FABRICATION AND PROPERTIES OF NICKEL NANOTUBES SYNTHESIZED BY TEMPLATE-ASSISTED ELECTROCHEMICAL DEPOSITION

Gulnar Kalkabay

A thesis submitted in partial fulfillment of the requirement of Nazarbayev University for the degree of Doctor of Philosophy

February 2020

Table of Contents

List of figures

List of tables

Acronyms and definitions

TM – track membrane;

PET – polyethylene terephthalate;

NS – nanostructure;

NT – nanotube;

NW – nanowire;

NP – nanoparticle;

Ni – nickel;

SEM – scanning electron microscopy;

EDA - energy dispersive analysis;

XRD - X-ray diffraction analysis;

TEM - transmission electron microscopy;

MeV - megaelectron - volt;

keV - kiloelectron - volt;

ECD - electrochemical deposition;

EPD - effective pore diameter;

CD – chemical deposition;

nm - nanometer;

μm - micrometer;

UV - ultraviolet;

VT – track etching rate;

VB – the etching rate of intact polymer material;

NR – nanorods;

MWR - microwave radiation;

HTS - hydrothermal synthesis;

FAP – fluorapatite;

CT - computed tomography

Acknowledgements

I would like to express my sincere gratitude to all who helped and encouraged me and made their contribution to this work. These are:

Dr Alexander Tikhonov, my main supervisor, for valuable discussions and support during PhD study and for being nice person. You gave me a lot of freedom to perform and design experiments. You always corrected my mistakes and showed effective ways how to be scientist.

Dr Artem Kozlovskiy, my co-supervisor, for giving me opportunities to work in laboratory, for giving me knowledge in field of experimental physics, always taking own time to read and correct my work.

Dr Maxim Zdorovets, my external supervisor, for support and chance to work in laboratory of the Institute of Nuclear Physics.

I would like to express deepest gratitude to, Professor Luis Rojas-Solórzano, Director of PhD Studies in Science, Engineering and Technology, for creating friendly and professional atmosphere, his help to all students during PhD study.

I am also grateful to my family members who have supported me along the way.

Declaration

I declare that the research contained in this thesis, unless otherwise formally indicated within the text, is the original work of the author. The thesis has not been previously submitted to this or any other university for a degree, and does not incorporate any material already submitted for a degree.

Abstract

One of the important topics today is the controlled synthesis of nanostructured materials, in particular nanotubes (NT) or nanowires, the interest in which is due to the great potential for their use as devices in microelectronics [1], catalysts [2], biomedicine [3], sensors [4], etc. The interest in metal nanotubes is due to the great prospects for practical applications associated with a larger specific surface area for nanotubes compared to nanowires, the possibility of obtaining single-domain isotropic walls along the entire length and the unique magnetic properties. Although a large number of recent research aimed at perfecting methods for producing metal nanowires/nanotubes and studying their properties, there are still many blank spots and unresolved issues [5]. In particular, the controlled synthesis of nanotubes with a predetermined isotropic wall thickness along the entire nanotube length, well-ordered crystalline structure, controlled orientation of domain structures, and high corrosion resistance to external influences remains unsolved and research active. Nickel nanowires and nanotubes deserve special attention due to their unique structural, conductive and magnetic properties. While the popular template-assisted electrochemical deposition of nickel nanowires is not difficult, the synthesis of highly ordered nickel nanotubes with controlled properties needs further research. Although there are many works devoted to the Ni nanotubes synthesis, showing that Ni NTs strongly depends on fabrication method and parameters, mechanism of NT growth is still not fully explored.

The aim of this work is comprehensive study of template-assisted electrochemical deposition of nickel nanotubes with controlled isotropic geometry of the diameter and wall thickness. The driving motive is the search for optimal fabrication conditions of Ni nanotubes with a high degree of structural ordering, as well as establishing controlled nanotubes synthesis with given structural parameters and aspect ratio.

Electrochemical deposition of Ni nanotubes was studied at various synthesis conditions, including the composition and temperature of the electrolyte, the difference in applied potentials, alcohol additives and the acidity of the solution. Detailed model for the Ni nanotube growth and formation of nanotube walls in the pores of polymer templates is developed. According to the model, at the initial stage of Ni nanotube formation the transverse component of growth rate prevails, which is responsible for nanotube wall growth in width. At the next stage characterized by a decrease in current density due to the depletion of the electrolyte solution the nanotube grows uniformly in both transverse and longitudinal directions. Next, the concentration of metal ions dominate near the top end of the nanotube, resulting that the longitudinal component of the

growth rate of the nanotubes prevails and the tubes grow predominantly along the walls of the pores.

The influence of various factors such as difference in the applied potential, temperature and the level of acidity of the electrolyte solution on the wall thickness, grain sizes and the degree of texturing of nanotubes, was evaluated. In particular, it was found that an increase in the applied potentials in the range of 1.5 – 2.0 V and the deposition temperature range 35-50°C leads to the formation of nanotubes with one dominant direction of texture orientation and to the increase in the number of defects in the nanotubes crystal structure due to an increase in the average crystallite size and the degree of microstresses. Adding ethanol to the electrolyte increases Ni nanotubes conductivity due to an improvement in the crystal structure and decrease in amorphous inclusions. It was found that lowering the acidity level of the solution leads to a decrease in the nanotubes wall thickness and the size of crystallites. Based on the conducted experiments, the most optimal parameters for the synthesis of nanotubes were selected: the difference of the applied potentials is 1.5-1.75 V, pH = 3 and the electrolyte temperature is 25 °C. These parameters were used to fabricate Ni nanotubes for experiments to study the influence of the geometry of the template matrix on the structure of the resulting nanotubes, as well as for corrosion tests experiments.

The main magnetic characteristics of fabricated Ni nanotubes were explored. Ni nanotubes arrays coercivity and squareness ratio exhibit unusual dependence on nanotubes diameter: it rises for samples with nanotubes 100 to 300 nm diameters and falls down for nanotubes 400 and 500 nm diameters. Ni nanotubes corrosion resistance to external influences of aggressive media was studied. The kinetics of degradation of Ni nanotubes was determined depending on the acidity of the solution and time being in the solution. It has been shown that the main mechanism of degradation of nickel nanotubes is the formation of the metastable phase of nickel oxide, which decays due to instability, which leads to partial destruction of the structure. It was found that the speed of degradation of nanotubes depends on the degree of crystallinity of the initial nanotubes, as well as the acidity of the solution.

1. Introduction

1.1 Background

The unique properties of nanoscale objects are of a great interest in science. The difference in properties of the same elements in the macroworld can be caused by several reasons. The first is the fact that in macroscopic objects a domain structure is created in accordance with the principle of minimizing the total energy, but with a decrease in the geometric dimensions of object, after passing through a certain critical value, a single-domain state may occur. The unique physicochemical, electrical and magnetic properties of ferromagnetic nanostructures based on the elements of the iron triad (Co, Fe, Ni) and their alloys cause a great interest in them in academic and manufacturing sectors. Large aspect ratio of elongated nano-objects ensures the separation of the easy magnetization axis in them, and the hollow form of nanostructures (for example, NT), due to the absence of magnetic core, make possible uniform switching fields for reproducible results. The low bulk density of hollow nanostructures allows them to float in liquids (including biological) and makes them suitable for use in biotechnology (for example, when used as a basis for creating contrasting liquids), and the increased specific surface area provides the possibility of obtaining more functional links and, accordingly, the movement of more payloads in the delivery of drugs.

There is a wide choice of methods for metal nanotubes synthesis: ALD deposition, electroless deposition, electron-beam and optical lithography, implantation, etching. The popular bottom-up approach allowing good control on geometry and structure of synthesized nanostructures is template assisted electrochemical deposition. This method is based on the use of porous thin films templates, such as track membranes, and allows wide range of materials to be deposited into membrane pores.

It is convenient to use the method of electrochemical deposition for obtaining metallic NTs and nanowires in the tracks of a template matrix based on a polymer. The deposition of materials in the pores occurs by passing a direct current through the electrolyte solution, which allows obtaining composite nanostructures. In the process of deposition, metal is reduced at the cathode, on which the polymer template is fixed. The main advantage of this method is the ability to control the deposition rate of metals in the pores, by changing the magnitude of the current and the applied voltage, as well as the deposition time. By adjusting these parameters, you can get nanoscale objects with the desired structure.

Considering that the shape, size, crystal structure and, accordingly, the properties of the formed nano-objects substantially depend on the conditions of synthesis, it seems relevant to study the mechanisms of formation of Ni nanotubes in the pores of the ion-track membranes at different voltages of electrochemical deposition, analysis of the synthesis temperature on their microstructure, the study of reactivity and chemical resistance.

1.2 Key objectives and novelty

The object of the study is metal one-component nickel nanotubes obtained by electrochemical synthesis in the pores of polymer template matrices.

The aim of the research is to study the processes of formation of nickel nanotubes in the pores of template matrices depending on various synthesis conditions parameters (electrolyte temperature, electrolyte acidity, difference in applied potentials, template geometry) and to study its corrosion resistance.

The following objectives of the dissertation research were formulated:

1. Development of the detailed model for the formation of nickel nanotubes in the pores of polymer matrices;
2. Study of the structure and composition of synthesized nanostructures by modern physicochemical methods: energy dispersive analysis, scanning electron microscopy, X-ray diffraction analysis, transmission electron microscopy;
3. Investigation of the effect of potential difference, electrolyte temperature on the phase composition and crystal structure of Ni nanotubes;
4. Study of the influence of the geometry of template matrices on the structural and magnetic properties of Ni nanotubes;
5. Investigation of the kinetics of degradation and chemical resistance of synthesized Ni nanotubes under the exposure to solutions with different acidities.

The novelty of the dissertation research is in the following results:

1. The model is proposed for the formation of nickel nanotubes in the pores of polymer matrices. According to the model, at the initial stage of growth the transverse component of the growth rate dominate, which is responsible for the wall growth in width. When an equilibrium state is reached, which is characteristic of a decrease in the current density, due to the depletion of the electrolyte solution during the synthesis, an equiprobable ratio of rates is observed. Further in the process of nanotube formation the growth rate longitudinal component predominates and the nanotube grows along the pore walls.

2. The dependences of the influence of the temperature of the electrolyte solution and the difference of the applied potentials on the degree of texturing and the domain structure of the synthesized nickel nanotubes are established. It was found that an increase in the potential difference in range of 1.5–2.0 V and the deposition temperature in range of 25–50 °C increases degree of texturing and preferred grain orientation in the [111] crystallographic direction along the nanotubes.

3. Nanotubes wall thickness dependence on synthesis temperature, acidity level of the electrolyte solution and potential difference is shown. It was found that a decrease in the acidity level of the solution leads to a decrease in the wall thickness of nanotubes and the size of crystallites.

4. The kinetic curves of the degradation of nickel nanotubes in various media are established. The time dependences of the deformation of crystallographic parameters at different levels of medium acidity were obtained. It was shown that degradation of nickel nanotubes proceeds through formation of a metastable phase of nickel oxide. This unstable phase decomposes leading to partial destruction of the nanotube.

5. Magnetic properties of nickel nanotubes were analyzed. Ni nanotubes' shape anisotropy, low specific density, large specific surface, and uniform magnetic field make them possible candidate to be used in bio applications and drug delivery.

1.3 Dissertation contents

Chapter 2 starts with a brief historical review of the state-of-the-art in the field of nickel nanotubes discussing their advantages and stating importance of their research.
Chapter 3 describes methods of synthesis and physical and chemical characterization of nickel nanotubes.
Chapter 4 presents results on synthesis and characterization of nickel nanotubes and describes potential applications.
Chapter 5 summarizes the obtained results and sets goals for future research.

1.4 Role of collaborators

This thesis is based on my own research and was written by me, but collaborations had an important role in obtaining results. All aspects of this thesis have received advice and been reviewed by main supervisor Professor Alexander Tikhonov and co-supervisor Dr Artem Kozlovskiy. Important contribution was also received from the colleagues from Scientific and

Practical Materials Research Centre of the National Academy of Sciences of Belarus. Full list of my collaborations and publications is contained in section 1.5.

Conducting experiments on the preparation of template matrices for electrochemical synthesis, testing the regimes for obtaining nanotubes in polymer matrices depending on the conditions of electrochemical synthesis, determining the elemental composition and morphology of nanotubes by such device as scanning electron microscopy and methods of energy dispersive analysis, obtaining x-ray diffraction patterns and analyzing them, processing the results and graphical construction of the obtained dependences of changes in structural parameters and kinetics of degradation were carried out by me or jointly with employees of the Laboratory of Solid State Physics of the Astana Branch of the Institute of Nuclear Physics of the Ministry of Energy of the Republic of Kazakhstan. Irradiation was made by my co-supervisor. The magnetic characteristics and hysteresis loops of the synthesized nanotubes were obtained in the Cryogenic Research Department of the Belarusian Academy of Materials Science (Minsk, Belarus) during the scientific training together with the department staff. Preparation of scientific publications on the topic of the dissertation, discussion of the obtained results and analysis was carried out by me and with the staff of the above scientific centers directly involved in the experiments and with supervisors.

Papers 1, 2 contain predominately my own work, including conducting experiments, analysis of experimental results and writing. XRD data was obtained and analyzed with the help of my co-supervisor Dr A.Kozlovskiy. Ni nanotubes magnetic properties were analyzed in collaboration with researchers A.Shumskaya and E. Kaniukov from Minsk.

Papers 3, 4, 5 made in collaboration with scientists from Minsk. Synthesis of nickel nanotubes was made by me. Chemical model was proposed by colleagues from Minsk. Characterization of structural features was conducted by me and my co-supervisor.

Team of my supervisors, Professor A. Tikhonov, Dr A. Kozlovskiy and Dr. M. Zdorovets, made suggestions and feedback of my papers and this thesis. Colleagues from Minsk who are co-authors of my papers help me with equipment and modeling experiments and advice on applications of obtained nickel nanotubes.

1.5 Thesis outputs

Journal papers:

1. **Kalkabay G.,** Kozlovskiy A. et al. Study of the Reactivity of Ni Nanotubes in Media with Different pH //Crystallography Reports. – 2018. – Vol. 63. – №. 1. – P. 90-95. (IF=0.8)
2. **Kalkabay G.,** Kozlovskiy A. et al. Influence of temperature and electrodeposition potential on structural and magnetic properties of nickel nanotubes // Journal of Magnetism and Magnetic Materials. – 2019. - Vol.489. (IF=2.7)
3. A. L. Kozlovskiy, I. V. Korolkov, **G. Kalkabay**, M. A. Ibragimova, A. D. Ibrayeva, M. V. Zdorovets, V. S. Mikulich, D. V. Yakimchuk, A. E. Shumskaya, E. Yu. Kaniukov. Comprehensive Study of Ni Nanotubes for Bioapplications: From Synthesis to Payloads Attaching // Journal of Nanomaterials. – 2017. - V. 2017. - Article ID 3060972 - 9 pages, (IF=1.78).
4. M. D. Kutuzau, E. Yu. Kaniukov, E. Shumskaya, V. D. Bundyukova, **G. R. Kalkabay**, M.V. Zdorovets, D. B. Borgekov and A.L. Kozlovskiy. The behavior of Ni nanotubes under the influence of environments with different acidities //CrystEngComm. – 2018. – Vol.20. – P. 3258-3266 (IF=3.26).
5. Shumskaya, A., Bundyukova, V., Kozlovskiy, A., Zdorovets, M., Kadyrzhanov, K., **Kalkabay, G.,** Kaniukov, E. Evolution of morphology, structure, and magnetic parameters of Ni nanotubes with growth in pores of a PET template. // Journal of Magnetism and Magnetic Materials. – 2020. – Vol. 497. – P. 165913 (IF=2.7).

Conference proceedings and presentations:

1. G.Kalkabay, A.Shumskaya, E.Kaniukov, A.Kozlovskiy, M.Zdorovets, A.Tikhonov. Ni nanotubes: influence of deposition parameters on structure and magnetic properties. 4th International Conference “Nanotechnologies”, NANO – 2016, Tbilisi, Georgia, October 24 – 27, 2016.
2. G. Kalkabay, A. Tikhonov, A.L. Kozlovskiy, M.A. Ibragimova, D.I. Shlimas. Investigation of structural features of Ni nanotubes. NANO – 2016, Minsk, November 22-25, 2016.

3. A.Shumskaya, E.Kanyukov, A.Kozlovskiy, M.Zdorovets, A.Tikhonov, G.Kalkabay. Metallic nickel nanotubes: influence of deposition parameters on theirs structure and magnetic properties. European Chemical Bulletin, 2016, 5(12), p.531-535.

2. Literature review

This chapter contains brief review of the state-of-the-art in the field of nickel nanotubes research and applications, discusses unresolved issues to be addressed in thesis.

2.1 Ni nanotubes as one of the promising materials in nanotechnology

Today, significant attention is paid to methods for synthesis of nanostructures of various geometries, such as wires [1-3], tubes [4-6], spherical particles [7-10], dendritic structures [11-13]. Such a great interest in nanostructures is due to the wide range of possibilities of their application in microelectronics, photocatalysis, biomedicine, solar cells, etc. [14-20]. Various nanotubes are currently actively researched, as due to their geometry, they have a large specific surface area, large aspect ratios.

Among the variety of metal nanowires and nanotubes synthesized by various fabrication methods, magnetic nanostructures synthesized from a subgroup of iron (Ni, Co, Fe) are distinguished as a separate group. Interest in this class of nanomaterials is due to a wide range of their practical applications in the modern world, in field of microelectronics [21-26]. Metal nanotubes studied for obtaining single-domain structures with controlled magnetic and electrical properties. The interest in magnetic nickel nanostructures, in particular, nanotubes, is primarily due to their high stability to degradation and oxidation, as well as the absence of phase transformations in a fairly wide temperature range. Nickel nanotubes, unlike iron or copper ones, are highly stable to corrosion and degradation processes in various media, as well as the absence of oxidative processes for a long time in the air, while iron or copper structures in air become covered with a thin oxide film, which can subsequently make a negative contribution to the structural and strength properties. Also, the oxidation of the surface of nanotubes makes essential changes in the conductive or magnetic properties, which has a huge impact on the performance of nanotubes. In turn, high rates of resistance of nickel nanotubes to degradation and corrosion processes, as well as low toxicity indicators, make them a promising material for biomedicine as containers for targeted delivery of drugs [27-30]. In this case, unlike nanowires, the hollow structure of nanotubes makes it possible to use both outer and inner surface of the nanotube for drug transfer (see Figure 1).

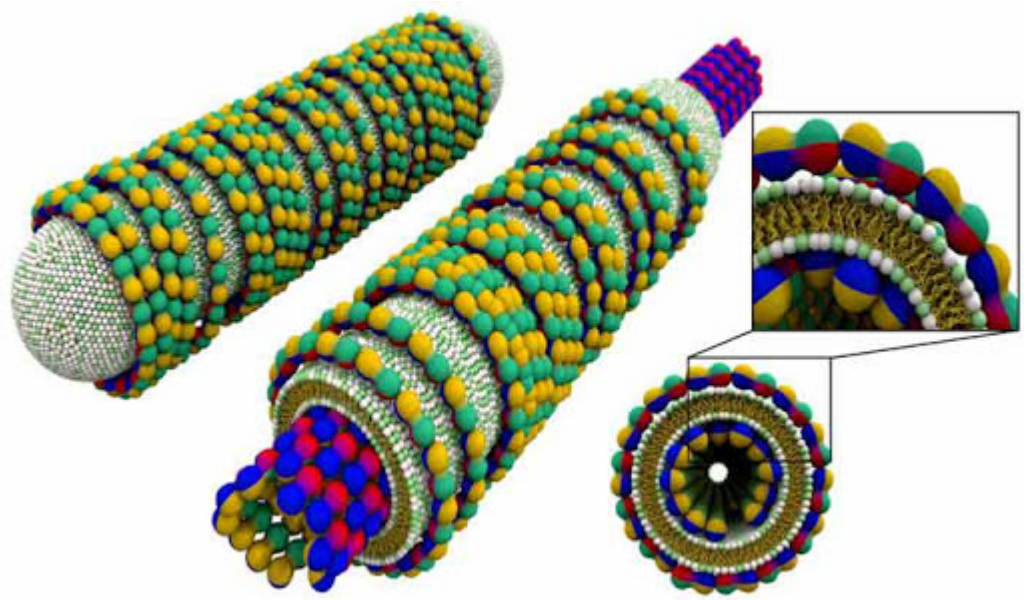

Figure 1. An example of using nanotubes as a container for targeted drug delivery [30]

Other useful applications of nickel nanotubes include fabrication of light and durable composite materials, special coatings, and ending with electronic devices, nanoscale sensors and devices. [31-34]. The interest in nickel nanotubes in microelectronics applications is primarily due to their high stability of structural ordering and the uniformity of the phase composition during synthesis, in contrast to other magnetic nanostructures based on cobalt or iron, which are known for the presence of several crystalline structures and phases. The presence of metastable phases in the structure of cobalt nanostructures, for example, makes them unstable to degradation and long-term storage, and also has a significant effect on their magnetic properties [35-37]. In turn, nickel nanotubes have only one phase state in a wide range of annealing temperatures or synthesis conditions [38]. Authors in [38] studied the resistance of nickel nanotubes to external influences, such as thermal heating. The authors present in detail the dynamical changing in structural properties and transformations of phase and also changes of nanotubes geometry as a result of dynamic heating in an oxygen-containing atmosphere. Figure 2 shows the dynamical changing in the geometry of nanotubes and also in the internal diameter.

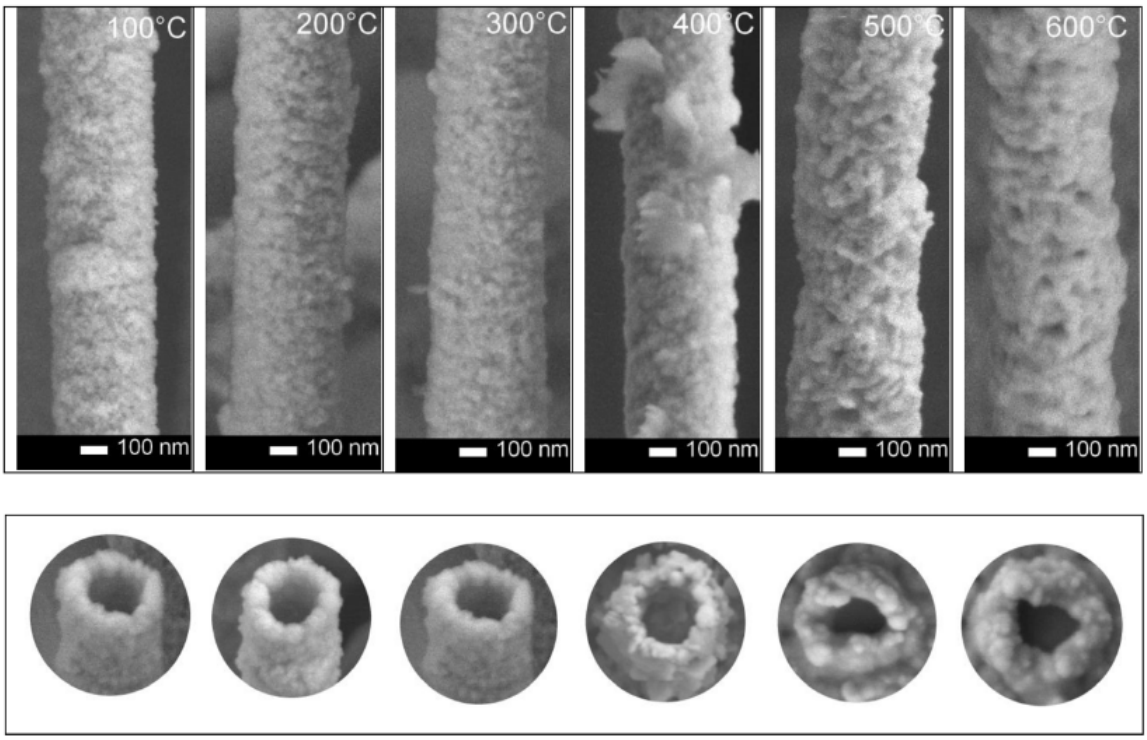

Figure 2. SEM images in morphology changing of Ni nanotubes after process of thermal annealing [38]

The authors showed that Ni-nanotubes thermal heating at a temperature 400°C and above leads to oxide growths and resultant decrease in the inner diameter.

In contrast to nickel nanowires, the fabrication of which by the method of template synthesis is not difficult, the formation of highly ordered nickel nanotubes with wall thickness isotropic along the entire length, as well as the ability to control the geometry of the walls and grain sizes has many unclear aspects and is of interest for further studies [39-43]. For example, in [44], a method was proposed for producing nickel nanostructures in the form of tubes, the production scheme of which is shown in Figure 3, and Figure 4 shows TEM images of the synthesized nanostructures.

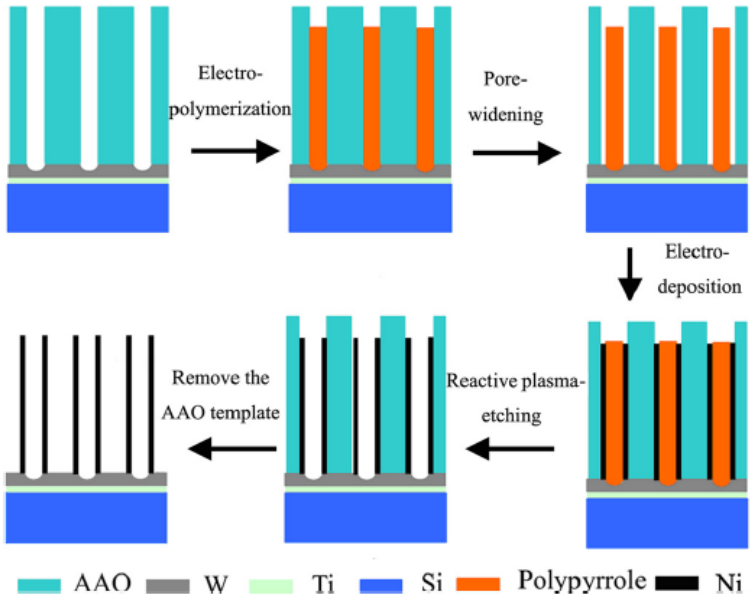

Figure 3. Fabrication process of Ni nanotube arrays [44]

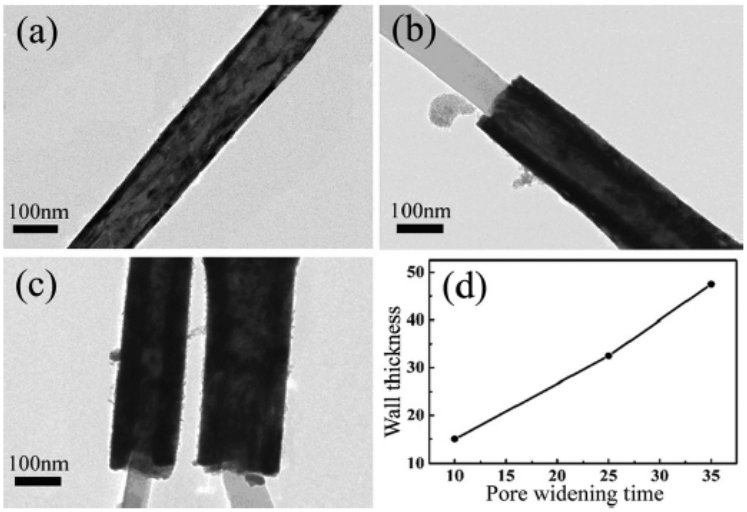

Figure 4. TEM images of Ni nanotubes with wall thicknesses of (a) 15 nm, (b) 32 nm, and (c) 47 nm, respectively; (d) the dependence of wall thickness on the pore-widening time [44]

The production technique presented by the authors of the work [44] makes it possible to control not only the geometry of nanostructures, but also the wall thickness of nanotubes. However, the small wall thickness leads to a weak degree of crystallinity of the nanotubes and strong anisotropy of magnetic properties.

Ability to control geometry and phase composition of Ni nanotubes is critically important for practical applications [45-51]. Nowadays much attention [52-53] is paid to the research and modeling of nickel nanotubes fabrication in the pores of template matrices, with the goal of

understanding the nucleation processes and fundamental aspects of the growth of nanostructures as well as such as crystalline structure formation and crystallite orientation.

An important feature for the synthesis of nanotubes is the detailed understanding of the growth mechanisms. Thus, in [52], a simple mechanism was proposed for the formation of NT and NW, depending on the geometry of the cathode, the deposited layer, and the deposition time (Figure 5). It is proposed that metal nanoparticles initially form and then stack inside the tubes to form nanotubes when the electric field reaches a certain value.

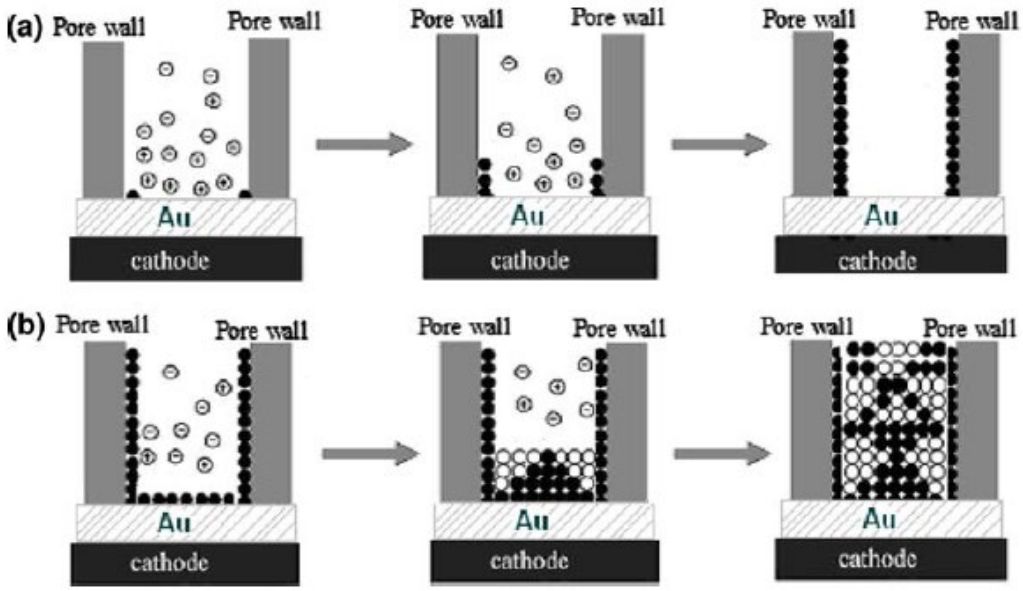

Figure 5. Schemes of the growth process a) of nanotubes; b) of nanowires (the white and black balls show various crystallographic orientations) [52]

Paper [54] describes the ECD for fabrication of Ni nanotubes of wall thickness varying from 10 to 70 nm controlled by adjusting the pH of the solution and the applied electrode potential. Gradual building of the nanotube wall was explained as assisted with hydrogen bubbles formation during nanotube growth process. In [57] fabrication of Ni nanotubes by electrodeposition in polycarbonate templates was described. Magnetic properties of Ni nanotubes are very important due to their practical applications, including memory and electronic devices, drug delivery bio-applications. Magnetic properties of nickel nanotubes were actively studied, for example [23, 56, 57]. With ongoing discussion and different hypothesis on nanotubes growth in pore membranes, the question on detailed mechanism still remains open and needs further research.

As a rule, the synthesis of nanostructures under real experimental conditions proceeds under nonequilibrium conditions, i.e. in the environment surrounding the system of nanotubes,

various flows of matter and energy arise, the direction and intensity of which determines the shape, size and properties of the formed nanostructures [53-59]. Knowing the intensity of the flows in the system, the degree of nonequilibrium of the system can be determined [60-62]. Under certain conditions in the experimental system, different nanostructures [63-69] can be obtained. At the stage of obtaining nanostructured materials related to nonequilibrium systems, even slight fluctuations in pressure, density, concentration, temperature, potential difference, and many other factors have a significant impact on their formation [69-71]. The main problem in obtaining accurate reproduction of nanotubes on an industrial scale is that nanostructures can have several energetically favorable states, the so-called multistable system [72-75]. The reproducibility of nanotubes fabrication can be increased by optimizing the effects (thermal, electromagnetic, chemical) at the synthesis stage, the intensity of which is determined at the stage of studying the processes of organization and self-organization of nanostructured materials. In experiments on nanotubes fabrication, it is especially important to take into account their instability and high reactivity, which can lead to aggregation, loss of properties when interacting with the environment, and also change internal structure [76-79].

In addition, the method of nanomaterials fabrication significantly affects the properties of nanostructures and its possible applications. Thus, the method of obtaining nanostructured materials should not only ensure the stability of the properties of materials, but also preserve these properties during their operation [80-83].

The study of the structural features and the possibility of control of the phase composition or processes of phase transformations in nanotubes, open up great prospects materials and devices based on nanotubes. Special attention is paid to the research for obtaining nanostructures not only with a given phase composition and crystal structure, but also with geometry, which plays one of the essential roles in the application of nanotubes [84-89]. Large specific surface area, high degree of crystal structure ordering, high mechanical strength and resistance to external influences are the main factors that determine the characteristics of nanomaterials. Among the variety of nanostructures of various geometries, such as nanoparticles, dendrites, spheres, rods, cylindrical structures in the form of wires or tubes can be distinguished into a separate category. Interest in nanotubes is due not only to their geometry, but also to the ability to control parameters such as height, wall thickness, or outer diameter.

Corrosion resistance of Ni nanotubes remains unexplored and needs a detailed study. Oxidation, which causes corrosion and degradation of material, can make NT unsuitable for a number of applications. Nanostructures subjected to corrosion process experience a degradation of practically important properties. Degradation leads to changes in NT magnetic and electrical properties, which are important for micro- and nanoelectronic applications. Degradation of

nickel NT in acidic and slightly acidic environments with the formation of toxic nickel oxides can lead to cell death in case of bio-application. Corrosion modifies NT structural stability and motion. In [90] authors studied corrosion behavior of carbon nanotubes-Ni composite coating. In this work, degradation of Ni nanotubes was studied by the thesis author and colleagues from Minsk.

2.2 Template synthesis to obtain nanotubes with controlled geometry

To date, dozens of methods for creating Ni nanostructures are known [91-99]. Fundamentally, all methods for producing nanostructures can be conditionally divided into two large classes: physical and chemical methods. Another distinction is whether one uses a top-down or bottom-up approach. It should be emphasized that the bottom-up approach is more characteristic of chemical production methods [95-99]. In the case of the bottom-up approach, template-based methods are usually preferred, as with sufficient control over the nanostructures geometry while technologically simple and economical. Most popular bottom up chemical deposition method to produce nanostructures with cylindrical geometry is template-assisted electrochemical deposition method. Here the template matrices are an integral part, the use of which gives a direct opportunity to control the nanostructures geometry, and also allows you to scale this production technology on an industrial or semi-industrial scale [100-103].

Template methods for the synthesis of nanostructures are based on the process of nucleation or reduction of metal ions on the activation centers of the pore walls of template matrices under the influence of external factors, such as the addition of buffers that promote nucleation and further growth of nanostructures [104]. For example, in [105], the authors considered the possibility of fabrication nickel nanowires and nanotubes using the sol-gel method and template matrices based on anodized alumina. By changing the synthesis conditions, the authors were able to control the geometry of the obtained nanotubes, as well as vary the height (see Figure 6).

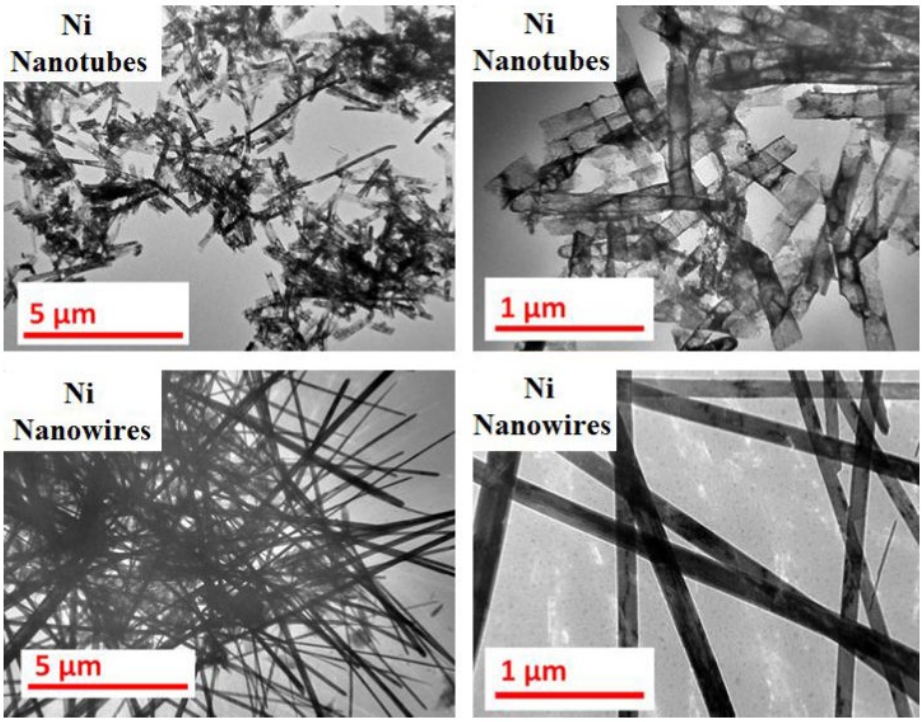

Figure 6. TEM images of the as-prepared Ni nanotubes and nanowires [105]

The authors of work [105] found that the use of the sol-gel method is most promising for the preparation of structurally ordered nickel nanowires, while the synthesized nanotubes had low crystallinity and low strength, which led to partial destruction with the slightest external impact. Moreover, the use of template matrices, as shown by the authors, allows one to control the height of the synthesized nanostructures, as well as their outer diameter. It is also worth noting that the use of template matrices makes it possible to control the geometry of the obtained nanotubes with high accuracy.

Among the variety of templates, much attention is paid to matrices based on anodized aluminum oxide (AAO), which allow one to obtain nanostructures with a high density per cm^2, which is 10^8-10^{11} pieces/cm^2. However, a high density leads to a limitation in external diameter not exceeding in most cases 100-200 nm [106,107]. Such a limitation leads to a decrease in the strength properties of the synthesized nanostructures, as well as a low degree of structural ordering, as evidenced, for example, by the results of the fabrication of nanotubes in the pores of template matrices based on AAO with a diameter of 20-50 nm (see Figure 7) [108].

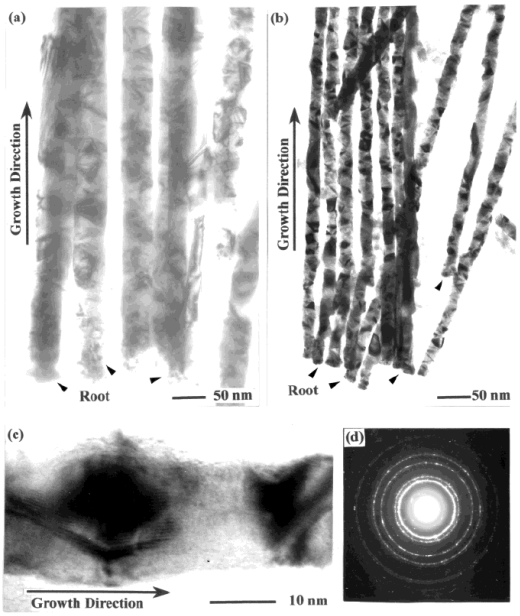

Figure 7. TEM images of the free Ni nanowires fabricated from the anodic alumina films formed in (a) oxalic acid; (b) and (c) sulfuric acid solution; (d) the corresponding electron diffraction pattern of (b) [108]

The most common template synthesis method utilizes chemical or electrochemical deposition for producing nanostructures. Moreover, method of template synthesis is suitable to precise control of nanotubes geometry as well as the structural properties and the degree of crystalline ordering. Template-assisted electrochemical deposition method allows to control these parameters with high accuracy and sufficient simplicity as well to control the phase composition of the synthesized nanotubes [110-114].

The possibility of using the template synthesis method to obtain nanotubes based on metals of the iron subgroup (Ni, Co, Fe) allows us to open new perspectives in the field of magnetic nanomaterials and devices based on them [114-119]. The interest in nanotubes is due to the great prospects for practical applications associated with a larger specific surface area for nanotubes compared to nanowires, the possibility of obtaining single-domain isotropic walls along the entire length, etc.

Nickel nanotubes deserve special attention as they have unique structural, conductive, and magnetic properties.

In turn, the solution to the problem of synthesis of nickel nanotubes with a controlled geometry can be the use of an electrochemical method for synthesis of nanotubes using polymer matrices as templates. This method makes possible to scale the synthesis technology not only in

laboratory conditions, but also on a semi-industrial scale with a high degree of repeatability of geometric and structural properties of the obtained nanotubes.

The aim of this research is comprehensive study of template assisted electrodeposition of nickel nanotubes with controlled isotropic geometry of the diameter and wall thickness, controlled crystal structure and ordering and also assessment of corrosion resistance to external influences of aggressive media of the obtained nanotubes.

3. Methodology

This chapter describes experimental details of our track-etched membranes based electrochemical synthesis of nickel nanotubes. It also describes used methods of physical and chemical characterization of obtained Ni nanotubes, including SEM, TEM, method of gas porosimetry, XRD, method of vibration magnetometry.

3.1 Obtaining template matrices for electrochemical synthesis

Ion track etching technique is a unique and practical tool for producing statistically distributed holes in polymer materials over a given area and density. Track-etched membranes are used as the matrix for the fabrication of nickel nanotubes.

To fabricate the template matrix, a film based on a HostFhan® type PET manufactured by «MitsubishiPolyesterFilm» (Germany) was used. Several materials can be used as template matrix for ion-track etched membranes, such as polycarbonate and PET. We used PET and not polycarbonate as PET is more economical and available material and has physical and chemical properties suitable for template based metal nanotubes synthesis.

PET (polyethylene terephthalate, better known as PET or lavsan) has a chemical formula $(C_{10}H_8O_4)_n$ - is a complex thermoplastic polyester typically produced by polycondensation of ethylene glycol with terephthalic acid (or its dimethyl ether). According to its physical properties, it is a solid transparent substance in an amorphous state and white, opaque in a crystalline state. It turns into a transparent state when heated to the glass transition temperature and remains in it with sharp cooling and rapid passage through the so-called "crystallization zone". PET is a durable, tough and lightweight material, non-toxic, a good dielectric. The physical properties of PET are presented in Table 1.

Table 1. Physical characteristics of PET

Properties	Unit of measurement	Value
Density	kg/m^3	1360-1400
Breaking stress at:	MPa	
Bending		50-70
Compression		80-120
Elastic modulus	GPa	2,5-3,0
Relative extension at break	%	2-4
The melting temperature	°C	255-265
Softening point		245-248
Glass transition temperature		70-80
Frost resistance		-50

One of the important parameters of PET is high intrinsic viscosity due to the relatively large length of the polymer molecule. As a result, PET has high chemical resistance to gasoline, oils, fats, alcohols, ether, diluted acids and alkalis. Polyethylene terephthalate is insoluble in water and many organic solvents, soluble only at 40-150 °C in phenols and their alkyl- and chlorine-substituted, aniline, benzyl alcohol, chloroform, pyridine, dichloroacetic and chlorosulfonic acids, methylene chloride, methyl ethyl ketone, ethyl acetate, carbon tetrachloride etc. It has increased resistance to water vapor.

PET is not chemically resistant to ketones, strong acids, alkalis, acetone, chlorobenzene, chloroform, methylene chloride, chloroethylene, trichlorethylene, tetrahydrofuran, hot water (above +60 °C), concentrated acetic acid, 40% hydrofluoric acid, 10% aqueous solution of potassium alkali, 50% aqueous alkaline sodium carbonate solution, aqueous solution of carbolic acid, 36% hydrochloric acid solution, 2% aqueous sulfuric acid solution. These properties make PET suitable for electrochemical deposition of wide range of materials using various electrolytes.

Polyethylene terephthalate (PET) films with a thickness of 12 μm, a pore density of 1-$4x10^7$ ion/cm^2 and diameters of 400±20 nm were used as templates in the work. These patterns were obtained using the ion-track technology method, which consists in irradiating a polymer film by heavy ions with an energy of 1.5-1.75 MeV/nucleon with a given ion flux density. This technique for producing template matrices using charged ion beams has been known for more than 50 years. It is one of the most accurate methods for obtaining template matrices with a given pore density and diameter.

A schematic representation of heavy-ion film irradiation is shown in Figure 8, taken from a dissertation by Holder of an Advanced Doctorate in Physico-mathematical Sciences Apel P.Y. [120], which is one of the founders of this area.

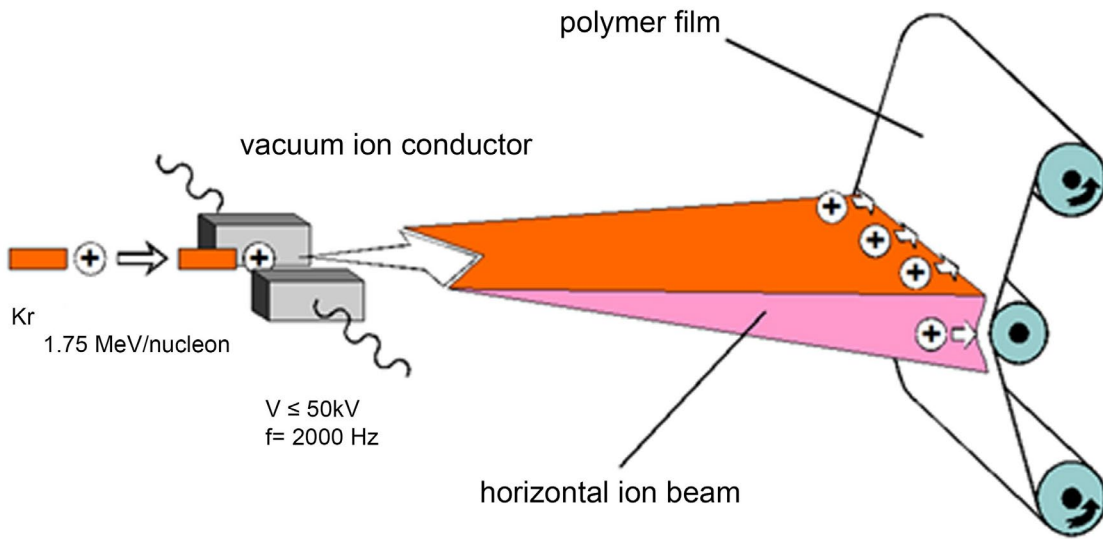

Figure 8. Schematic process of irradiation of polymer film [120]

After irradiation, the obtained films with latent tracks, the diameter of which does not exceed 3-10 nm [121,122], were treated with ultraviolet radiation to embrittle chemical bonds near the latent track and subsequent chemical etching to the desired diameter. A 2.2 M sodium hydroxide solution heated to a temperature of 85±2°C using a water bath was used as an etchant solution. The diameters were controlled by etching a series of samples depending on the etching time and then determining the diameters using scanning electron microscopy (SEM). The etching uniformity was controlled by comparing the diameters of the obtained tracks of the front and back of the film in order to prevent the effect of the formation of conical pores or asymmetric pores. Figure 9 shows typical SEM images of template matrices on the front and back sides, as well as a side chip of the template, showing the cylindrical geometry of the resulting pores. According to obtained data, the difference between the diameters of the front and back is not more than 1-3 %, which at a film thickness of 12 μm indicates the absence of a pronounced effect of conical pores.

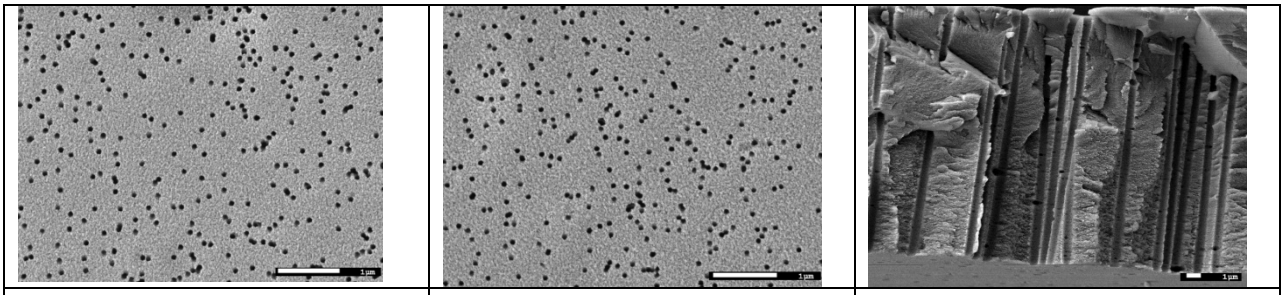

Front side	Back side	Side cleavage

Figure 9. SEM images of a PET film after etching

Figure 10 shows a diagram of the dependence of changes in pore diameters on etching time, measured by counting the diameters on the front and back sides in an amount of 50 pieces. Further increase in the etching time above 5 minutes led to the formation of larger, fused together pores, which are not suitable for the electrochemical growth of nanostructures.

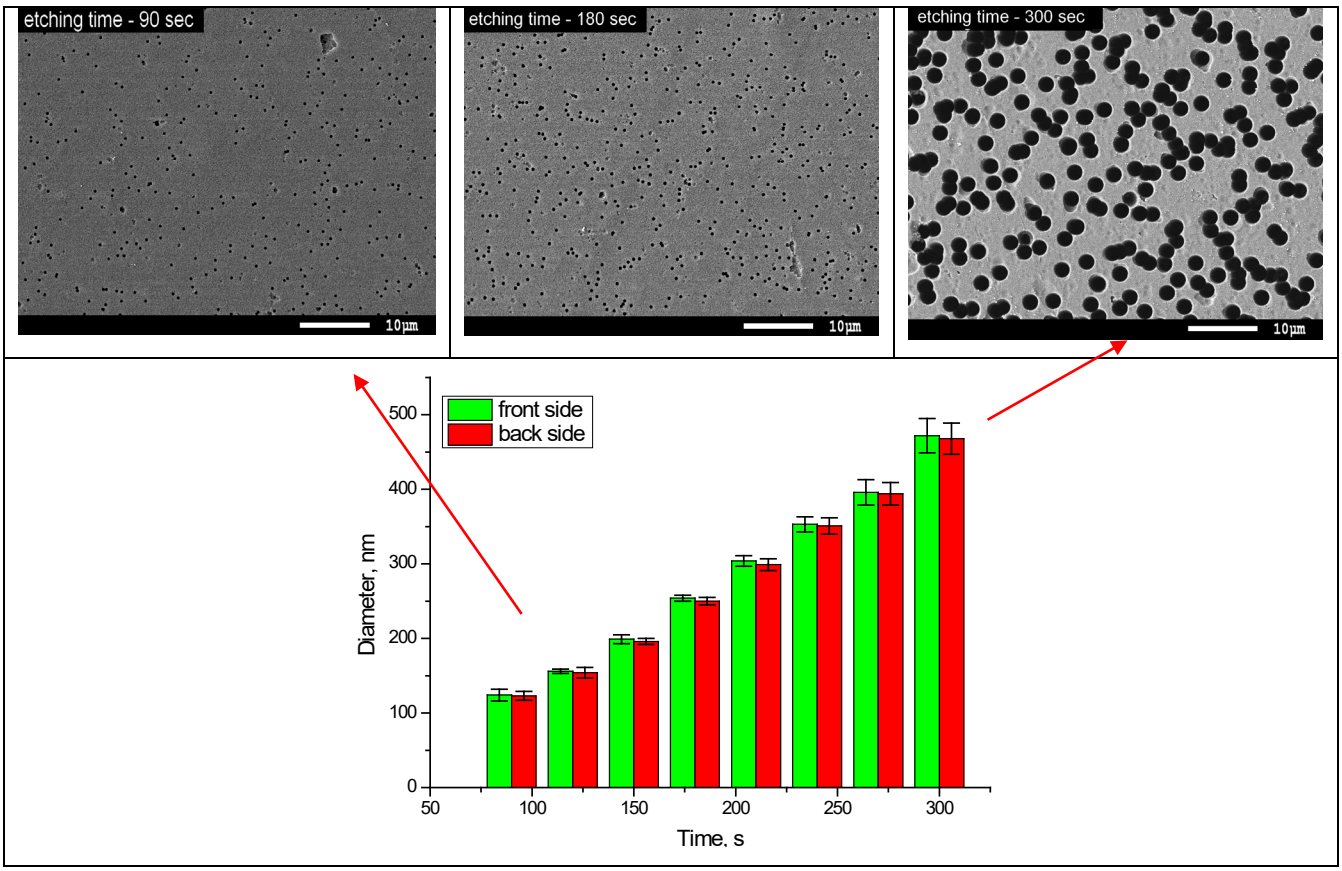

Figure 10. SEM images of PET pore membranes and a diagram of the dependence of pore diameters with etching time.

The choice of films with pore diameters of 400±20 nm as templates is due to the fact that these diameters of metal nanotubes are most often used in various fields of microelectronics, biomedicine, etc. The film thickness of 12 μm allows varying with high accuracy the geometry of the obtained nanotubes, which plays significant role in the study of the properties of nanotubes.

3.2 Electrochemical method for nanotubes synthesis

We synthesize nanotubes by template assisted electrochemical deposition, the method of electrochemical synthesis from aqueous solutions of electrolytes. In this method the restoration of metal salt ions dissolved in aqueous solutions occurs under the action of an electric field created by applying a potential difference between the anode and cathode. As a rule, the recovery of metal positive ions occurs on the surface of the cathode due to the addition of an electron and reduction to a metallic state. In this regard, the use of different patterns on the cathode surface

can make it possible to obtain nanostructures of various geometries [123-129]. Initially, this method was used to obtain nanowires that were formed inside the pores of template matrices, with conductive layer on one side of the template that completely covers the pores of the matrix. As a result of this deposition, the formed conductive layer upon application of the potential difference led to the fact that metal ions were restored uniformly over the entire surface of the conductive layer in the channel and, as a result, nanowires were obtained.

In this work, a conductive layer is a thin golden layer, the thickness of which is less than 30-40 nm. Using this layer allows you to leave the pores of the matrix open, only forming near the edge of thin rims of gold, the thickness of which does not exceed 10-15 nm, according to scanning electron microscopy. As a result of the deposition of such a conductive layer, the formation of nanostructures occurs only near this ring, thereby forming nanotubes. Varying the applied potentials difference, one can change not only the growth rate of nanostructures, but also the geometry. Moreover, the use of this method of applying a contact conductive layer leaves open the question of the initial processes of formation of the walls of nanotubes, as well as various synthesis conditions, which this dissertation is aimed at solving.

Figure 11 shows a typical scheme for nanotubes fabrication in the pores of PET based template matrices, with the subsequent release of the synthesized nanotubes from the polymer matrix by chemical etching in a highly concentrated sodium hydroxide solution.

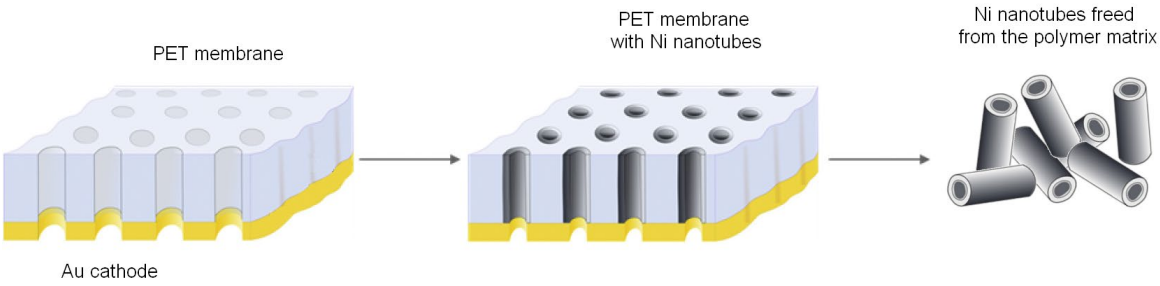

Figure 11. The scheme for producing nanotubes

The main electrolyte solution for the fabrication of Ni nanotubes was $NiSO_4 \times 6H_2O$ (100 g/l), H_3BO_3 (45 g/l), $C_6H_8O_6$ (1.5 g/l). The addition of boric acid and ascorbic acid served as buffer additives in order to increase the reduction efficiency of metal ions on the walls of pores during the synthesis. The potential difference was varied from 1.25 V to 2.0 V. Varying the synthesis conditions by changing the applied potentials difference, as well as the temperature of the electrolyte solution during deposition, was dictated by the search for optimal conditions for obtaining highly ordered nanotubes with controlled geometry.

Table 2 presents the data of electrolyte solutions used in the experiment to determine the effect of various metal salts, as well as alcohol additives on structural changes in the synthesized nanotubes.

Table 2. Data of solutions of electrolytes

№	Electrolyte	Synthesis conditions
1	$NiSO_4 \times 6H_2O$ (100 g/l), H_3BO_3 (45 g/l), $C_6H_8O_6$ (1.5 g/l)	Temperature - 25°±2°C pH=3 Potential difference – 1.5-2.0V
2	$NiCl_2 \times 6H_2O$ (100 g/l), H_3BO_3 (45 g/l), $C_6H_8O_6$ (1.5 g/l)	
3	$NiSO_4 \times 6H_2O$ (50 g/l), $NiCl_2 \times 6H_2O$ (50 g/l), H_3BO_3 (45 g/l), $C_6H_8O_6$ (1.5 g/l)	
4	$NiSO_4 \times 6H_2O$ (100 г/л), H_3BO_3 (45 g/l $C_6H_8O_6$ (1.5 g/l), Ethanol (100 ml/l)	
5	$NiCl_2 \times 6H_2O$ (100 g/l), H_3BO_3 (45 g/l), $C_6H_8O_6$ (1.5 g/l), Ethanol (100 ml/l)	
6	$NiSO_4 \times 6H_2O$ (50 g/l), $NiCl_2 \times 6H_2O$ (50 g/l H_3BO_3 (45 g/l), $C_6H_8O_6$ (1.5 g/l), Ethanol (100 ml/l)	

All reactions of fabrication Ni nanotubes during deposition process are described below.

$$NiSO_4 \rightarrow Ni^{+2} + SO_4^{-2}$$
$$Ni^{+2} + 2e \rightarrow Ni^0(s) \downarrow$$
$$NiCl_2 \rightarrow Ni^{+2} + Cl_2^{-2}$$
$$Ni^{+2} + 2e \rightarrow Ni^0(s) \downarrow$$

In the process of synthesis, the sulfates and nickel chlorides dissociate into ions and cations of salts, after that the ions are reduced near the cathode. This process makes possible formation of nanotubes walls. In this fabrication, changes in the applied potential difference made formation of nanotubes with a given composition of phase.

The pH of the solution plays significant role in the nanotubes fabrication. Change of pH level leads to an irregular growth of nanotubes. Ascorbic acid was added for control of pH level of solution. Ascorbic acid is used as buffer for maintaining the level of pH. Addition of ethyl

alcohol was made for assessment of the effect of surfactant additives. These surfactant additives change the rate of fabrication and the structural properties of nanotubes.

3.3 Characterization of the structural properties of synthesized nanotubes

To study the structural features of the nanotube morphology we used the method of scanning electron microscopy performed with a high resolution JEOL-7500F electron microscope at an accelerating voltage of 5.0 kV in the SEI shooting mode.

The elemental composition of the nanotubes synthesized at various conditions were studied by energy dispersive analysis performed on a Hitachi TM3030 electron microscope with a Bruker XFlash MIN SVE microanalysis system at an accelerating voltage of 15 kV.

The crystallographic characteristics, the phase composition and the degree of perfection of the crystal structure were determined by analyzing X-ray diffraction patterns obtained on a D8 ADVANCE X-ray diffractometer using Cu Ka-radiation from an X-ray tube and a graphite monochromator on a diffracted beam. X-ray diffraction patterns were recorded in the Bragg-Brentano geometry, in the angular range 2θ=30-90°, which covers all the main diffraction reflections of the studied nanotubes.

The study of macromagnetic properties was carried out using vibrational magnetometry on a universal measuring system «Liquid Helium Free High Field Measurement System (CryogenicLTD)». The measurements were carried out by the induction method by measurement of induced electromotive force of induction in signal coils oscillating with certain frequency magnetized sample within the range of magnetic fields 3 T at temperature 300 K.

4. Fabrication and properties of nickel nanotubes: growth mechanisms and dependence on synthesis parameters

This section is devoted to the study of the formation of nanotubes at varying fabrication conditions, such as difference in applied potentials, electrolyte temperature and alcohol additives in the electrolyte solution. The initial stages of nanotubes growth are studied and explained. The driving motive is the search for optimal conditions for the production of Ni nanotubes with a high degree of structural ordering, as well as establishing controlled synthesis of nanotubes with given structural parameters and aspect ratio.

4.1. Investigation of nanotube formation at the initial stages of growth

Despite a large number of studies addressing the processes of formation of nanotube walls in the pores of template matrices, the detailed mechanism of the initial stages of growth remains unclear. Understanding this mechanism will significantly expand the ability to control nanotubes fabrication with a given geometry, as well as to answer fundamental questions related to the formation of nanostructures.

The method of electrochemical synthesis is one of the most promising methods for the controlled production of nanostructures of a given geometry, as well as phase and elemental composition. There are many different factors that can be changed to control the structure of the synthesized nanostructures, as well as varying the geometry from nanotubes to wires [130-133]. However, the detailed description of the initial stage of the formation of the walls of nanotubes is not yet fully developed.

As it was indicated in Section 2, for the template matrices for the synthesis, we used PET polymer films 12 μm thick and 400±20 nm in pore diameter, with a contact golden layer of 30-40 nm thickness deposited on one side. Figure 12 represents scheme of the main stages of obtaining nanotubes and a chronoamperogram of the synthesis process, indicating the main stages of synthesis.

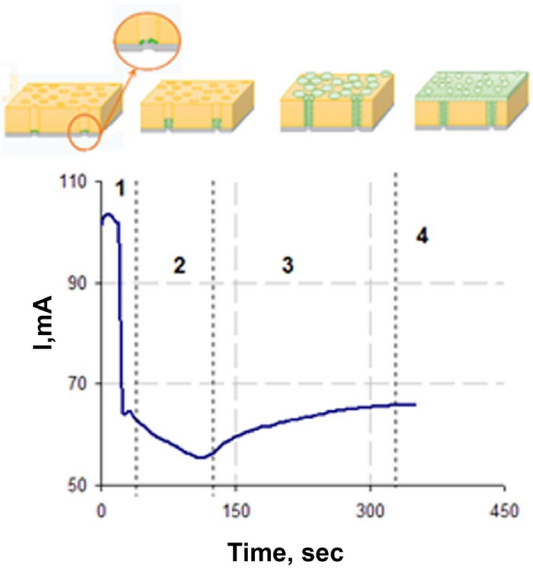

Figure 12. Chronoamperogram of the synthesis process of nanotubes

It is well known that fabrication of nanotubes by ECD or reduction of metal ions along the pore walls of template matrices consists of 4 main stages. The first stage corresponds to the beginning of filling the pores of the template and is characterized by a sharp drop in the current strength. It happens as a result of nucleation at the cathode, which is the gold rim formed by magnetron sputtering. The second stage is characterized by the growth of nanotubes along the pore walls of the template matrix until it is completely filled. The first two stages are the main ones in the process of nanostructure formation, since it is precisely at these stages that the basis for the geometry of the resulting nanotubes is laid, in particular the wall thickness. The synthesis process itself in the second stage continues until the length of the nanotube becomes equal to the thickness of the template. In the third stage, after the metal reaches the surface of the template, it begins to grow in three dimensions (volume growth) above the surface of the polymer film with the formation of “covers” growing from the walls of the nanotubes. Since the effective surface area of the deposition increases as a result of this process, the recorded current also increases. The third stage continues until the mutual overlapping of metal islands located in the places of localization of nanotubes. The fourth stage corresponds to the formation of a continuous metal layer on the surface of the template, as a result of which I reaches saturation. This value corresponds to the synthesis current, measured on a metal electrode of the same area with the same applied voltage. It should be noted that the behavior of I(t) in the chronoamperogram depends on the parameters of deposition and the shape of the pores.

For a more detailed understanding of the process of formation of the walls of nanotubes, at the first stage of synthesis, when the formation of the first crystallites occurs as a result of the

restoration of metal ions, we consider the first six minutes corresponding to the rise and fall of the current in the chronoamperogram.

Figure 13 shows a typical chronoamperogram of the process of formation of Ni nanotubes. Applied potentials difference was 1.75 V. The chronoamperogram is divided into 6 stages, which correspond to 1 minute of deposition.

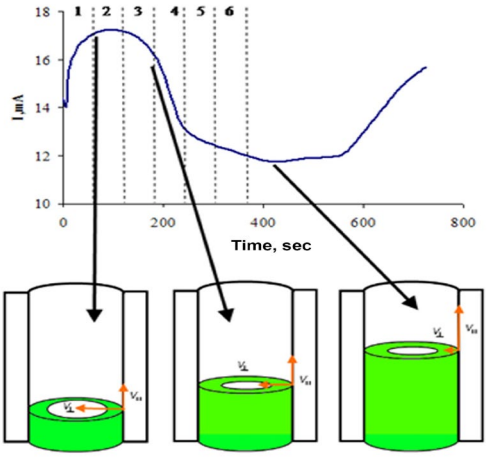

Figure 13. Chronoamperogram stages of the formation of Ni nanotubes walls in template pores

The sharp increase in current in the first seconds of the deposition process is due to the processes of charge separation motion in the electrolyte solution under applied potentials difference, as well as the formation of a liquid gap from the electrolyte formed as a result of the penetration of the electrolyte solution into the pores and subsequent contact with the copper plate used as the cathode. A small plateau characteristic of 2-3 minutes of deposition is the most important stage in the formation of nanotube walls. Due to the good hydrophilicity of the polymer matrix used as a template, the electrolyte solution can penetrate into the pores unhindered. In this case, as a result of applying the potential difference, the induced ionization and subsequent reduction of ions to a metal deposit near the cathode surface leads to a partial depletion of the electrolyte solution and, thereby, creating a gradient of metal ions. The reduction of metal ions to a metal precipitate in our case occurs near the gold ring at the pore edge with greater intensity than in the rest of the volume, as a result of which a stable metal ring is formed from reduced nickel.

Our proposed hypothesis for the mechanism of nanotube growth is following. The growth of nanotubes walls is governed by two growth rates - $V_{\perp}$ is the transverse velocity of the formation of the tube walls in thickness, $V_{\parallel}$ is the longitudinal velocity of the formation of the

tube walls in height. At the first stage, corresponding to 1-3 minutes of wall formation, $V_{\perp}$ prevails, resulting in the formation of a ring of a certain thickness, which can vary from the applied potentials difference, as well as the electrolyte solution and ion mobility. In this case, the rate of reduction of ions to a metal precipitate in the case of depletion of the electrolyte solution decreases sharply, while each subsequent formed nanotube layer is, in fact, a cathode surface on which further restoration of the metal precipitate and grain enlargement take place. At this stage, the alignment of the velocity values and the subsequent predominance of the longitudinal growth rate $V_{\parallel}$ are observed. The hypothesis is confirmed by detailed SEM images of the minute stage of formation of the walls of nanotubes represented in Figure 14 [134].

The predominance of the longitudinal growth rate at the second stage of growth is due to the fact that in the filled pore volume, where the nanotube wall has already formed, the concentration of metal ions decreases, thereby creating a gradient of the difference in the concentration of ions in the pore, with the predominance of the concentration of metal ions in the place where the nanotube has not yet formed. As a result, the growth is more intense near the top end of the growing nanotube, where the concentration of ions is higher. This leads to the predominance of the longitudinal component of the nanotube growth rate and predominant nanotubes growth in height.

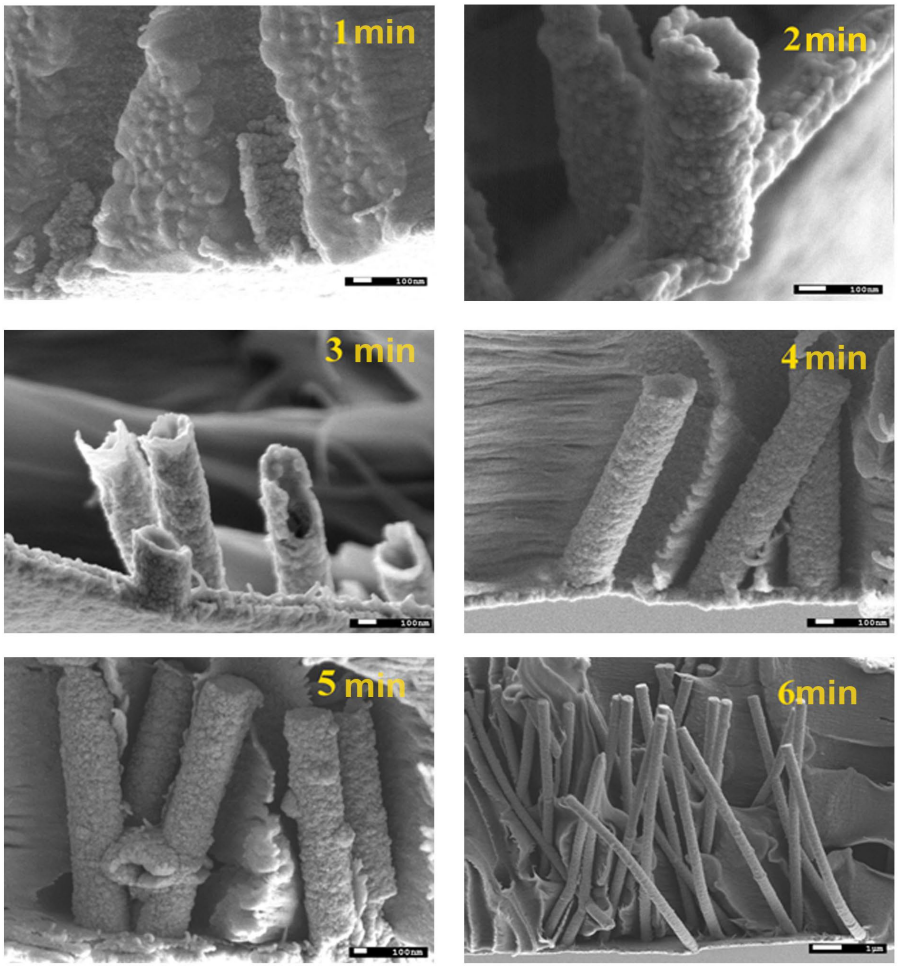

Figure 14. Formation of the walls of Ni nanotubes obtained using SEM

As can be seen from Figure 14, in the first minutes of deposition the formation of thin walls located near the gold contact adjacent to the surface of the copper plate-cathode is observed. The formed metal precipitate has a conical shape with a denser base. An increasing in the deposition time increase the wall thickness and length of the formed metal precipitate, while the taper remains until the height of the formed nanotubes exceeds 3-4 microns. Further growth of nanotubes occurs evenly, without a visible increase in wall thickness.

Figure 15 shows graphs of changes in the dimensional characteristics (wall thickness and height) of Ni nanotubes depending on the deposition time.

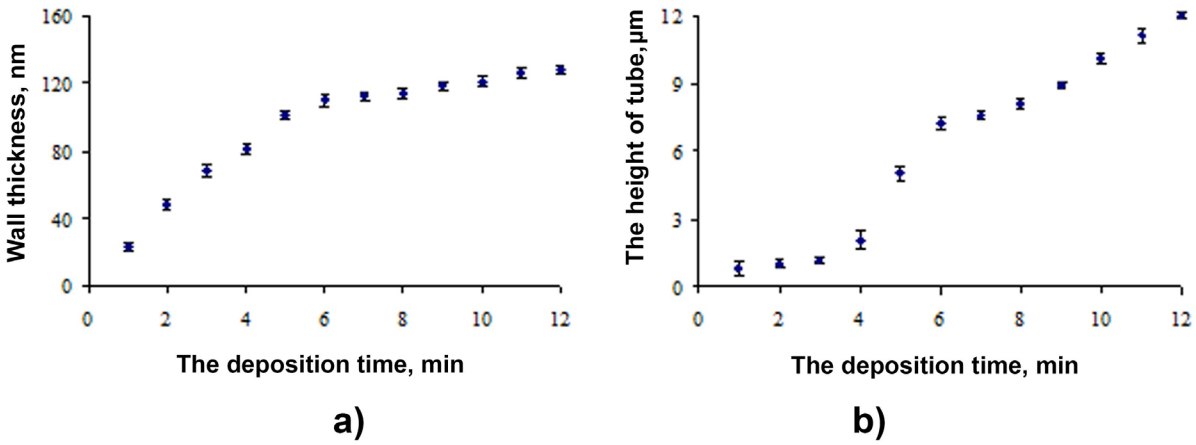

Figure 15. Graphs of changes in the dimensional characteristics a) dependence of changes in wall thickness during deposition; b) dependence of the height of the tube during deposition

Figure 15a shows that the change in the wall thickness of nanotubes in the synthesis process consists of two stages. Range of time 0-4 minutes shows the first stage, at this stage a sharp increase in wall thickness occurs, which can be explained by the process of nucleation of nanoparticles from an electrolyte solution near gold contacts, resulting in a depletion of the electrolyte solution in this area. It makes decreasing in the current on the chronoamperogram. Moreover, according to the graph of the dependence of the change in the tube height during the synthesis process shown in Figure 15b, the tube growth in height at this stage is minimal. We can make an assumption that at this stage there is a three-dimensional growth of tubes in the pores of the matrix, as a result of which a cathode surface is formed for further tube growth. With an increase in the deposition time, depletion of the electrolyte solution is observed in this area. It makes decreasing in the growth of thickness of nanotubes walls. The second stage shows increasing in the height of the tube, while the wall thickness is practically unchanged. Two-dimensional growth of the tubes occurs along the walls of the pores, which is typical for an approximately constant value of the current density on the chronoamperogram.

One of the important characteristics of nanotubes obtained by electrochemical synthesis is their structural and crystallographic parameters, which characterize the degree of perfection of the crystal structure, phase composition, crystal lattice parameters and also the degree of texturing or grain orientation. The most interesting is the dynamics of these parameters at the initial stages of nanotube growth, since they determine the degree of perfection of the resulting nanostructures and their entire subsequent evolution. Figure 16 shows dynamical changing in the XRD patterns of the studied nanotubes during deposition process [134].

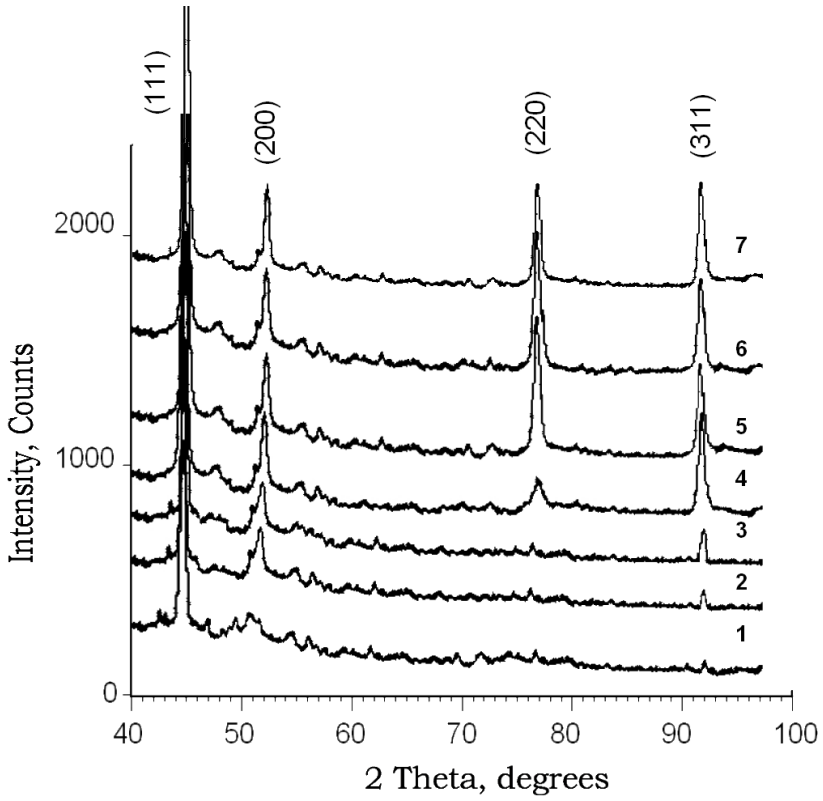

Figure 16. XRD patterns of Ni nanotubes at different stages of growth 1) 1 minute of growth; 2) 2 minutes of growth; 3) 3 minutes of growth; 4) 4 minutes of growth; 5) 5 minutes of growth; 6) 6 minutes of growth; 7) 12 minutes of growth

The general appearance of XRD patterns indicates that the obtained nanotubes are polycrystalline objects with a pronounced dynamics of changes in structural ordering, as well as changes in the degree of texturing and grain orientation during the formation of nanotubes. In this case, the position of the X-ray reflections shows the lack of any oxide compounds in the structure of the nanotubes, and all the observed reflections are characteristic of the face-centered nickel phase. Data presented on the diffractograms show, that in the first minutes of synthesis (1-2 minutes), there are low-intensity peaks with Miller indices (111) and (200), with a clear predominance of the peak (111), which indicates the predominant growth of crystallites in this direction by initial stages of growth. In this case, a strong broadening of the (111) and (200) reflections shows the presence of microdistortions in the nanotube at the initial stages of growth, as well as small crystallite sizes. The size of crystallite does not exceed 5-10 nm. When deposition time increases, according to the X-ray diffraction data, an increasing in the intensity and narrowing of the peaks (111) and (200), as well as the appearance of additional peaks with Miller indices (220) and (311) can be observed. This fact indicates the appearance of a crystalline texture in the samples. Moreover, the narrowing of the peaks and decreasing in the

asymmetry of the diffraction peaks indicate an increase in the degree of structural ordering in nanotubes as they grow in the pores of the template matrices. A further increase in the growth time, according to the obtained diffraction patterns, makes the formation of crystallites in nanotubes with various texture orientations. This formation is typical for polycrystalline objects. The degree of texturing was estimated using the method of determining texture coefficients according to Harris formula (4.1):

$$TC_{hkl} = \frac{I_{hkl}}{I_{0hkl}} \Big/ \frac{1}{n} \sum \frac{I_{hkl}}{I_{0hkl}} \qquad (4.1)$$

where I_{hkl} is the experimentally obtained intensity of the reflex, I_{0hkl} is the corresponding intensity according to the JCPDS base, n is the number of reflexes. Table 3 shows the calculation results.

Table 3. Texture coefficient data

$2\theta^o$	(hkl)	TC(hkl)						
		1 minute	2 minutes	3 minutes	4 minutes	5 minutes	6 minutes	12 minutes
44.505	(111)	0.9415	1.4131	1.4721	1.4874	1.5140	1.5211	1.5231
51.844	(200)	-	0.3341	0.5231	0.6427	0.9983	1.1562	1.1621
76.366	(220)	-	-	-	0.3532	0.4351	0.7531	0.7536
92.939	(311)	-	0.1214	0.2313	0.5224	0.5854	0.6531	0.6541

Texture coefficients *TC* greater than unity indicate the preferred orientation of crystallites in nanotubes along the corresponding directions. The calculated TC_{hkl} values confirm the assumption about the polycrystalline structure of Ni nanotubes with a dominant [111] direction at the initial stages of growth, as well as a large variation in texture orientations with increasing nanostructure growth time and also the lack of a pronounced texture in nanotubes at the final stage of formation. Such a dynamics of texture changes may be due to the fact that at the initial stage, when the growth of nanotubes occurs due to the formation of small crystallites, near the golden ring, all the formed crystallites have a preferential orientation due to the small contribution of the tube growth to height. In the case when the longitudinal and transverse

growth rates become equal, the formed grains begin to occupy the most favorable position for them in the structure, thereby forming different texture orientations. There are known cases when the orientation of grains and the changes in the degree of texturing for magnetic nanostructures are controlled by applying an external magnetic field during synthesis or by changing the pH of an electrolyte solution, thereby significantly affecting not only the texture but also the growth rate [135-137]. In contrast to the studies cited above, in this experiment, the influence of external factors was excluded, in order to avoid additional factors affecting the formation of nanotubes.

Table 4 presents the calculated data on changes in crystallographic parameters obtained by the analysis of XRD patterns. The calculation of the crystal lattice parameter was made using the Nelson — Taylor extrapolation function (4.2):

$$a = f\left[\frac{1}{2}\left(\frac{\cos^2\theta}{\sin\theta} + \frac{\cos\theta}{\theta}\right)\right], \qquad (4.2)$$

The value and the error in determining the parameter *a* are determined by linear extrapolation of this function to the zero value of the argument (θ = 90°). The references value is estimated using international ICDD PDF-2 database (03-065-2865 Ni Cubic Fm-3m (2 2 5)) a=3.52400 Å.
The dislocation density (δ) contains information on the improvement of the crystal structure and is calculated according to formula (4.3).

$$\delta = \frac{1}{L^2} \qquad (4.3)$$

where L is the crystallite size. The average crystallite size according to the Scherrer equation (4.4):

$$\tau = \frac{k\lambda}{\beta\cos\theta}, \qquad (4.4)$$

where k = 0,9 is the dimensionless particle shape coefficient (Scherer constant), λ=1,54Å is the X-ray wavelength, β is FWHM, θ is the diffraction angle (Bragg angle).

Table 4. The calculated data on changes in crystallographic parameters obtained by the analysis of XRD patterns

Time of fabrication	Crystal lattice parameter , Å	The average crystallite size, nm	Dislocation density, δ (m^{-2}) * 10^{15}
1 minute	3,5243±0,0011	9,3±0,7	11,51
2 minutes	3,5240±0,0057	10,2±0,9	9,61
3 minutes	3,5210±0,0020	12,2±0,8	6,71
4 minutes	3,5192±0,0008	14,5±1,2	4,72
5 minutes	3,5141±0,0023	17,1±1,0	3,41
6 minutes	3,5131±0,0011	21,9±1,2	2,11
12 minutes	3,5121±0,0021	23,1±1,5	1,87

Data presented in Table 4 show, that increasing in the time of fabrication leads to increasing in the average crystallite size. This fact is associated with the nucleation of nanoparticles, from which the tube wall is formed. However, after the longitudinal component of the growth rate begins to prevail during the growth process, the average crystallite size remains practically unchanged. The increasing in the crystallite size makes decreasing in the dislocation density. This fact indicates the ordering of the crystal structure of the tube during synthesis. Figure 17 shows the data on the changes in the degree of structural ordering of Ni nanotubes obtained by analyzing the shape and intensity of diffraction reflections by approximating diffraction patterns using pseudo-Voigt functions.

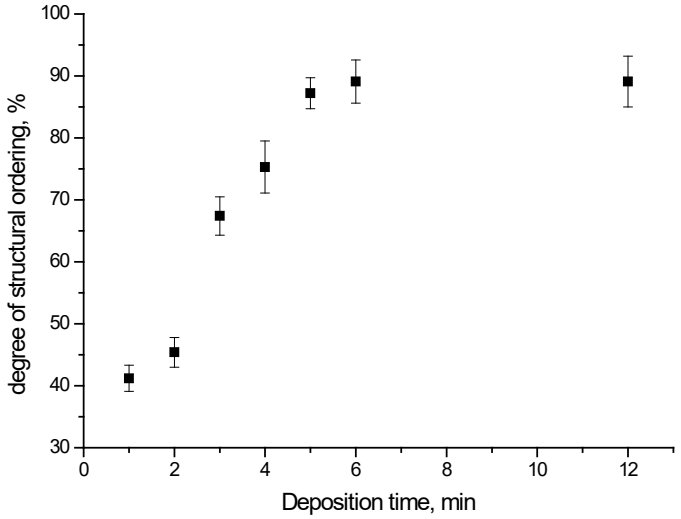

Figure 17. Changes with deposition time in the degree of structural ordering of Ni nanotubes during deposition process.

Presented data show that increase in the deposition time above 3 minutes makes a sharp increase in structural ordering and the perfection of the crystal structure due to a decrease in the density of dislocations and the concentration of defects in nanotubes. When the longitudinal growth rate begins to prevail during the formation of nanotubes, the degree of perfection of the nanotubes remains almost unchanged.

Thus, based on the obtained time dependences of the processes of fabrication of Ni nanotubes, a model of controlled growth of nanotubes was proposed, and the initial stages of the formation of nanotubes were considered in detail by changing the ratio of the contributions of the longitudinal and transverse growth rates.

Notes.

- The main results of this section were published in [134].
- The proposed growth model of Ni nanotubes and also data XRD analysis, was used later by a team of coauthors to describe the mechanisms of formation of nanostructures, as well as their practical application, a detailed description of which is presented in the monograph section [138]. The XRD patterns and the data of scanning electron microscopy, were obtained jointly with the co-leader A.L. Kozlovsky, as well as the employees of BelNAN for material science A.E. Shumskaya, E.Y. Kanyukov.

4.2. Effect of synthesis conditions on the structural properties and degree of texturing of Ni nanotubes

According to the proposed model of the formation of Ni walls of nanotubes, at the initial stage of crystallization of nuclei and their subsequent growth, an important role is due to the magnitude of concentration of ions in the electrolyte solution near the cathode surface, as well as the mobility of the ions in the solution. One of the important factors that can have a significant effect on the mobility of ions in a solution is the temperature of the electrolyte and the difference in applied potentials. Their influence is as follows.

Changing the temperature of the electrolyte solution makes the ions more mobile, which allows them to quickly move through the volume. However, an increase in the temperature of the electrolyte solution can be accompanied by negative factors due to the appearance of a large number of gaseous bubbles of oxygen and hydrogen, which arise as a result of dissociation of water, which leads to t boiling of the electrolyte solution. Formed oxygen and hydrogen bubbles rush to the surface and can passivate the anode. Also, part of the formed gas bubbles in the pores of the template matrix can lead to clogging and the effect of anisotropic growth of nanotubes in the pores.

Changing the difference in applied potentials also has its pros and cons. The positive aspects of the increasedpotentials difference can be attributed to the fact that when crossing the threshold associated with the values of the potentials of metal recovery from an electrolyte solution, the rate of formation of a metal precipitate increases sharply. A change in the growth rate have considerable effect on the degree of texturing and orientation of crystallites in nanotubes. However, these processes with large potential differences are reason of severe structural distortions and deformations of the nanotube due to the appearance of regions with a high degree of overstrain in the structure and also the appearance of hydrogen inclusions in the nodes and interstices of the crystal lattice.

Based on the foregoing, this section presents the study of Ni nanotubes synthesis at different applied potentials in the range 1.25 V to 2.0 V (the step was 0.25 V) and different temperature of the electrolyte solution 25°C, 35°C and 50°C. The limitation in applied potentials at 2.0 V is based on the results of our preliminary experiments, which showed that an increase in the potential difference above 2.0 V leads to a sharp increase in the growth rate, which leads to an uncontrolled process of tube formation with a low degree of structural ordering. The limitation on the maximum temperature of the electrolyte at 50°C is also based on experimental data related to the effect of the rapid evolution of hydrogen gas and oxygen leading

to passivation of the anode and the appearance of strong anisotropy along the height of the synthesized nanotubes in the template.

Formation of Ni nanotubes, as well as determination of growth rate of nanotubes, was monitored by analyzing chronoamperograms of the deposition process. Figure 18 shows the experimental curves *I(t)* of the process of deposition of nanotubes into the pores of template matrices with varying electrolyte temperatures and applied deposition potential differences

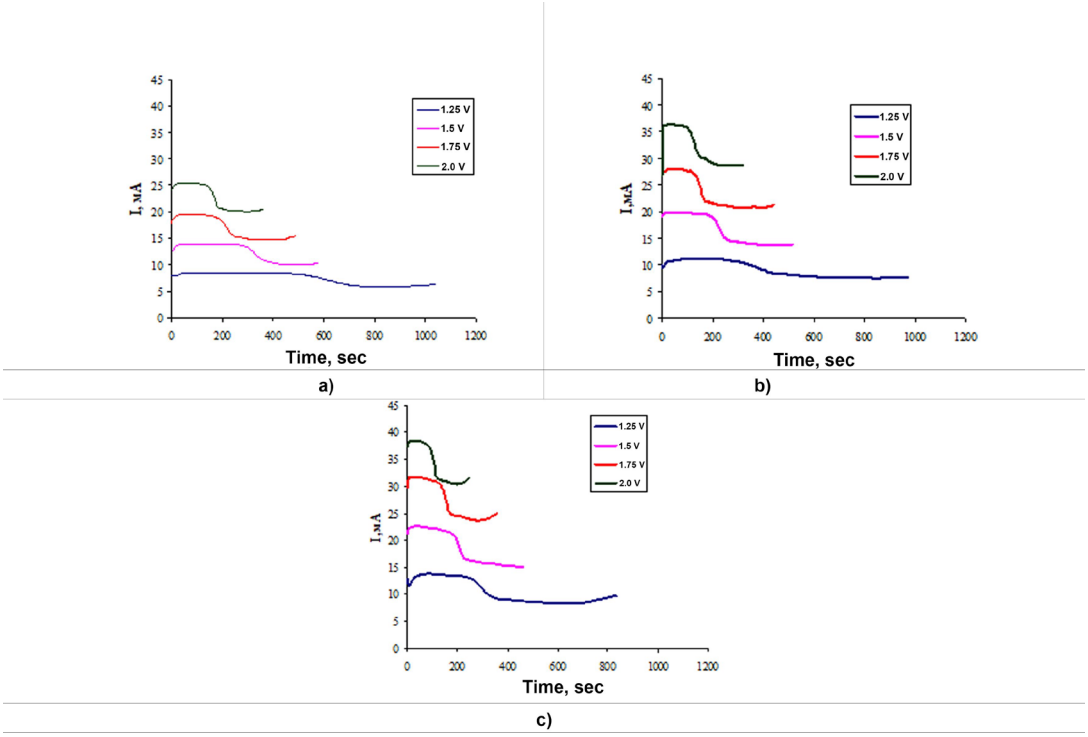

Figure 18. Chronoamperograms of the deposition process at electrolyte temperatures a) 25ºC; b) 35ºC; c) 50ºC

According to the presented data, all of the obtained chronoamperograms has a qualitatively identical appearance, consisting as shown earlier of 3 main stages of growth: the stage of initialization of the synthesis and ionization of ions in solution, the stage of nucleation, the stage of two-dimensional growth of nanotubes inside the pores of the template matrix.

Presented data show, that an increase in the applied potentials difference and also in temperature of the electrolyte solution, makes significant changes in the time intervals of the initial stages of growth, which indicates that a change in the deposition conditions leads to a change in the ratio of the longitudinal and transverse growth rates. Also, an increase in the potential difference leads to a more significant increase in the current density at the initial stage of nucleation, which indicates changes in the mobility rate of ions in solution and also an increase in the concentration of ions near the cathode. It should be noted that increasing in the temperature of the electrolyte also makes increasing in current density. However, it is not so

pronounced as with an increasing in the potential difference. Analyzing the time dependences of the change in the current strength, it was noted that with an increase in the applied potentials difference, as well as with the temperature of the electrolyte solution, it leads to a decrease in the time of the nucleation stage and, consequently, to a decrease in the wall thickness. In the case of the large applied potentials differences, the longitudinal growth rate at the initial stage of crystallite nucleation begins to prevail, as a result of which the growth of nanotubes in height occurs much faster. In this case, it is worth noting for anomalously large times the nucleation stage with an applied potentials difference of 1.25 V, which in some cases make up more than half of the total deposition time. This abnormal behavior can be explained by the fact that, for a given applied potential difference of 1.25 V, the ionization rate is quite low due to a slight excess of the applied potential difference over the value of the electrode reduction potential of $Ni^{2+} + 2e^- \rightarrow Ni^0$ (0.25 – 1.0 V), resulting in the nucleation process is much slower than with large potential differences. In such situation, the wall thickness of the nanotubes is quite large, and the geometry of the nanostructures is close to a wire with a very small inner diameter or its complete absence.

With increasing current density due to an increase in the potential difference on the electrodes during the growth of nanostructures, adsorption of hydrogen impurities, salt anions, and hydroxides is observed, some of which precipitate on the surface of the template matrix, but some of the precipitate formed can be included in the crystal structure of pores of nanotubes. Thus, the effect of the applied potentials difference on the formation of impurity deposits on the surface of template matrices during electrochemical deposition, which has a negative effect on the growth of nanostructures, was shown in [139]. In this case, impurities entering the crystal structure of nanotubes can have a large deformation effect on the construction of the crystal structure. The resulting impurities on the surface of the template matrix block the movement of metal ions, and thereby passivate the cathode. Since, during electrochemical deposition, metal ions are brought along normal to the cathode surface, blocking the growth sites can change the movement of ions to the cathode and reduce the growth rate. Such a deposit localizes (blocks) the growth of nuclei on the pore walls, creates an additional dielectric layer between the cathode and the nucleus, thereby slowing the growth of the walls of nanotubes, and making their structure porous and brittle. At lower current densities, such particles have time to move away from the pore surface; moreover, the nanostructures are more uniform, however, due to an increase in the influence of ion migration, the wall thickness increases, up to overgrowing (formation of nanowires) [139].

Based on the obtained chronoamperograms, volumetric deposition rates were calculated for various temperatures and deposition potentials (Figure 19).

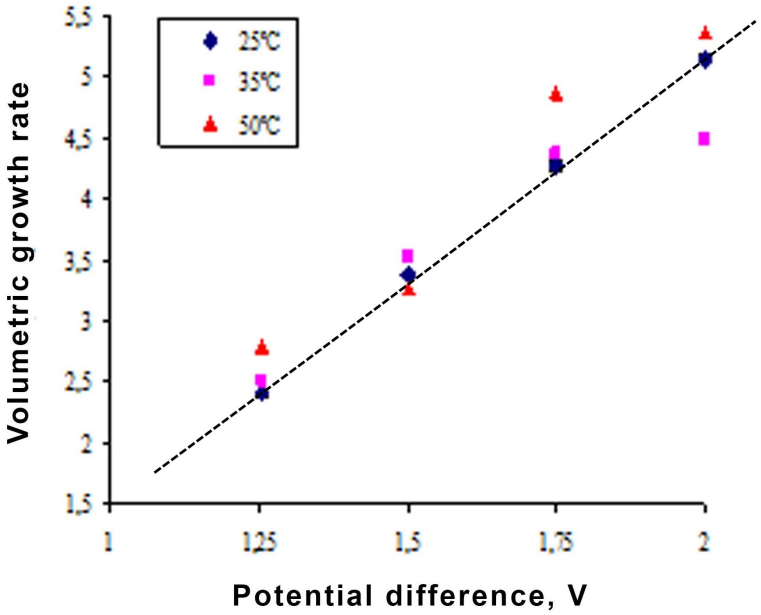

Figure 19. The dependence of the volumetric growth rate on the applied potential difference and solution temperature.

As can be seen from the graph, the volumetric deposition rate is directly proportional to the change in the applied voltage, but they have more complex temperature dependence. It should be noted that at room temperature, that increasing in the potential difference leads to linearly deposition rate increasing, however, with increasing temperature, an ever greater deviation from this dependence is observed. The deviation from linearity can be explained by the fact that at high temperatures the rate of ion formation during the decay of molecules increases, there is a fast generation of hydrogen leading to the electrodes passivation.

The geometrical characteristics and sizes of nanotubes were determined using scanning electron microscopy and manometric determination of gas permeability. Typical SEM images of nanotubes are shown in Figure 20.

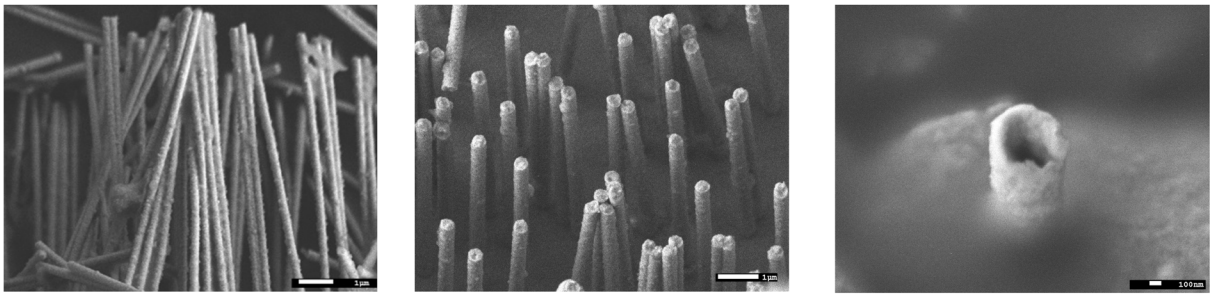

Figure 20. SEM images of Ni nanotubes obtained at 1.75 V and a temperature of 25°C

Presented micrographs show that the nanotubes are isotropic and cylindrical, with a length of 12 μm and an external diameter of 400±10 nm, which corresponds to the pore sizes of the initial template matrix. Studying the pore diameters and the inner diameters of the nanotube templates in the PETF was made by the manometric method for determining gas permeability, based on measuring the change in gas pressure in a closed chamber at a pressure in the range from 8 to 20 kPa with a step of 4 kPa.

The determination of the diameters d of the pores of the template matrices and the inner diameters of NTs located in the PET templates was carried out by the manometric method for determining gas permeability. This method is based on measuring the molar air flow density Q depending on the pressure difference Δp in a closed chamber on both sides of the template, which varied in the range from 0.008 to 0.020 MPa with a step of 0.004 MPa. The analyzed gas, passing through the reducer, enters the feed chamber of the cell. The sample gas flow is regulated by the system; the pressure is measured using a manometer. The cell has a drainage substrate made of a porous neutral material capable of withstanding a pressure drop of up to 0.3 MPa without deformation. A template matrix fixed on a drainage substrate divides the cell into two chambers: a feed chamber and a leakage chamber. A pressure of 0.008 to 0.02 MPa is created in the feed chamber, while in the leakage chamber it is 0.1 to 1 Pa. Penetrating through the template matrix, the gas enters the differential mercury manometer.

According to the readings of the manometer, the pore diameter of the template matrix is calculated. The values of the diameters d were determined in accordance with Fick's law from the ratio:

$$Q = \frac{nd^3}{6l}\sqrt{\frac{2\pi}{RTM}}\Delta p$$

where l – template thickness (nanotube length), R – universal gas constant, M – molar air mass, n – surface pore density (fluence of irradiation of PET films during process of obtaining a template), T – temperature.

The obtained results of changing the nanotube diameters using the gas permeability method are in good agreement with the data of SEM images. Both methods provide good accuracy of ~5%.

Based on the obtained calculation data for the internal pore diameter, a changes in wall thickness from various deposition conditions was constructed (Figure 21) [140]. Figure 21 data was obtained by comparing and incorporating results of both methods.

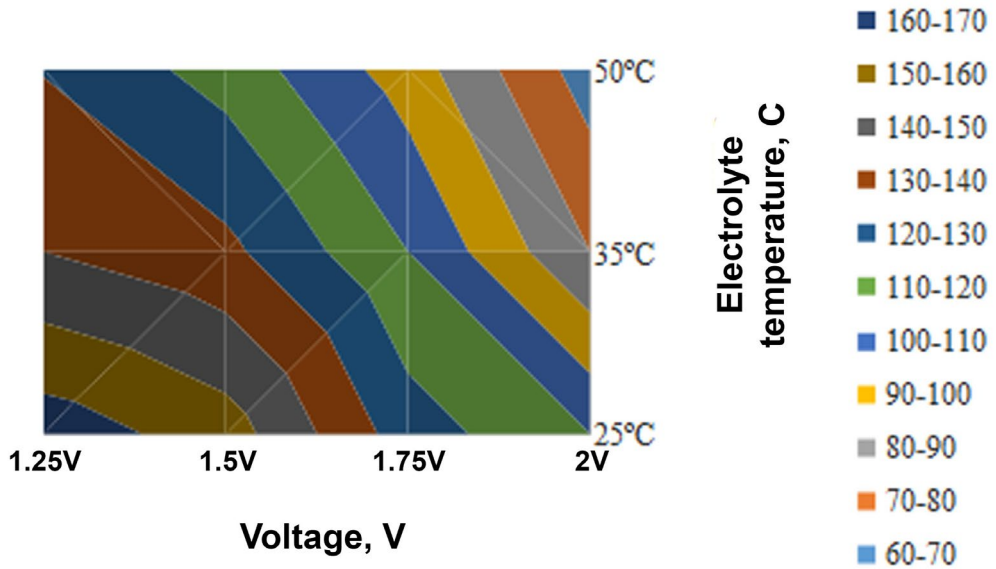

Figure 21. Diagram of changes in wall thickness from various deposition conditions [140, 141]

Presented data in Figure 21 show, that an increase in the difference between the applied potentials and the temperature of the electrolyte solution, a decrease in the wall thickness is observed, which confirms the proposed model of Ni nanotubes growth.

To determine the influence of deposition conditions on the crystal structure, an XRD analysis of the obtained samples was carried out under various synthesis conditions. Since the studied samples during the analysis were in the polymer matrix, a wide halo peak with an angular peak of $2\theta = 20 - 35^{o}$ and a small peak of $2\theta = 52 - 55^{o}$ corresponding to the matrix are observed in the diffractogram. In this case, all diffraction patterns had low-intensity peaks, which are characteristic of diffraction by nanoscale objects (Figure 22a-c). The broadening of the peaks indicates the polycrystalline structure of Ni nanotubes.

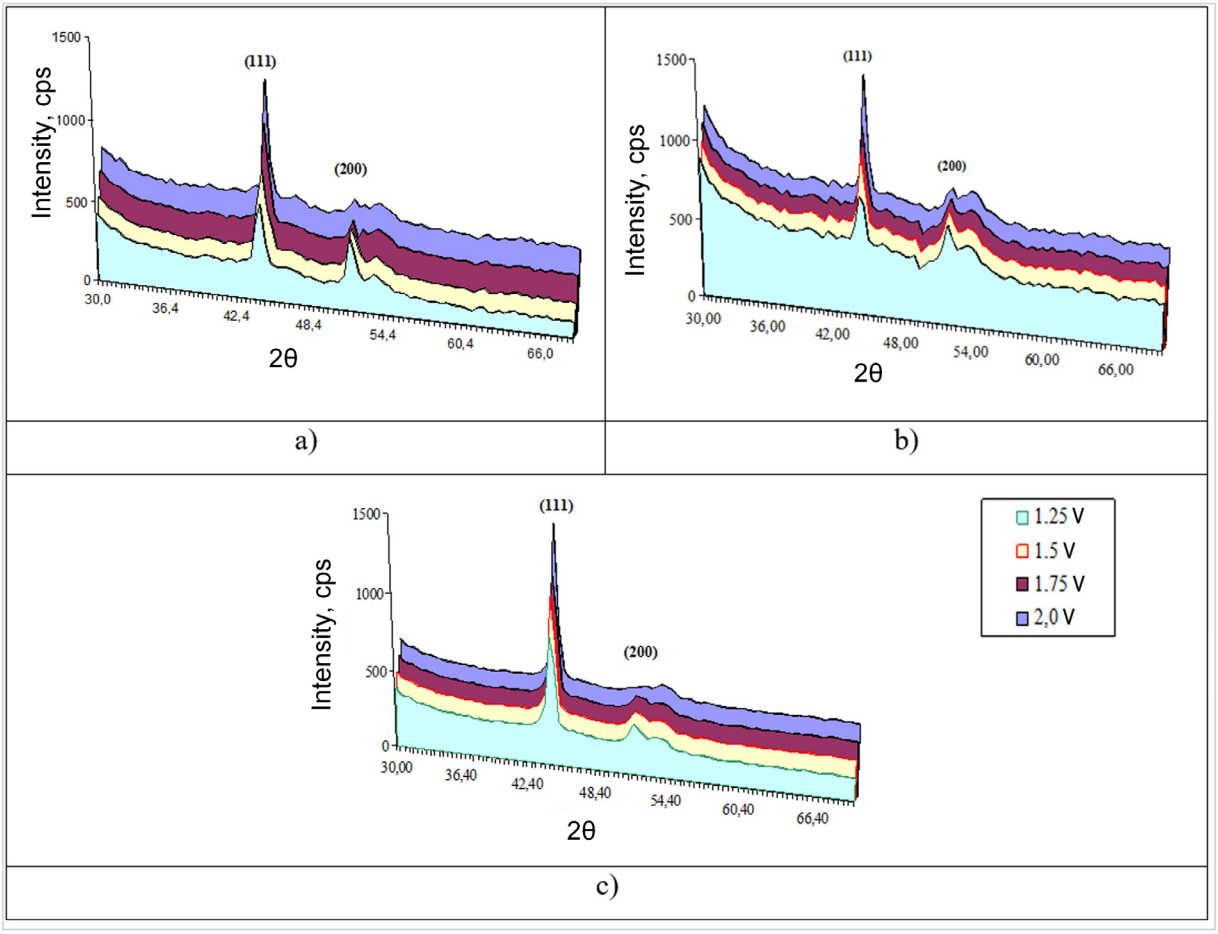

Figure 22. XRD patterns of Ni nanotubes a) 25ºC; b) 35ºC; c) 50ºC [140, 141]

Analysis of the diffraction patterns showed that the obtained Ni nanotubes possess an fcc phase with crystal lattice parameters that depend on deposition parameters. Moreover, with an increase in the potential difference during the synthesis, corresponding Ni nanotubes XRD pattern shows an increase in the peak intensity with Miller indices (111) and a decrease in the peak intensity (200), which indicates the increased prevalence of the [111] oriented grains in the crystal structure of the obtained nanotubes.

Values of texture coefficients (calculated using equation of Harris) larger than 1 indicate predominance of the grains with corresponding crystallographic orientation along the nanotubes.

Table 5 shows the calculated results.

Table 5. The calculated texture coefficients for [111] and [200] directions for different samples obtained at different temperatures and applied voltage.

2θº	(hkl)	TC(hkl)											
		25ºC				35ºC				50ºC			
		1.25B	1.5B	1.75B	2.0B	1.25B	1.5B	1.75B	2.0B	1.25B	1.5B	1.75B	2.0B
44.559	(111)	1.3415	1.4762	1.5741	1.7831	1.3541	1.5413	1.6107	1.8741	1.4531	1.5731	1.7762	1.9102
51.930	(200)	0.9714	0.8224	0.6741	0.5421	0.8702	0.7055	0.5467	0.4531	0.5431	0.4211	0.3513	0.2365

The average crystallite size (Figure 23b) was calculated according to the Scherrer equation. An analysis of the data obtained showed that with an increase in the potential difference and the temperature of the electrolyte, an increase in the average crystallite size occurs. The (111) interplanar spacings for the obtained samples at different potential differences are shown in Figure 23c.

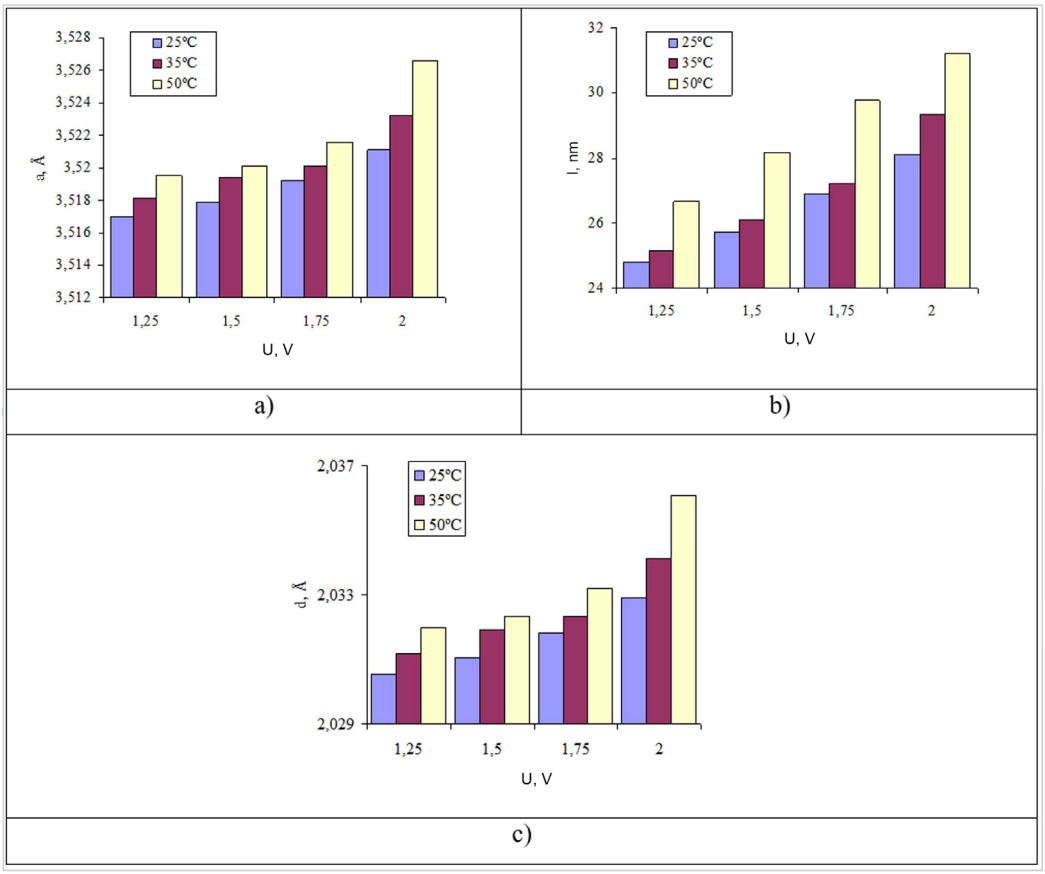

Figure 23. Effect of potential difference on a) the unit cell parameter; b) the average crystallite size; c) the (111) interplanar distance

The obtained data show that an increase in the potential difference leads to an increase in the unit cell parameter and the interplanar distance and, consequently, the degree of microstresses in the structure of nanotubes. As a result, an increase in the potential difference and the electrolyte temperature leads to an increase in the number of defects in the crystal structure of nanotubes, due to an increase in the average crystallite size and the degree of microstresses. However, with the increase in potential difference, a predominance of the texture direction [111] in the structure of nanotubes is observed.

Thus, by changing the crystal structure of Ni nanotubes and the conditions of electrochemical deposition, one can obtain ordered arrays of nanotubes with desired properties.

Notes.

- The main results of this section were published in [140].
- Obtaining X-ray diffraction patterns and their analysis was carried out together with the staff of the Laboratory of Solid State Physics AB of INP.
- Obtaining samples under given synthesis conditions was performed personally by the author at the Laboratory of Solid State Physics AB of INP.

4.3. The effect of electrolyte acidity on the structural properties of Ni – nanotubes

This section presents the results of detailed research of the influence of the acidity level of an electrolyte solution on the properties of synthesized nanotubes, as well as the rate of their formation. In the majority of works [141-144] devoted to the electrochemical reduction of metal ions from electrolyte solutions, special attention is paid to the pH level or acidity of the medium, as well as to strict control over its maintenance during the entire deposition process. This is due to the fact that, depending on the acidity of the medium, the rate of ionization of ions and their migration can have large differences, which in the future can lead to heterogeneity of the formation of the walls of nanotubes. Moreover, in the case of nickel electrochemical reduction, as is known from the literature [145-149], when the pH of the solution changes, there are strong changes in the mechanisms of discharge-ionization processes, and also at low pH values, NiOH hydroxide compounds can form in the solution the appearance of which leads to severe distortion of the crystal structure and partial amorphization of nanotubes due to the formation of oxide inclusions.

Consider the influence of synthesis conditions (acidity of an electrolyte solution) on the geometric characteristics of nickel-based NTs. As a result of studying the potentials of various electrode processes, it was found that their values depend on the following three factors: 1) on the nature of the substances involved in the electrode process. 2) on the ratio between the concentrations of these substances and 3) on the temperature of the system. This dependence is expressed by equation (4.5):

$$E = \frac{E^{o} + \frac{2.3RT}{zF}\lg([O_x])}{[Red]} \qquad (4.5)$$

where,

E^{o} - standard electrode potential;

R - gas constant;

T - absolute temperature;

z - the number of electrons involved in the process;

F - Faraday constant;

[O_x] and [Red] - products of concentrations of substances involved in the process in oxidized and reduced forms.

The physical meaning of the value E^o becomes clear when considering the case where all concentrations (activity) of the substances involved in a given electrode process equal to one. Under this condition, the second term of the right part of the equation turns to zero (lg = 0) and the equation takes the form:

$E = E^0$

Concentrations (activity) equal to one are called standard concentrations. Therefore, the potential corresponding to this case is called standard potential. The standard electrode potential is the potential of a given electrode process at concentrations of all substances involved in it equal to one.

Thus, in the equation of the electrode potential, the first term E^o takes into account the influence on its value of the nature of the substances, and the second

$\frac{\frac{2.3RT}{zF}\lg([O_x])}{[Red]}$ - their concentration. In addition, both terms change with temperature.

For normal electrochemical measurements of standard temperature (25 ° C = 298K), when substituting constant values [R = 8.31 J/(mol*K), F = 96 500 C/mol], the equation takes the form (4.6):

$$E = \frac{E^o + \frac{2.3*8.31*298}{z*96500}\lg([O_x])}{[Red]} = \frac{E^o + \frac{0.059RT}{z}\lg([O_x])}{[Red]} \qquad (4.6)$$

Let us consider what form the general equation of the electrode potential takes in the case of nickel. The electrode process is expressed by equation (4.7):

$$Ni^{2+} + 2e = Ni^0 \qquad (4.7)$$

The oxidized form of the metal is nickel ions (Ni^{2+}), and the reduced form is atoms (Ni^0). Therefore,

$[Ox] = [Ni^{2+}]$, a = const, since the concentration of atoms in a metal at a constant temperature is a constant value. Including the value of this constant in the value, we obtain (4.8):

$$E = -0.250 + \frac{0.059}{z} lg[Ni^{2+}] \qquad (4.8)$$

If the redox reaction proceeds with the participation of water and hydrogen ions or hydroxide ions, then the size of the solution medium must also be taken into account. Hydrogen ions in an aqueous solution are oxidizing agents. They can be directly reduced to hydrogen molecules or participate in the reduction of other particles to form water molecules.

In this case, from the Nernst equation it is easy to determine the quantitative effect of pH on the equilibrium potential of the system. Consider, for example, the electrode process (4.9):

$$MnO_4^- + 8H^+ + 5e = Mn^{2+} + 4H_2O \qquad (4.9)$$

This half-reaction occurs when potassium permanganate reacts with most reducing agents in an acidic environment. The concentrations of all substances involved in the electrode process under consideration, except for water, are variables. For this process

$E^0 = 1.507\ V$

The electrode potential equation has the form (4.10-4.11):

$$E = \frac{E^o + \frac{0.059}{5} \lg([MnO_4^-])}{[Mn^{2+}]} + \frac{8 * 0.059}{5} lg[H^+] \qquad (4.10)$$

$$E = 1.507 + \frac{0.012 \lg([MnO_4^-])}{[Mn^{2+}]} - 0.095pH \qquad (4.11)$$

As the above example shows, in the case of electrochemical processes involving hydrogen, the concentration of hydrogen ions is included in the numerator of the logarithmic term of the potential equation. Therefore, the electrode potentials of such processes depend on the medium of the solution and have the greater magnitude the more acidic the solution.

During the electrochemical reduction of nickel, hydrogen ions do not directly participate in the reductive half-reaction at synthesis temperatures of 25°C, as was shown in Section 4.2, but they

affect the state of the oxidized and reduced ions in solution, thereby changing the metal reduction potential from the electrolyte solution.

Figure 24 shows experimental chronoamperograms of the process of deposition of Ni nanotubes obtained at various applied potential differences at a room temperature of 25°C. In this experiment, the influence of the temperature of the electrolyte solution above 25°C was not considered, since at high temperatures of the electrolyte solution the effect of the generated hydrogen will be complex and it is not possible to separate the contribution of pH and temperature in this case.

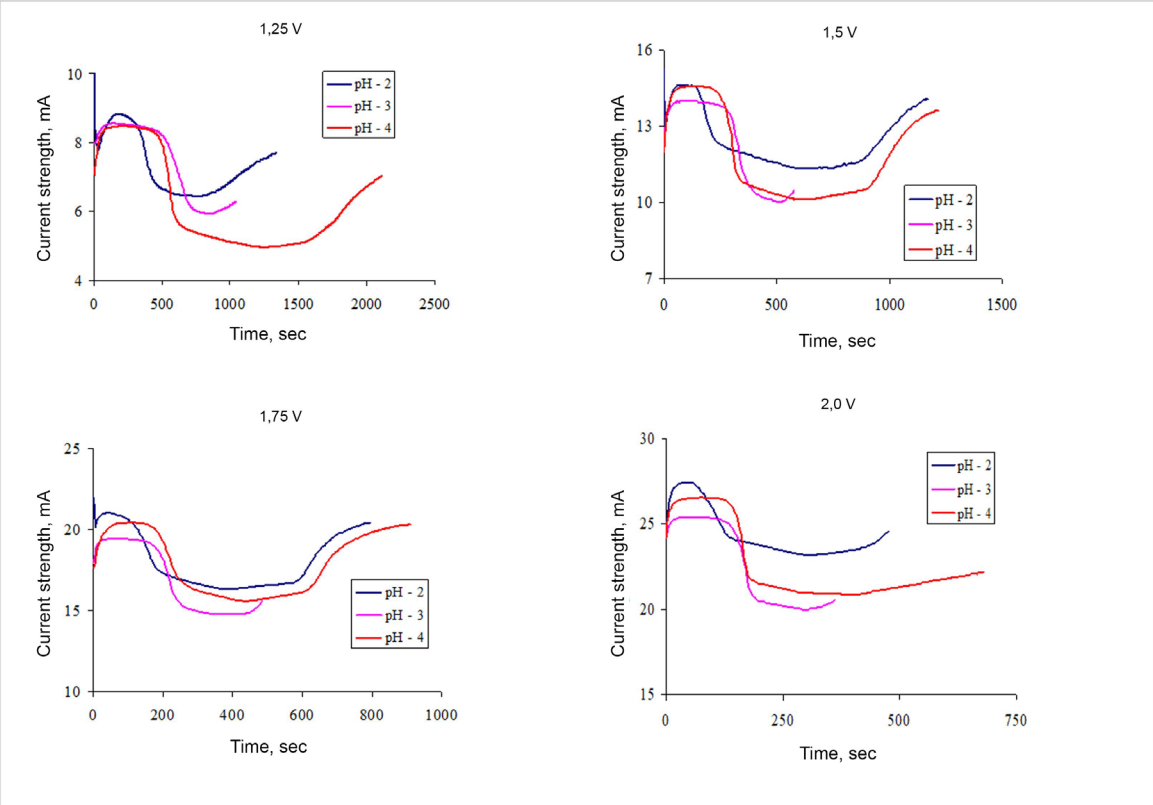

Figure 24. Chronoamperograms of process of deposition of Ni nanotubes

The analysis of the obtained chronoamperograms showed the following: with a change in the degree of acidity, pH to 2 and 4, an increase in current strength is observed at the beginning of the deposition process. Moreover, at pH = 2, a decrease in the time of the nucleation stage is observed, while at pH = 3 and 4, the nucleation time is comparable in magnitude, however, pH = 4, the time of the second stage is two times longer than at pH = 3. Figure 25 shows diagram of changes in the wall thickness of nanotubes depending on the level of acidity:

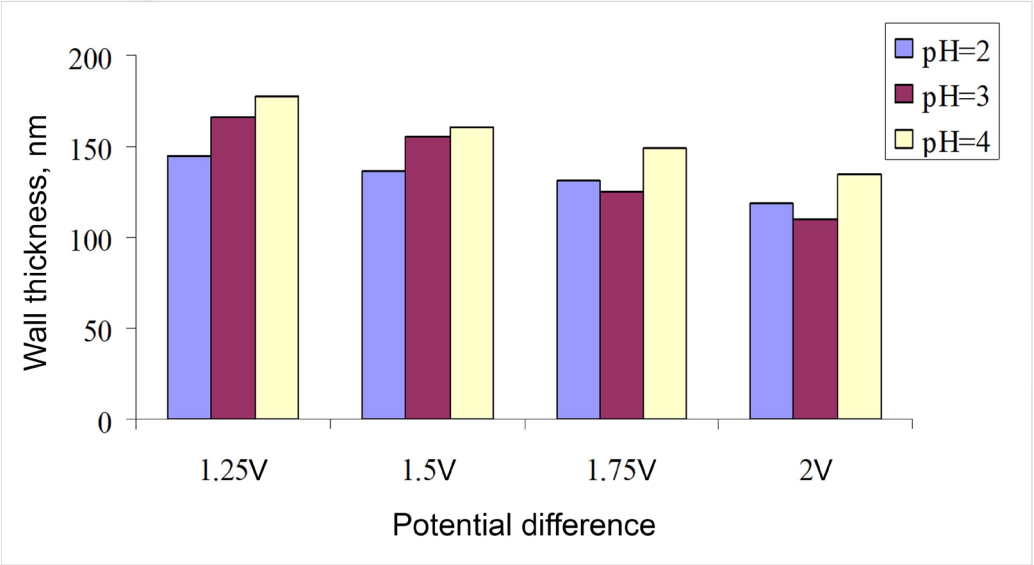

Figure 25. Diagram of changes in wall thickness depending on deposition conditions

As can be seen from the presented diagram, with an increase in the potential difference, a decrease in the wall thickness is observed. The smallest difference in wall thickness at different pH level is observed at a potential difference of 1.75 and 2.0 V, which, as was shown in Section 4.2, is caused by a change in the ratio of the longitudinal and transverse growth rates of nanotubes, due to the predominance of the longitudinal growth rate at large potential differences. However, it can be seen that in the case when the pH of the solution is 3, an increase in the applied potentials difference to a greater decrease in the wall thickness, while at pH=2, changes in the geometry of the nanotubes with an increase in the applied potentials difference are minimal. Decreasing the acidity of the solution to 4 leads to a more intensive decrease in wall thickness at potential differences from 1.25 V to 1.5 V than in the case of a further increase in the applied potentials difference. Moreover, at a given acidity pH=4, the geometry of the nanotubes obtained at a difference in applied potentials of 1.25 V is close to wires without a clearly defined inner diameter.

Consider the effect of boric acid on the formation of nanostructures. Boric acid has long been considered as a buffering agent in the processes of electrochemical synthesis. The presence of boric acid in the electrolyte enhances the deposition of metals, due to its ability to lower the metal reduction potential. In this case, boric acid plays a key role in the electrodeposition of nickel nanotubes by forming a surface bound nickel-borate complex on the pore walls. Figure 26

shows a diagram of the formation of tube walls in tracks of template matrices due to the addition of boric acid to the electrolyte solution.

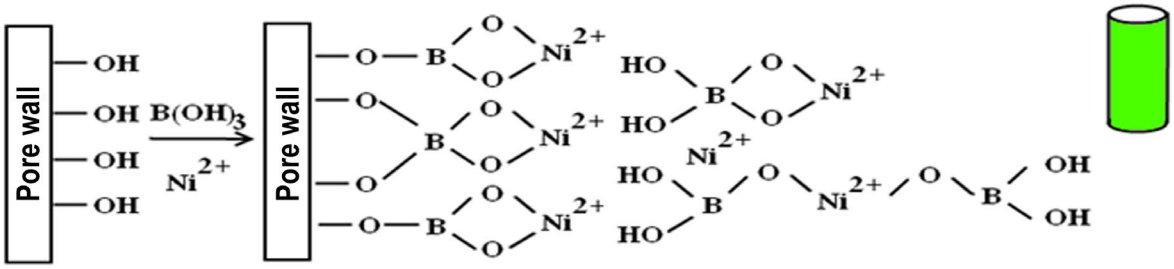

Figure 26. Scheme of the formation of walls of Ni nanotubes

As can be seen from these results, boric acid plays an important role in the growth of nickel nanotubes. Boric acid forms a nickel-borate complex with nickel; it can also easily bind to hydroxyl groups that are on the surface of tracks of PET templates. An increase in the concentration of boric acid leads to small potential differences leading to a predominance of the transverse growth rate of nanostructures for a sufficiently long time, as a result of which nanowires can form, without an inner diameter.

To identify the effect of the potential difference on the elemental composition of the obtained nanostructures, an energy dispersive analysis of the samples was carried out. No oxide compounds were found in the NT structure, which indicates the absence of oxidative and corrosive processes in the process of preparation, sample preparation, and also storage in air. In the energy dispersion spectra with acidity levels 2 and 3, the most intense peaks of the Ni Kα-series (7.474 keV) are observed, while the contribution of the Lα peaks (0.849 keV) is insignificant. However, with an acidity degree of 4, an increase in the contribution of Ni Lα peaks is observed, which may be due to a rearrangement of the crystal structure and the appearance of additional texture axes.

To study changes in the crystal structure of Ni nanotubes as a result of electrochemical deposition at different degrees of acidity of the electrolyte solution and potential difference, an X-ray diffraction analysis was performed. All reflections in the diffraction patterns of the samples under study have low intensities characteristic of diffraction by nanoscale objects. The broadening of the peaks indicates the polycrystalline structure of Ni nanotubes. The most intense reflection observed in the diffractograms corresponds to the [111] peak of the fcc phase of Ni, while the intensity of the peak [200] in the diffractograms is low. As a result of processing the

obtained X-ray diffraction patterns, the unit cell parameters *a* of the studied samples were determined. The processing results are presented in Figure 27.

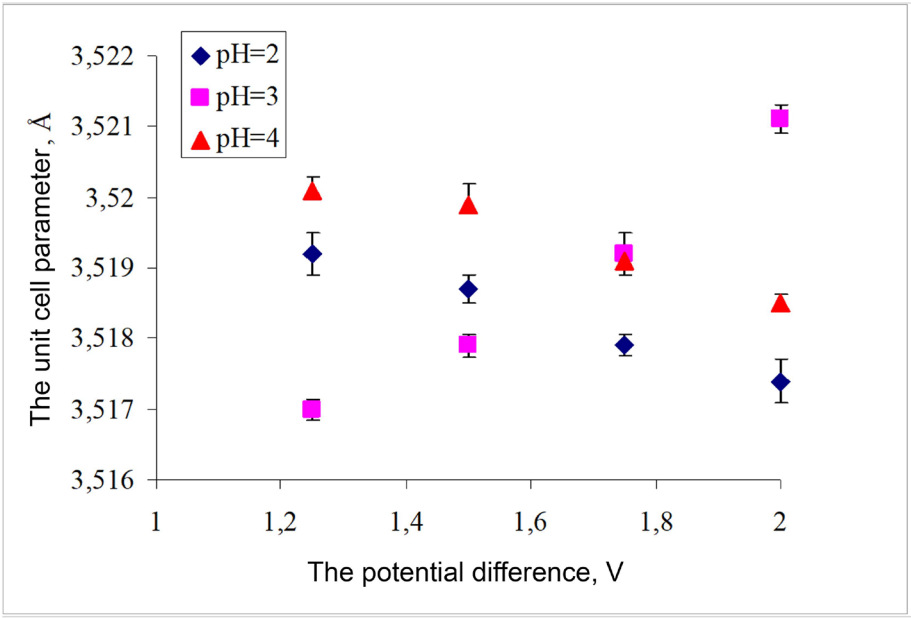

Figure 27. Unit cell parameter dependence on the potential difference at different degrees of acidity of the electrolyte solution during electrochemical deposition

The analysis of the results showed the following: when the degree of acidity of the electrolyte solution is 3, a linear increase in the unit cell parameter is observed, while at the acidity level of the electrolyte solution 2 and 4, a decrease in the unit cell parameter is observed. A change in the unit cell parameter can be associated with the formation of point defects in the crystal structure that can cause distortions in the crystal structure.

Point defects arise mainly during the growth of nanostructures, while point defects are distributed unevenly in volume. Increasing in the potential difference during deposition leads to increasing the rate of formation of the nanotube walls, and diffusion processes in the pores of the template matrices begin to play an important role.

At high deposition potentials which are equal to 1.75 and 2 V, as was shown in Section 4.2, the formation of hydrogen is observed, which is capable of incorporating into the crystalline structure, thereby causing the formation of additional defects in the structure.

Let us consider the effect of defects formed in the crystal structure on the change in the interplanar spacing between atoms characteristic of the (111) diffraction reflex. The calculation results are shown in Figure 28.

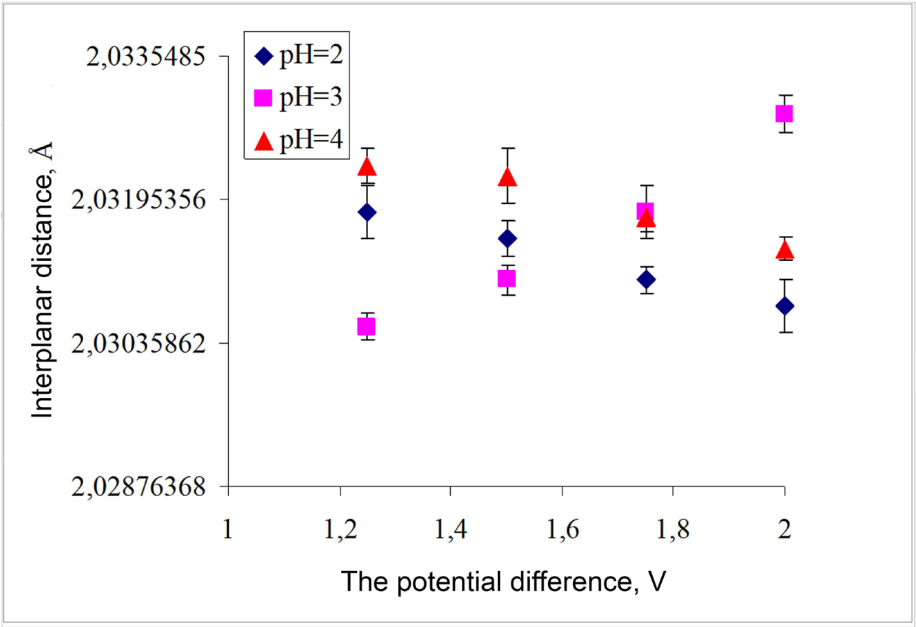

Figure 28. Dependence of interplanar distance on the potential difference at different degrees of acidity of the electrolyte solution

As can be seen from the graph of the dependence of the change in interplanar spacing on the potential difference at an acidity level = 3, an increase in interplanar spacing between atoms is observed, which indicates a change in the crystal structure and confirms the hypothesis that the defects affect the structure. An increase in the potential difference during deposition leads to an increase in the number of defects in the structure. However, a change in the acidity level of electrolyte solution pH=2 and pH=4 leads to a decrease in interplanar spacing, which can be explained by the following fact: a change in the acidity of the solution to 4 leads to an increase in the transverse component of the tube formation rate, which leads to an increase in wall thickness, and the structure becomes more ordered. Also, as a result of a change in the acidity of the solution, a decrease in the effect of the generated hydrogen on the formation of the crystal structure of nanotubes is observed.

Figure 29 shows a graph of the dependence of the change in the average crystallite size, calculated according to the Scherrer equation, on the potential difference at different degrees of acidity of the electrolyte solution during electrochemical deposition.

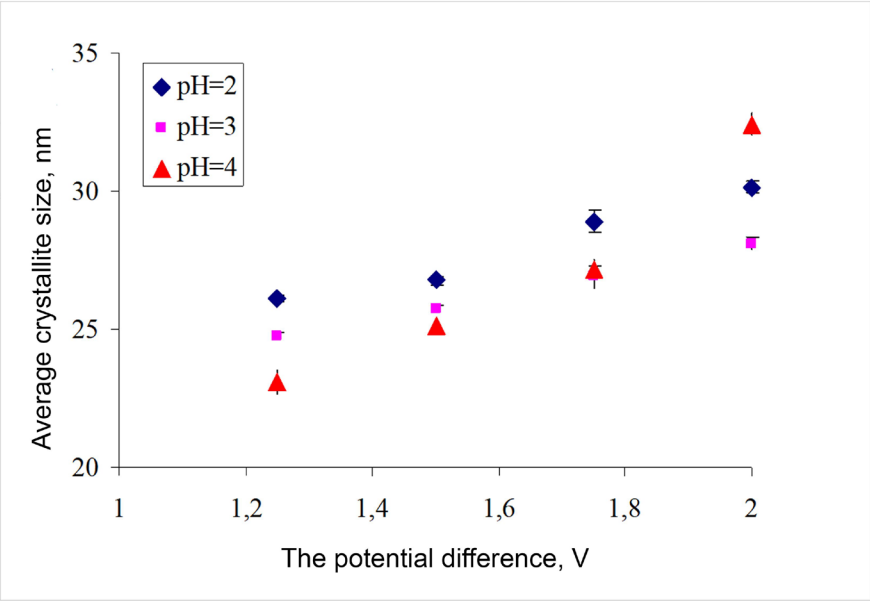

Figure 29. Dependence of change in average crystallite size on the potential difference at different degrees of acidity of electrolyte solution

Graph shows, that increase in the potential difference leads to an increase in the average crystallite size, while at acidity levels 2 and 3, a linear change in size is observed, while at acidity level 4 a deviation from linearity is observed, which is due to a change in the rate of crystallite formation during growth at a large difference in deposition potentials (1.75 V and 2.0 V).

Thus, by changing the acidity level of the solution and the potential difference, it is possible to obtain nickel-based nanotubes with given geometric parameters, crystal structure and wall thickness.

Notes.

- The analysis of structural parameters based on X-ray diffraction patterns and their analysis was carried out jointly with the staff of the Laboratory of Solid State Physics AB of INP.
- Obtaining samples under given synthesis conditions was performed personally by the author at the Laboratory of Solid State Physics AB of INP.
- The analysis of the geometry of the synthesized nanostructures under various conditions was carried out by the author personally.

4.4 Determination of the influence of ethyl alcohol additives on the deposition rate of Ni nanostructures, as well as the degree of structural distortion

This section presents the results of a research of the influence of ethyl alcohol on the change in the rate of formation of nanotubes, as well as the degree of structural distortion resulting from their formation. The use of ethanol as a surfactant is due to a decrease in the surface tension of the liquid as result of adsorption at the interface of the electrolyte solution, the pore wall of the template matrix. It makes process easier to distribute and reduce interfacial tension during the formation of nanostructures. As is known from the literature, the ethyl alcohol or other surfactants in the synthesis process is used to change not only the rate of metal ion reduction reaction or the formation of crystallites, but also to reduce distortions and deformations in the structure. Surfactants are widely used in solid-state synthesis processes in the preparation of complex multiphase nanostructures or ceramics, where the use of additives leads to a significant decrease in interfacial boundaries and the formation of stable phase formations. In electrochemical synthesis, surfactants are primarily used to change the rate of formation of structures [150-154].

Also, an important factor, according to many researchers, is the initial metal salts, since the use of nickel sulfates, chlorides or nitrates can also have a huge impact on the deposition rate of nanostructures, since the reduction potentials and reaction mechanisms of the formation of a metal precipitate from various solutions have significant differences [155-158]. To assess the effect of the potential difference, as well as the use of various metal salts for electrochemical synthesis and ethanol on the properties and geometry of the synthesized nanotubes, the deposition rate of nanostructures was calculated by the gravimetric method using analytical weights to weigh the samples before and after deposition. A detailed description of the synthesis conditions used, as well as electrolyte solutions with various additives, is presented in section 3, Table 1. The rate was converted to current units using the formula (4.12):

$$i = \frac{\Delta m \cdot n \cdot 26.3 \cdot 10^3}{t \cdot S \cdot A} \qquad (4.12)$$

where Δm is the change in the mass of the sample, n is the valency of the deposited metal, t is the deposition time, S is the area of the deposited surface, A is the atomic weight. The value of the coefficient of efficiency of the formation of nanostructures was estimated using the formula (4.13):

$$K = \frac{i_0}{i_u} \qquad (4.13)$$

where i_0 and i_u are the exchange currents under different experimental conditions. Figure 30 shows graphs of changes in the coefficient of efficiency of the formation of nanostructures without the addition of ethanol and with the addition of ethanol.

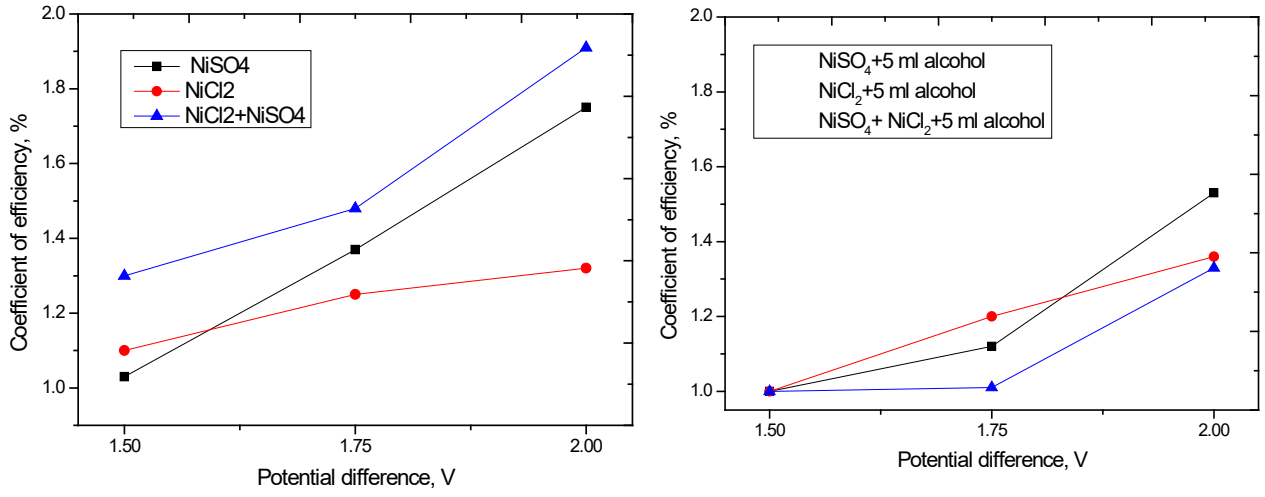

a) b)

Figure 30. Dynamics of changes in the deposition coefficient (coefficient of efficiency) of nanostructures: a) without the addition of ethanol; b) with the addition of ethanol

Figure 30a shows that the greatest efficiency in the formation of nanostructures is the use of an electrolyte based on a mixed composition (nickel sulfate + nickel chloride). Increasing in the potential difference for a given electrolyte increases the formation rate by more than 1.9 times. However, high rates of formation of the walls of nanotubes at large potential differences can lead to the introduction of impurity inclusions in the structure, which can affect the crystal structure and conductive properties. At large potential differences during the deposition process, a fast evolution of hydrogen was observed. It passivated the anode and led to an irregular growth of nanotubes. The addition of ethanol to electrolytes leads to a decrease in the coefficient of growth efficiency, while hydrogen evolution was not observed at large potential differences.

With the addition of alcohol the deposition coefficient decreases, together with the decrease in formation of gas hydrogen bubbles, which affect the distortion and deformation of the structure, and also prevent the tubes from growing in width, thereby increasing the contribution of the longitudinal growth rate.

The addition of alcohol also affects the rate of movement of metal ions in the electrolyte solution and, thereby, decreases the rate of formation of nanotubes.

Figure 31 represents SEM images of the synthesized nanotubes with and without the addition of ethanol [159].

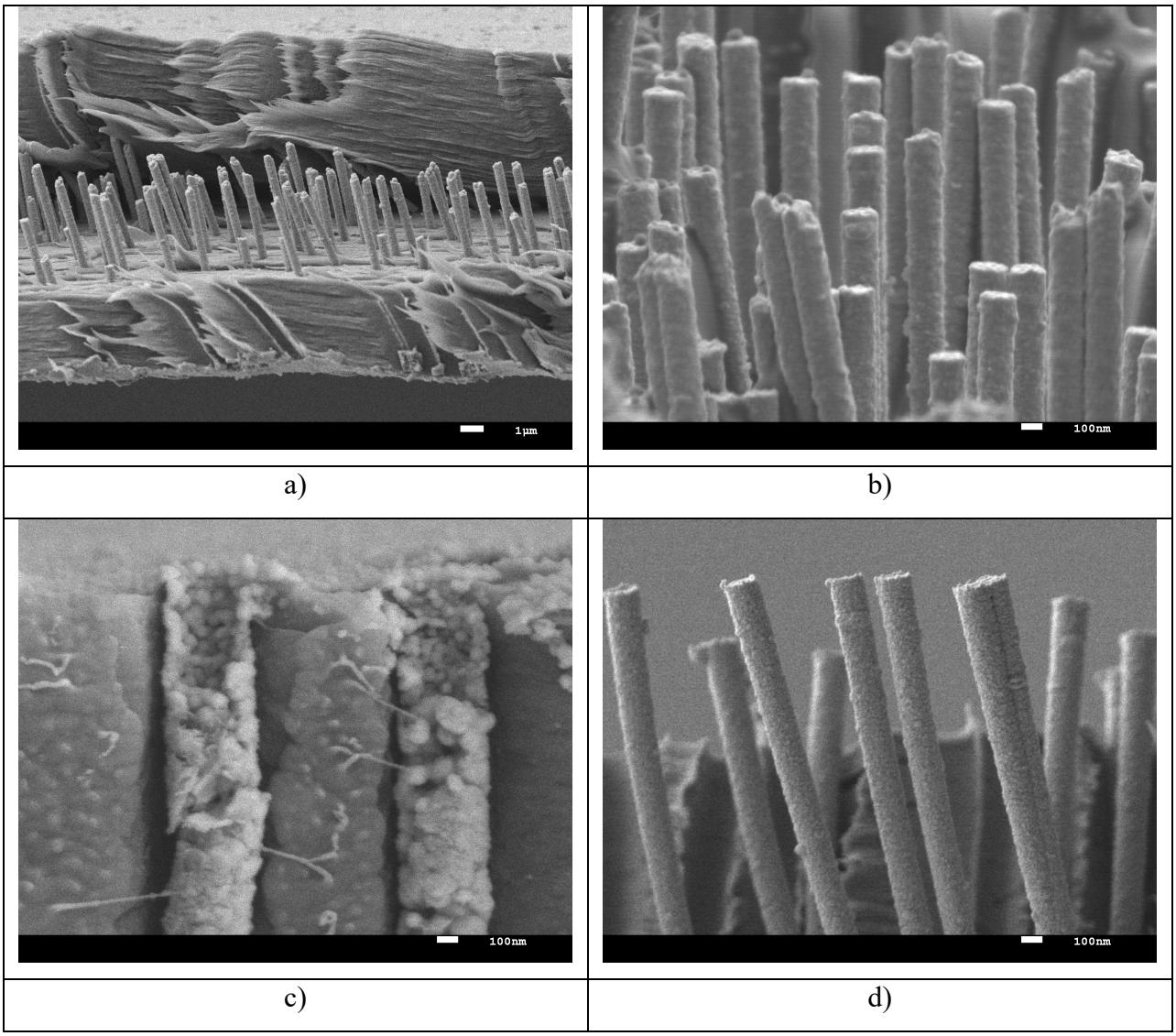

Figure 31. SEM – images of synthesized nanotubes: a,b) electrolyte – 1, U=1.5 V; electrolyte – 1, U=1.5 V; c) electrolyte – 1, U=2.0 V; d) electrolyte – 4, U=2.0 V [159].

Presented images show, that with a potential difference of 1.5 V, nanostructures in the form of tubes are obtained. However, when the applied potential difference is 2.0 V, porous inclusions appeared in the walls of the nanotubes. It may be due to the influence of the impurity formation of the structure of the nanotubes. Moreover, the addition of ethanol is the reason of the absence of amorphous inclusions in nanotubes with a potential difference of 2.0 V.

To study the influence of adding alcohol on the structural properties and phase composition, the method of x-ray diffraction analysis was applied. Figures 32-34 show X-ray diffraction patterns of the samples under study [159].

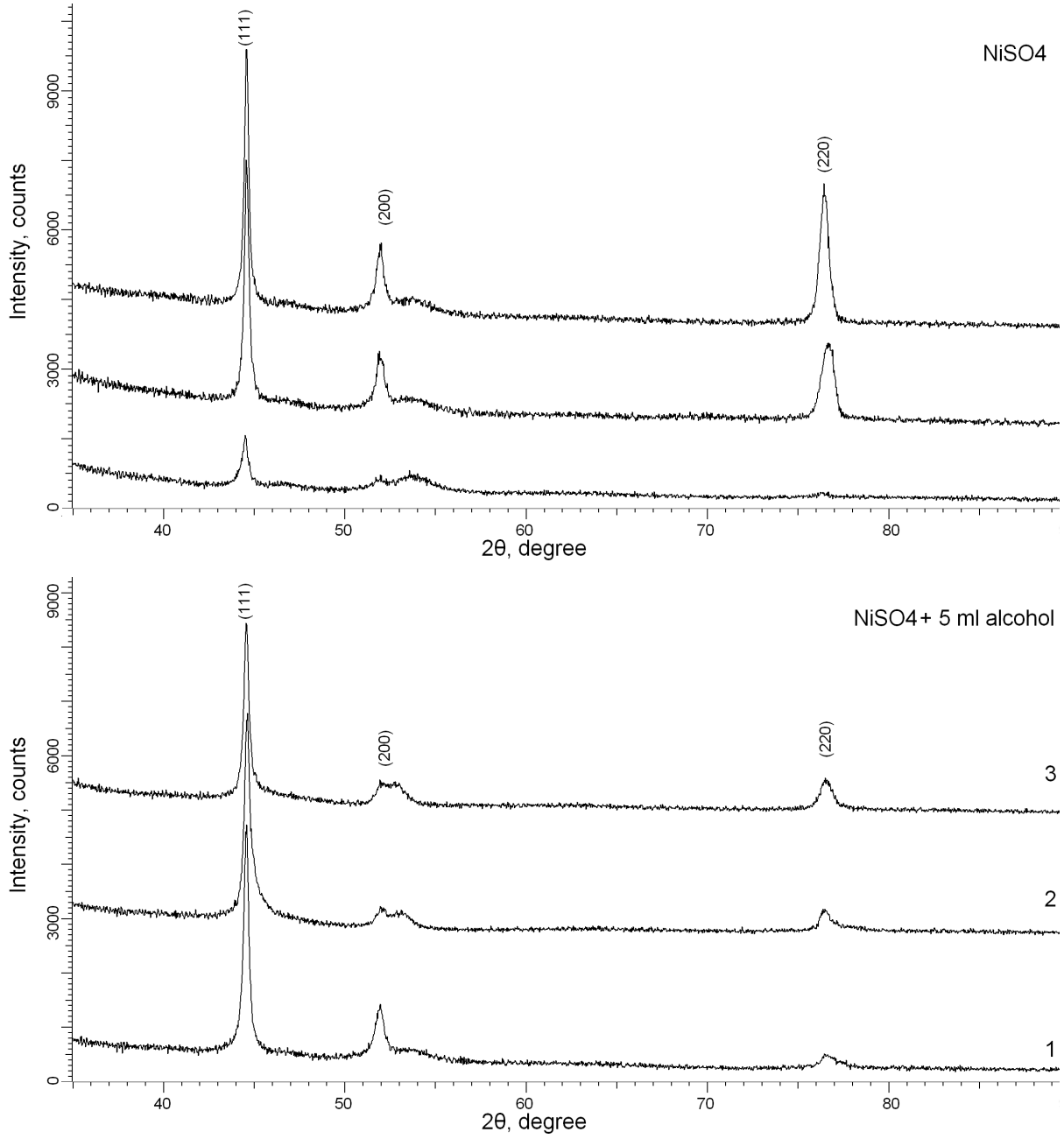

Figure 32. XRD patterns of samples deposited from solutions 1 and 4

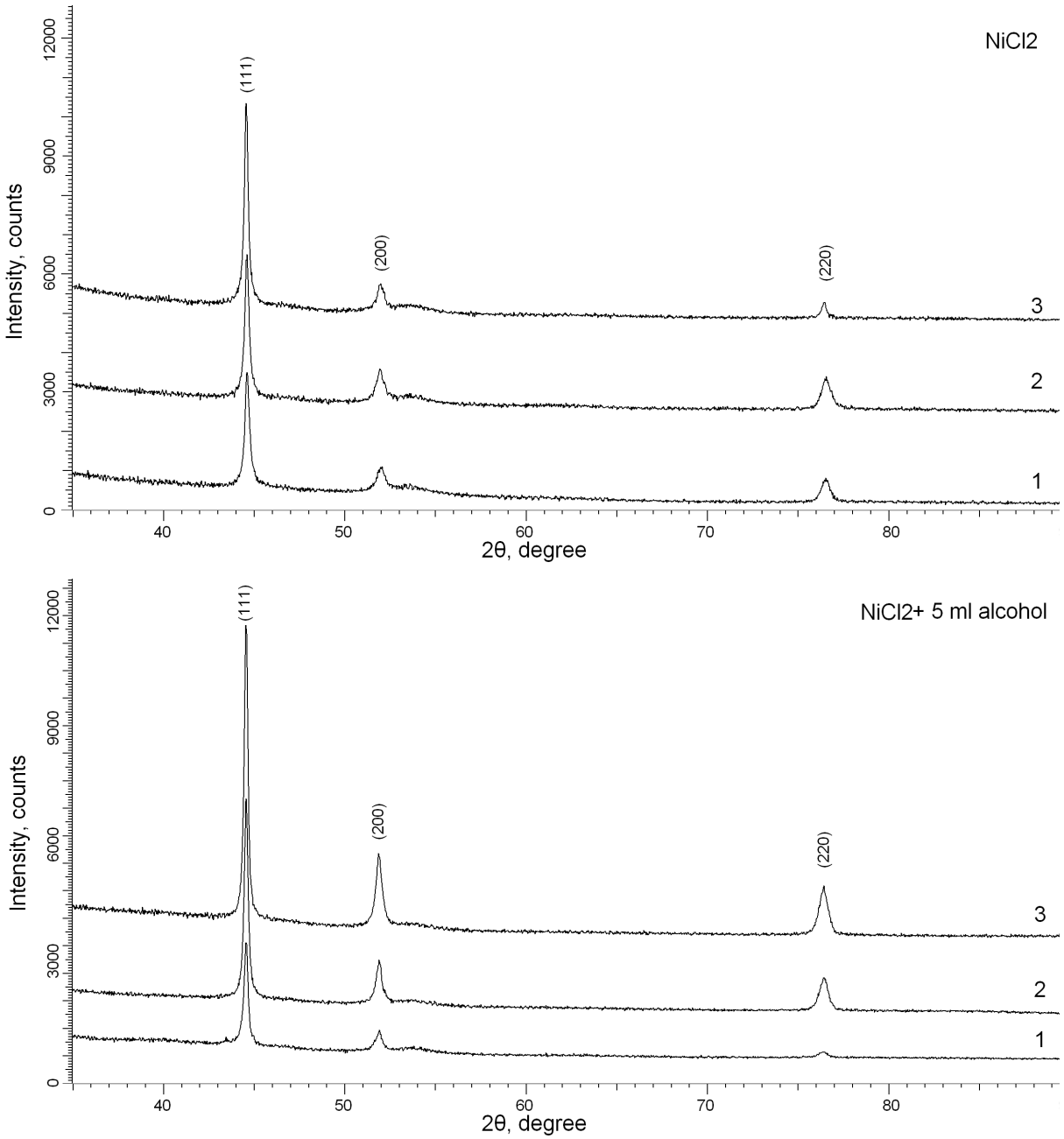

Figure 33. XRD patterns of samples deposited from solutions 2 and 5

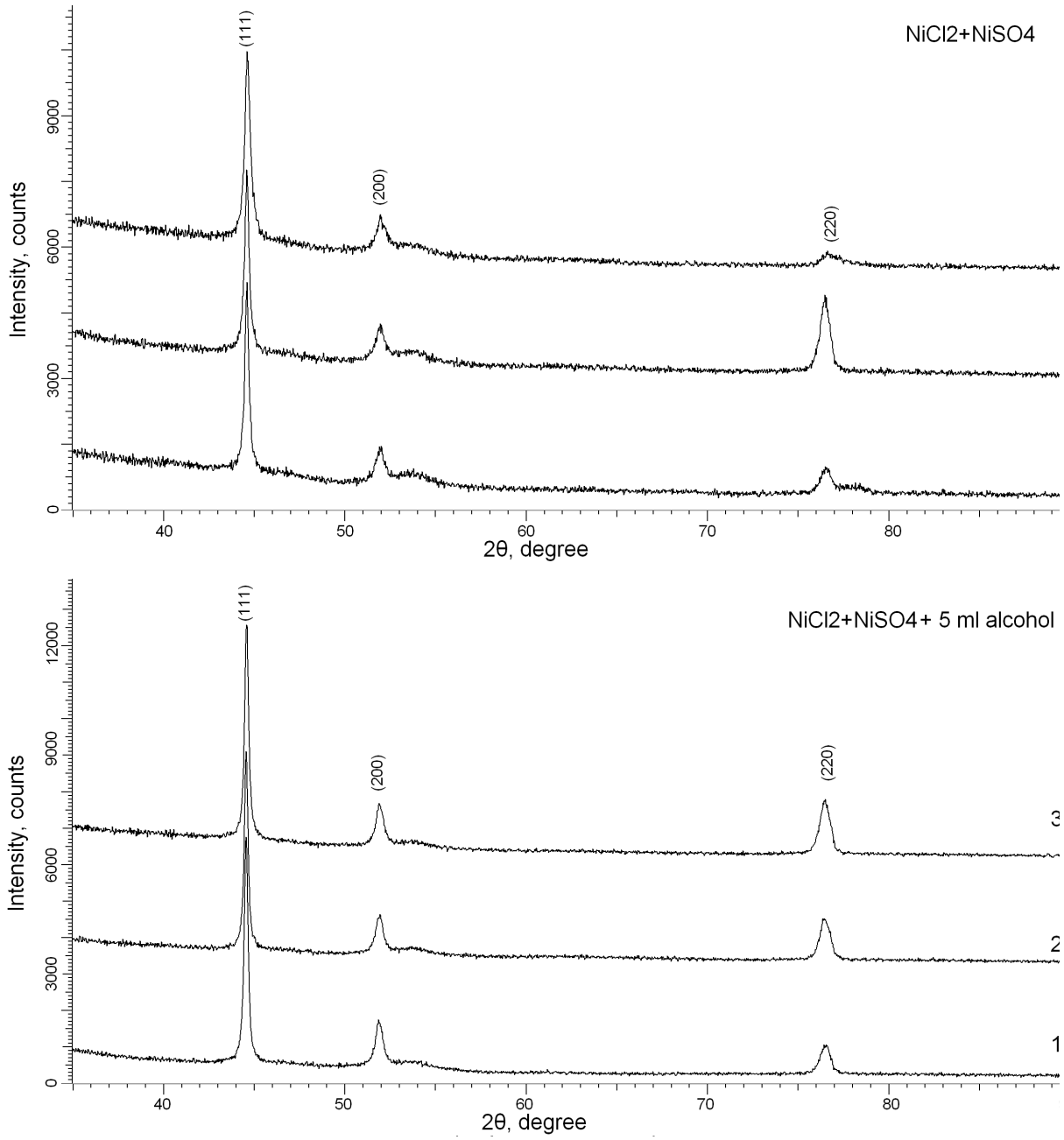

Figure 34. XRD patterns of samples deposited from solutions 3 and 6

An analysis of XRD patterns shows that the samples under study are polycrystalline structures with an fcc phase and cubic syngony of the space group Fm-3m (225). Moreover, according to the data obtained, no impurity oxide phases are observed in the structure of nanotubes. Degree of texturing of the obtained nanotubes depends on both applied potential difference and content of the electrolyte solution. Based on the obtained diffraction patterns, the crystallographic characteristics (crystal lattice parameters, average crystallite size, density) were calculated. The crystal lattice parameter was calculated using the Nelson – Taylor extrapolation function (4.14):

$$a = f\left[\frac{1}{2}\left(\frac{\cos^2\theta}{\sin\theta} + \frac{\cos^2\theta}{\theta}\right)\right], \qquad (4.14)$$

The value and the error in determining the parameter a are determined by linear extrapolation of this function to the zero value of the argument (θ = 90°). The average crystallite size was determined by the Scherrer equation. A change in the parameters of the crystal lattice, caused by distortions and deformation in the structure, leads to a change in the volume of the crystal lattice and, consequently, the density of the material. The density of the material was calculated using the formula (4.15):

$$p = \frac{1.6602\sum AZ}{V_o}, \qquad (4.15)$$

where V_0 is the volume of the unit cell, Z is the number of atoms in the crystal cell, A is the atomic weight of the atoms. Based on the change in intensities, the texture coefficients were calculated according to Harris formula (4.16).

$$TC_{\text{hkl}} = \frac{I_{hkl}}{I_{0hkl}} \Big/ \frac{1}{n}\sum \frac{I_{hkl}}{I_{0hkl}}, \qquad (4.16)$$

where I_{hkl} is the experimentally obtained reflex intensity, I_{0hkl} is the corresponding intensity according to PDF#2, n is the number of reflexes.

Table 6 presents the crystallographic data of Ni nanotubes obtained at different electrolyte solutions at different voltages.

Table 6. Crystallographic data of Ni nanotubes obtained at different electrolyte solutions at different voltages.

N of solution	Potential difference, V	Unit cell parameter, Å	The average crystallite size, nm	Density, g/cm^3	TC (hkl)		
					(111)	(200)	(220)
1	1.5	3.51901	30.28±2.12	8.945	2.425	0.231	0.245
	1.75	3.51341	25.68±1.87	8.988	2.152	0.342	0.563
	2.0	3.51482	22.36±1.83	8.978	1.852	0.563	0.942
2	1.5	3.51224	24.79±2.13	8.997	2.234	0.424	0.221
	1.75	3.51426	24.51±2.11	8.982	2.452	0.342	0.213
	2.0	3.51706	33.95±2.65	8.960	2.532	0.231	0.345
3	1.5	3.51385	24.19±1.98	8.985	2.653	0.231	0.134
	1.75	3.51441	24.53±1.87	8.981	2.422	0.441	0.321
	2.0	3.51107	21.97±1.64	9.006	2.134	0.541	0.445

4	1.5	3.51601	35.08±1.89	8.968	2.451	0.215	0.214
	1.75	3.51262	22.56±1.52	8.994	2.343	0.436	0.316
	2.0	3.51542	20.07±2.18	8.972	2.134	0.674	0.542
5	1.5	3.51566	28.17±1.76	8.971	2.435	0.342	0.213
	1.75	3.51705	29.43±2.11	8.961	2.134	0.314	0.763
	2.0	3.51566	27.91±1.52	8.971	2.325	0.432	0.212
6	1.5	3.51724	25.41±1.63	8.958	2.312	0.453	0.321
	1.75	3.51653	25.98±1.62	8.964	2.314	0.422	0.425
	2.0	3.51461	24.74±1.98	8.979	2.123	0.532	0.763

As can be seen from the data presented, a change in the fabrication conditions and the electrolyte solution are reason of changes in the basic crystallographic characteristics. For electrolyte solutions №1 and №2, an increase in the potential difference leads to a decrease in the density of nanotubes as a result of the formation of amorphous inclusions in the structure, and for an electrolyte solution №3, a slight increase in density is observed with an increase in the potential difference. Moreover, the addition of surfactant additives makes a decrease in amorphous inclusions and an increase in the density of nanotubes. Increasing in the potential difference makes changes in texture coefficients as well as increasing in the degree of polycrystallinity of nanotubes. A change in the FWHM of the main diffraction lines in the X-ray diffraction patterns indicates a change in the crystallinity of the synthesized samples. When approximating the lines in the diffraction pattern by the required number of symmetric pseudo-Voigt functions, the width of the recorded FWHM lines was determined, which made it possible to characterize the perfection of the crystal structure and evaluate the degree of crystallinity. The evaluation results are presented in Figure 35.

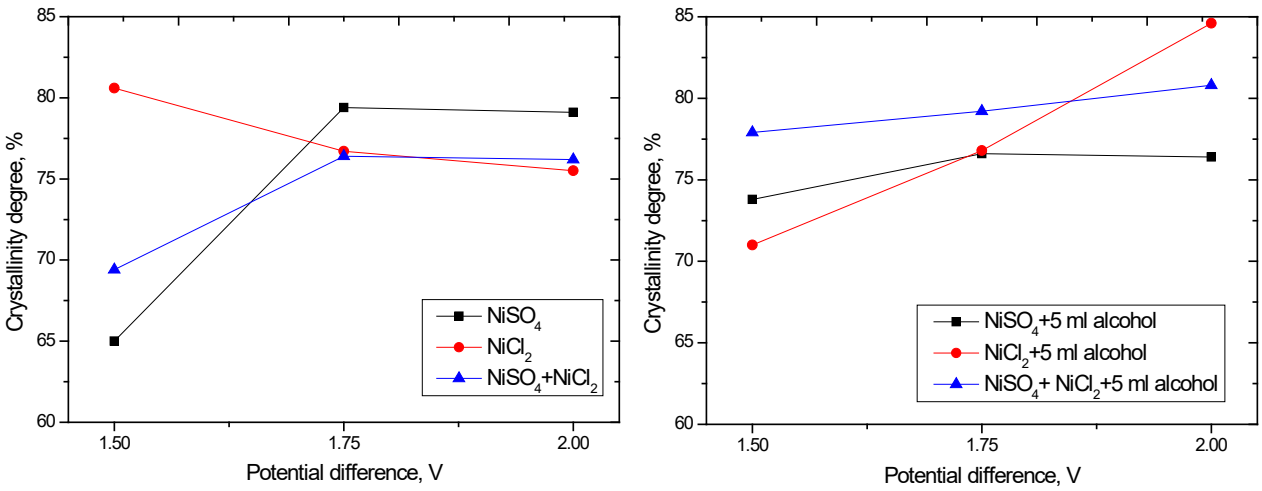

a) b)

Figure 35. Degree of crystallinity of the studied nanotubes for different electrolyte solutions: a) solutions 1,2,3; b) 4,5,6.

By analyzing the magnitude of the diffraction maxima width and area under the line, we can evaluate the grain sizes and the contribution of various defects. In this case, the broadening of the widths of diffraction lines can be due to microstresses in the structure, which are associated with the accumulation of dislocations, as well as the crushing of crystallites associated with crystallization processes. An analysis of the angular dependence of physical broadening allows one to evaluate the influence of both factors. To assess the impact, the Williamson-Hall method was used, which is based on relation (4.17):

$$\beta^2 = W_{size}{}^2 + W_{strain}{}^2, \qquad (4.17)$$

$$W_{size}{}^2 = \left(\frac{\lambda}{D \cdot \cos(\theta)}\right)^2,$$

$$W_{strain}{}^2 = \left(4 \cdot \varepsilon \cdot \tan(\theta)\right)^2,$$

where β is the physical broadening of the diffraction maximum, λ is the x-ray wavelength (1.54 Å), D is the crystallite size, θ is the Bragg diffraction angle, ε is the magnitude of microstresses in the lattice. According to the data obtained, the main contribution to the broadening and change in the shape of diffraction peaks at large potential differences is made by the microstresses arising in the course of synthesis crystallization. Moreover, the addition of ethanol makes decreasing in the degree of microstresses and deformations in the nanotube.

Microstresses were calculated by an analysis of the displacement of diffraction peaks according to equation (4.18):

$$microstrain = \frac{d_{exp} - d_0}{d_0}, \quad (4.18)$$

where d_{exp}, d_0 are the interplanar distances experimentally measured, the reference value according to the PDF 2 database. The strain coefficient of the structure was calculated using equation (4.19):

$$\varepsilon = \left| \frac{a_0 - a}{a_0} \right|, \quad (4.19)$$

where a_0 and a are the reference and experimentally obtained values of the unit cell parameter. Table 7 presents the results of changes in microstresses and strain coefficient in nanostructures.

Table 7. Microstress and strain factor data

№	Potential difference, V	The degree of microstresses in the structure	Strain factor
1	1.5	0.054	0.211
	1.75	0.065	0.251
	2.0	0.097	0.370
2	1.5	0.046	0.177
	1.75	0.067	0.235
	2.0	0.089	0.315
3	1.5	0.052	0.144
	1.75	0.065	0.223
	2.0	0.087	0.239
4	1.5	0.043	0.188
	1.75	0.054	0.232
	2.0	0.059	0.268
5	1.5	0.034	0.134
	1.75	0.042	0.213
	2.0	0.052	0.275

6	1.5	0.045	0.102
	1.75	0.064	0.186
	2.0	0.078	0.231

Presented data show, that an increase in the potential difference makes the formation of additional stresses in the structure that arise as a result of the formation of amorphous inclusions and regions with a high degree of imperfection. As a result, an increase in the distortion of the crystal lattice and a change in interplanar distances are observed in the structure, which lead to an increase in microstresses in the crystal structure. In turn, the addition of ethanol to the electrolyte solution leads to an increase in crystallinity and a decrease in deformation and distortion in the crystal structure, which can have a significant effect on the performance of nanotubes, such as conductive properties.

For the potential practical application of nanostructures, one of the significant characteristics is conductive properties. Parameters such as chemical composition, crystal structure, geometric characteristics, and surface morphology affect the transport characteristics of nanostructures. The specific conductivity of arrays of nanostructures was calculated by the formula (4.20):

$$\sigma = \frac{dI}{dU}\frac{l}{A}, \qquad (4.20)$$

where l is the length of the nanotubes, A is the area, dI/dU is the tangent of the angle of inclination I–U.

The results of the change in conductivity are presented in Figure 36.

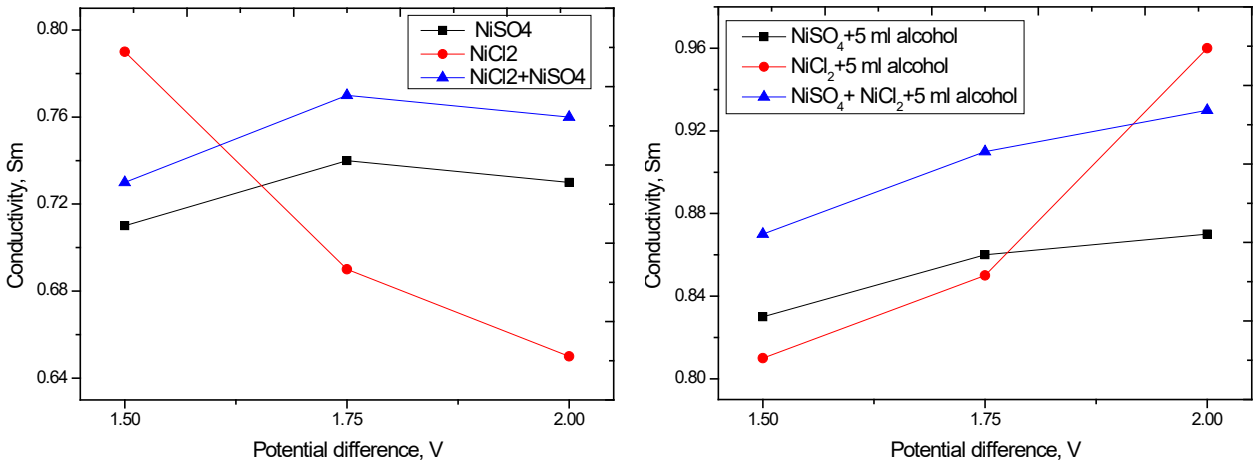

a) b)

Figure 36. Specific conductivity of Ni nanotubes fabricated using different electrolyte solutions: a) solutions 1,2,3; b) 4,5,6.

Presented data show that an increasing in the potential difference to 2.0 V for electrolyte solutions №1-3 leads to large distortions and deformations of the crystal structure and the formation of amorphous inclusions in the structure. It makes to a decrease in conductivity. Moreover, the addition of surfactant additives is reason of increase in conductivity. It happens due to the high degree of crystallinity of the nanotubes and the more perfect structure of the nanotubes. One of the important factors affecting the performance of nanostructures and the crystal structure is the concentration of dislocations in the structure, the change of which directly affects the conductive characteristics. The dislocation density (δ) contains information on the improvement of the crystal structure and is calculated according to formula (4.21).

$$\delta = \frac{1}{L^2}, \qquad (4.21)$$

where L is the volumetric grain size.

Figure 37 shows the dynamics of changes in the density of dislocations depending on the synthesis conditions.

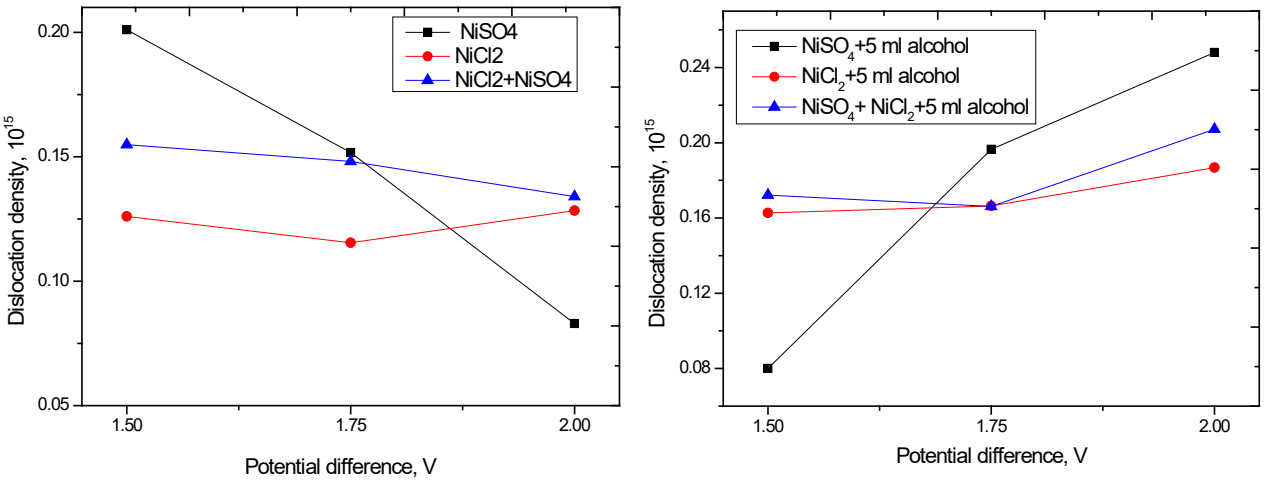

a) b)

Figure 37. Dislocation densities of Ni nanotubes fabricated at different electrolyte solutions: a) solutions 1,2,3; b) 4,5,6.

Graph shows that an increase in the potential difference makes a decrease in the dislocation density due to amorphous inclusions in the structure. In this case, the addition of ethanol leads to a decrease in amorphous inclusions in the structure and a change in grain sizes and an increase in the dislocation density, which leads to the creation of additional charge carriers in the structure and to a change in the ballistic nature of charge transfer in nanotubes.

Notes

- The results of this study were published in [159].
- The analysis of structural parameters based on X-ray diffraction patterns and their analysis was carried out jointly with the staff of the Laboratory of Solid State Physics AB of INP.
- Obtaining samples under given synthesis conditions was performed personally by the author at the Laboratory of Solid State Physics AB of INP.
- The analysis of the geometry of the synthesized nanostructures under various conditions was carried out by the author personally.

4.5 The influence of the geometry of the template on the degree of texturing and magnetic properties of Ni nanotubes

One of the factors affecting the properties of nanotubes, as well as their magnetic characteristics, is the aspect ratio, which, in the case of using template matrices with a given thickness, can be changed by varying the pore diameter. Changing the pore diameter can have a significant effect not only on the aspect ratio, but also in the case of using the same synthesis conditions, by changing the pore diameter and changing the contact area, it can lead to a change in the degree of texture and grain orientation. This section presents the results of research of the influence of pore geometry, in particular, variations in their diameters from 100 to 500 nm, on the properties of Ni nanotubes obtained with a applied potential difference of 1.75 V.

The changes in the pore diameters make it possible to change the Ni nanotubes morphology, structure, and the physical properties. Figure 38a shows SEM images of Ni nanotubes with different outer diameters and Figure 38b - dependence of the wall thickness on pores diameter.

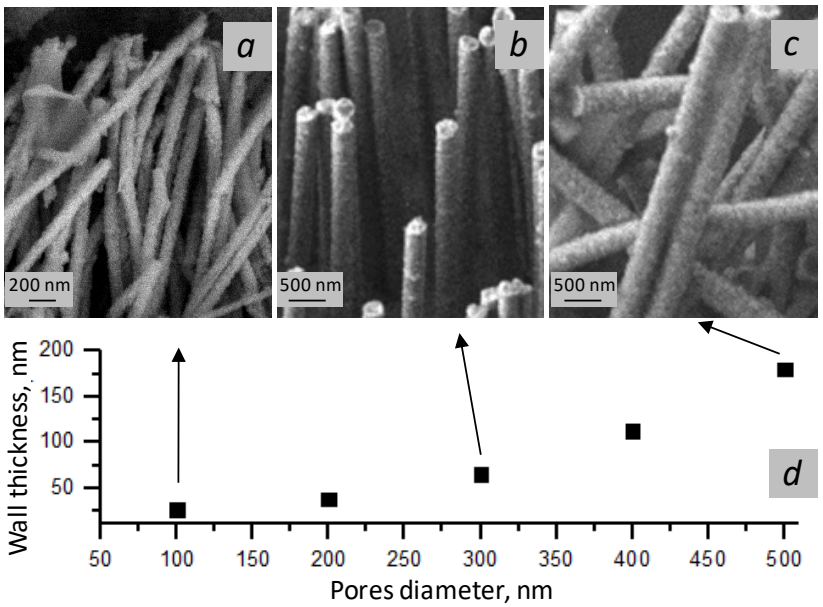

Figure 38. SEM images of obtained nanotubes: a) 100 nm; b) 300 nm; c) 500 nm; d) dependence of Ni nanotubes wall thickness on pores diameter at constant deposition potential.

From SEM images, it can be seen that nanotubes have a similar morphology, differing only in the size of the outer diameters, which are determined by the template pore parameters. In all cases, the length of the nanotubes corresponds to the thickness of the PET membrane. A

detailed study of the wall thickness of the nanotubes (internal diameters) shows that wall thickness monotonically increase with nanotubes outer diameter increasing (Fig. 38b). We used manometric method. At smallest diameter (it equals to 100 nm) wall thickness is about 25 nm and the nanotubes are fragile and at the maximum diameter (500 nm) the wall thickness reaches 170 nm and the structures are quite strong.

Figure 39 shows XRD patterns of the obtained nanotubes with different outer diameters.

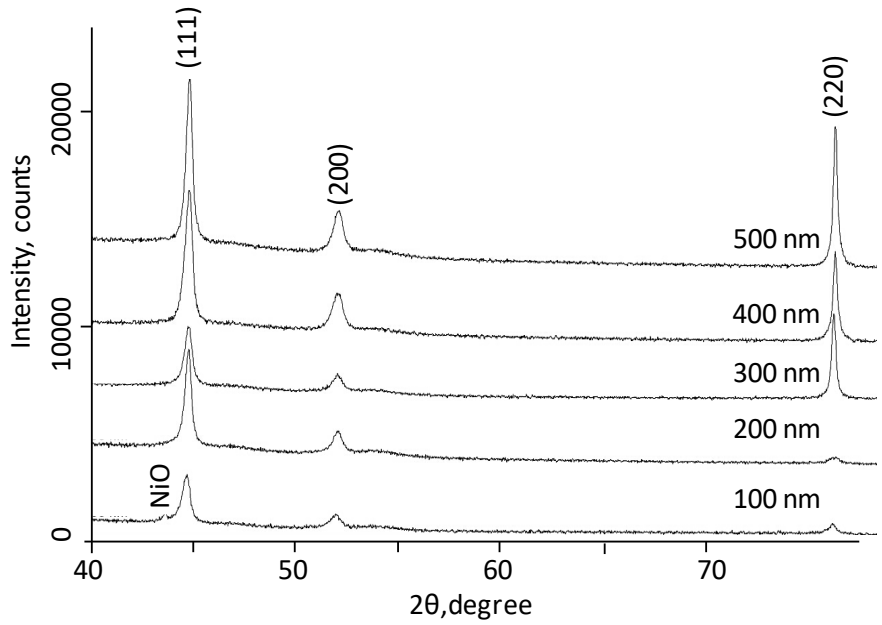

Figure 39. XRD patterns of Ni nanotubes fabricated in PET with various diameters

Ni nanotubes with diameter of 100 nm have a low-intensity peak characteristic of NiO which felt off for other samples. The fast rate of synthesis in small pores volume makes the formation of amorphous inclusions and disorder regions in the nanotubes. It happens due to oxygen ions coming into the crystal lattice during the fabrication. The content of the nickel oxide phase in the structure does not exceed 6-8%.

The degree of texturing of the crystallites in nanotubes with different diameters were determined by analyzing texture coefficients TC_{hkl} (Table 8)

Table 8. Texture coefficients of Ni nanotubes fabricated in PET with pores of various diameters

(hkl)	TC_{hkl}				
	100 nm	200 nm	300 nm	400 nm	500 nm
(111)	2.311	2.156	1.151	1.031	1.297
(200)	0.365	0.642	0.456	0.675	0.667
(220)	0.324	0.202	1.393	1.294	1.036

Increasing in the diameter of nanotubes makes to rise of the contribution of the texture plane (220) and, consequently, an increasing in the degree of polycrystallinity of nanotubes.

According to the proposed model of the formation of nanotube walls, which is based on the assumption of two rates of growth of nanotubes (longitudinal and transverse), as well as a change in their contributions during growth, the formation of amorphous inclusions at Ni nanotubes with small diameters can be explained as follows. In the case of a small pore volume, at large potential differences (1.75 V) the pore contains a small volume of electrolyte solution. At the initial stages of growth, when the nucleation of nanotube walls occurs, any bubble formation can lead to partial or complete clogging of the pores due to its small diameter, which leads to uneven growth of the walls, as well as their amorphization associated with uneven growth and deformation of the structure as a result of intrusion oxygen and hydrogen in the lattice internodes. At the same time, in a small volume, the formation of walls occurs rather quickly and the longitudinal growth rate prevails in the structure, which leads to the rapid filling of the entire pore volume and the formation of thin-walled tubes with a thickness of no more than 20-30 nm. In this case, a small wall thickness leads to weak crystalline and chemical bonds, and embedded oxygen or hydrogen can lead to the formation of oxide phases and thereby deforming the crystalline structure of nanotubes.

Table 9 shows main parameters of crystal structure.

Table 9. Main parameters of crystal structure of Ni nanotubes with various diameters

Pores diameters, nm	Lattice parameter, Å	Coherent scattering region, nm	Crystallinity, %	Microstrains, m2·1015
100	3.5149	23.9	63.5	0.074
200	3.5094	26.5	68.7	0.054
300	3.5066	31.8	78.6	0.031
400	3.5052	29.1	87.6	0.04
500	3.5034	31.3	93.2	0.032

Presence in nanotubes of oxide impurities and disorder regions decreases the degree of crystallinity. Increasing the pore diameter while keeping constant deposition potential increases the synthesis time and leads to better ordered nanotubes. Analyzing diffraction peaks area and FWDH allows to estimate the contribution of various defects in nanotubes structure. Decreasing of Ni nanotubes outer diameters broadens the XRD peaks, which occur as a result of

microstrains in the structure associated with the accumulation of dislocations, as well as the splitting of crystallites during crystallization processes. Large number of different deformations and distortions of the crystal structure is observed for nanotubes with the smallest diameters. It happens due to the influence of different impurity inclusions (in particular, the oxide phase). An increase in the diameter of nanotubes leads to a decrease in microstresses and deformation in the lattice. When the diameter of nanotubes increases we observe decreasing microstresses and lattice deformation. However, for sample with nanotubes of 500 nm diameter the amount of distortions in the structure increases, which may be due to the appearance of additional texture orientations. Analyzing the lattice parameter (reduced), and also the degree of crystallinity (increased), it becomes obvious that with diameter increasing the samples ordering significantly improves, which confirms the assumption above that the different rate of deposition in the pores of different diameters affects the nanotubes structural properties.

The hysteresis loops for samples are shown on Figure 40. Table 10 represents main magnetic characteristics.

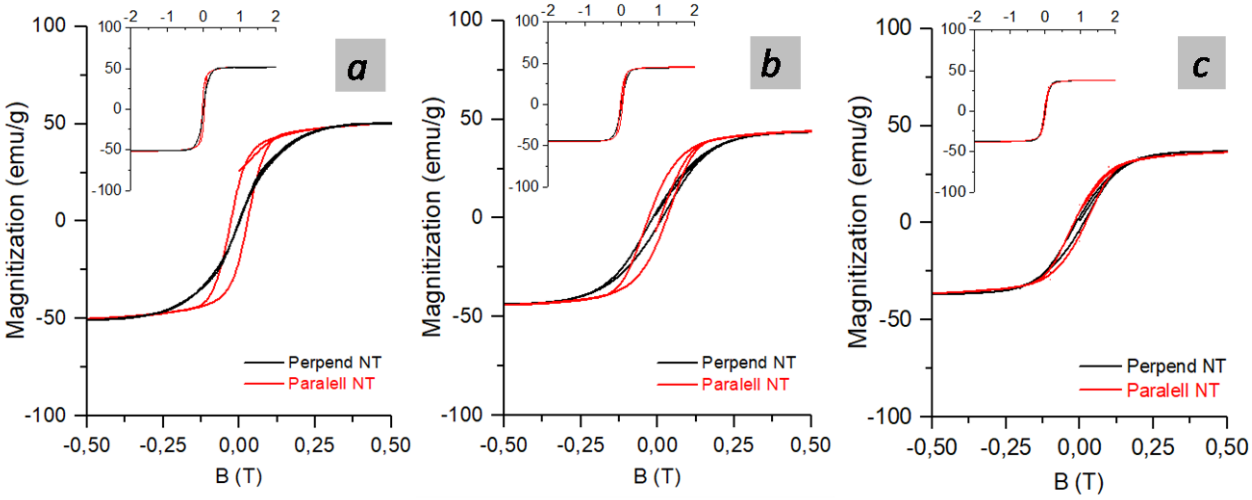

Figure 40. Hysteresis loop of Ni nanotubes with diameters: a) 100 nm; b) 300 nm; c) 500 nm.

Table 10. Main magnetic characteristics of Ni nanotubes

Pores diameter, nm	Main magnetic characteristics			
	Parallel to nanotubes axis		Perpendicular to nanotubes axis	
	H_C, Oe	M_r/M_s	H_C, Oe	M_r/M_s
100	210	0.36	128	0.05
200	250	0.38	135	0.078
300	510	0.47	300	0.27
400	300	0.37	150	0.24
500	240	0.25	160	0.14

There is an interesting dependence of pore Ni nanotubes diameter on its magnetic properties. Coercivity and squareness ratio rise for samples from 100 to 300 nm diameter and fall down at 400 and 500 nm. Several structural factors play a dominant role on Ni nanotubes magnetic properties. According to Tables 7 and 8, with the increase in diameter of nanotubes we observe the growth of crystallinity degree and crystallites size, change in lattice parameter, and the redistribution of texture coefficients corresponding to the main growth direction. As it was mentioned above, the deterioration of crystallinity, presence of defects and stresses decreases magnetization and affects other magnetic parameters. Redistribution of peaks on XRD-diagram and correspondent texture coefficients with increase in nanotube diameter indicate that the main nanotubes growth direction changes from [111] to other crystallographic directions, leading to the changes in magnetic properties.

Notes

- The analysis of structural parameters based on X-ray diffraction patterns and their analysis was carried out jointly with the staff of the Laboratory of Solid State Physics AB of INP.
- Obtaining samples under given synthesis conditions was performed personally by the author at the Laboratory of Solid State Physics AB of INP.
- The analysis of magnetic characteristics, as well as obtaining hysteresis loops, was carried out jointly with the employees of the cryogenic research department of BelNAN in materials science, Minsk, Belarus.

4.6. Assessment of the corrosion resistance of Ni nanotubes when exposed to acidic and neutral environments

Having examined the influence of various factors, such as the applied potentials difference, the temperature of the electrolyte solution, the degree of acidity of the electrolyte solution, the addition of alcohol additives and the replacement of sulfate salts with chloride salts, as well as their combination, it was found that nanotubes obtained with an applied potentials difference of 1.75 V possess the best structural characteristics. However, for the practical application of nanotubes, in particular, in conditions of contact with liquid media, including acids and alkalis, it is necessary to know the rate of degradation of nanostructures, as well as the corrosion mechanisms resulting from contact with the medium.

Significant properties of nanotubes are resistance to oxidation and destruction in media with different acidity, which is determined by the concentration of H^+ and OH^- ions. In absolutely pure water, which does not even contain dissolved gases, the concentrations of these ions are equal. The hydrogen index (pH) is a value that characterizes the concentration of hydrogen ions in solutions. For deionized water, the pH value is in the range of 6.5 - 7, which is typical for a neutral and slightly acidic environment. This section presents the results of studying the processes of oxidation and destruction.

The effect of medium acidity on the crystal structure of Ni nanotubes was studied using the method of x-ray phase analysis. It should be noted that low-intensity peaks characteristic of the diffraction of nanoscale objects were observed in the diffraction patterns of the studied samples (Figure 41a-c). According to the XRD results, the initial samples of Ni nanotubes are polycrystalline structures with an fcc phase with a predominant texture plane [111] and with a crystal cell parameter a=3,5192 Å, which is slightly larger than the reference value (a=3,5154 Å, PDF # 031051). Analysis of diffraction patterns showed that with an increase in residence time in an acidic medium with pH=1, peak intensities decrease, peaks characteristic of the oxide compound NiO with Miller indices (100) and (220) appear on day 10, and peak intensities of oxide compounds on day 20 increases, a peak characteristic of the trivalent compound of nickel Ni_2O_3 with Miller indices is also observed (102). For a medium with an acidity level of pH=5 on day 10, a decrease in the peak intensity of an oxide peak at θ=43.3º is observed, a clear manifestation of oxide phases is observed on the 20th day. For a medium with pH=7, the peak characteristic of the oxide compound NiO appears only after 20 days. The appearance of oxide compounds NiO is characteristic of structures with an atomic ratio of $Ni_{91}O_9$, the trivalent

compound Ni_2O_3 appears at an atomic ratio of $Ni_{64}O_{36}$ in a medium with pH=7, which indicates a high oxidation rate of nanotubes in acidic media [160].

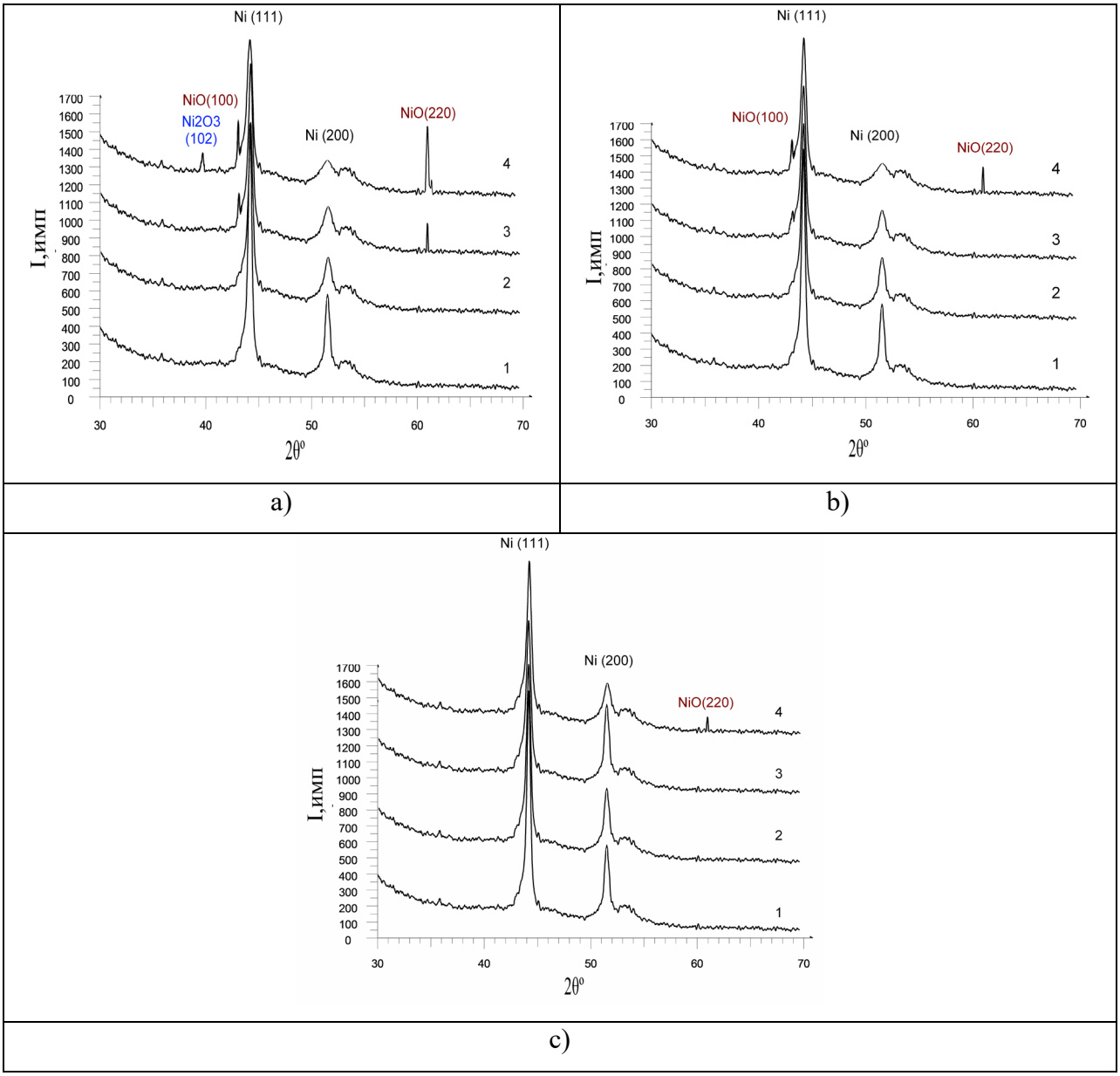

Figure 41. XRD patterns of Ni nanotubes before and after being in media with pH=1 (a); pH=5 (b); pH=7 (c): 1) initial; 2) 5 days; 3) 10 days; 4) 20 days [160]

Changes in the intensity and shapes of the peaks of diffractograms provide insight on the amorphization of the structure and partial degradation of nanotubes in acidic media after 10 days in the medium. Figure 42a shows a graph of the change in the parameter of the crystalline cell *a* as a function of the time spent in a medium with different pH, using the Nelson — Taylor extrapolation function. The increase in parameter *a* for a medium with pH=1 can be explained by the appearance of oxide phases NiO and Ni_2O_3 in the crystal structure, for which the value of parameter a is much higher (*a=4,1770* Å PDF 471049 and PDF # 140481). For a medium with

pH=7, a slight increase in the crystal cell parameter is observed, which indicates a low oxidation rate of nanotubes in neutral media.

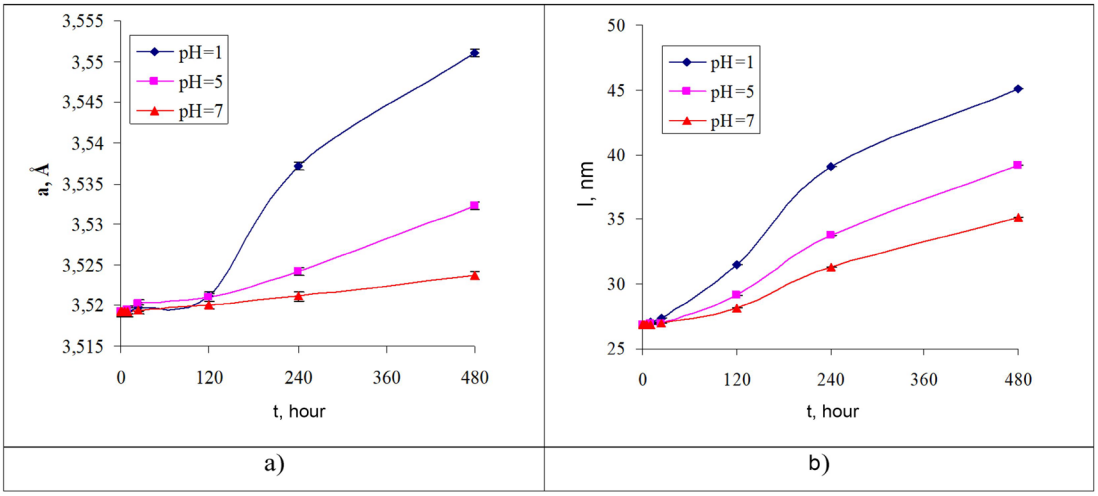

Figure 42. Characteristics of the crystal structure of the obtained samples of nanotube arrays: a) unit cell parameter; b) average crystallite size [161]

The increase in the average crystallite size (Figure 42b) can be explained by the appearance of oxide phases NiO and Ni_2O_3, as well as the formation of disordered regions in the crystal structure resulting from oxidation processes and subsequent degradation.

The dynamics of crystallite shape and orientation of Ni nanotubes as a result of oxidation were determined by studying the texture of nanotubes by evaluating texture coefficients. The crystallographic texture or degree of texturing refers to the preferred direction of orientation of certain crystallographic planes and directions in different grains of the polycrystal relative to the outer planes and directions. Texture coefficients were calculated using the Harris formula. The calculation results are shown in Table 11.

Table 11. Texture coefficient data

hkl	pH=1				pH=5				pH=7			
	initial	5 days	10 days	20 days	initial	5 days	10 days	20 days	initial	5 days	10 days	20 days
(111)	1.6414	1.6313	1.2132	1.0421	1.6414	1.6396	1.5951	1.3402	1.6414	1.6399	1.6032	1.4921
(200)	0.9424	0.8234	0.7622	0.3144	0.9424	0.9341	0.8562	0.7533	0.9424	0.9313	0.9023	0.8453

Values of texture coefficients greater than unity indicate that increased number of grains in the correspondent crystallographic orientation is along the array of nanotubes. The number of reflections (n) represents the maximum value of the texture coefficients. An analysis of the data

showed that with an increase in the contribution of oxide compounds to the crystalline structure in an acidic medium with pH=1, a decrease in the degree of texturing is observed, which leads to amorphization of the structure of nanotubes, while for neutral media the change in texture coefficients is insignificant.

One of the important characteristics of the kinetics of structural change is the rate of the oxidation reaction and subsequent degradation, which means the change in the concentration of substances per unit time. Figure 43 shows the kinetic curves of changes in the atomic ratio of nickel and oxygen in the crystal structure of nanotubes. An analysis of the obtained curves showed that the highest oxidation rate of nanotubes is observed in acidic media with pH=1, which confirms the results of elemental and X-ray diffraction analysis. In an aggressive environment, Ni nanotubes are partially oxidized, losing electrons, and passing into nickel (II) oxide:

$$Ni^{0} - 2e = Ni^{+2}$$

The nickel (II) oxide formed refers to bertollides with varying oxygen stoichiometry. With a large amount of oxygen in the structure, it transforms into nickel (III) oxide $Ni_2O_3 \cdot H_2O$ or NiOOH. In this case, the complete oxidation of nickel ions occurs:

$$Ni^{+2} - 1e = Ni^{+3}$$

But since the oxidation state of +3 is not characteristic of nickel, compounds with a given valency are not stable; therefore, hydrated forms of nickel (II) oxide fall apart with the elimination of oxygen.

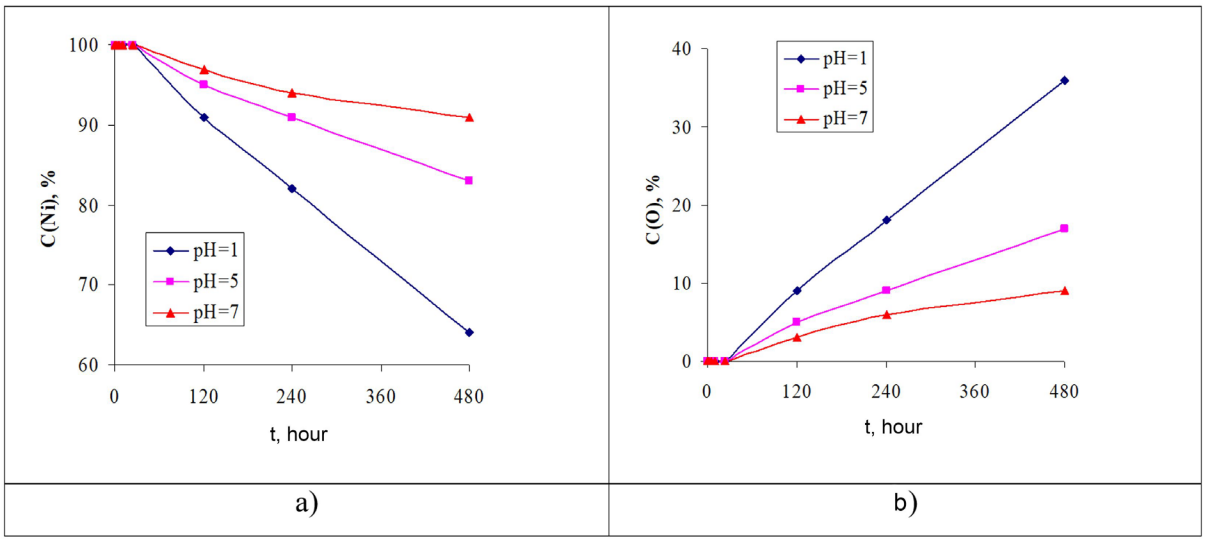

Figure 43. Kinetic curves of changes in the atomic ratio of nickel (a) and oxygen (b) in the crystal structure of nanotubes [160]

Figure 44 shows the anamorphoses of kinetic curves for the oxidation and degradation reactions of Ni nanotubes.

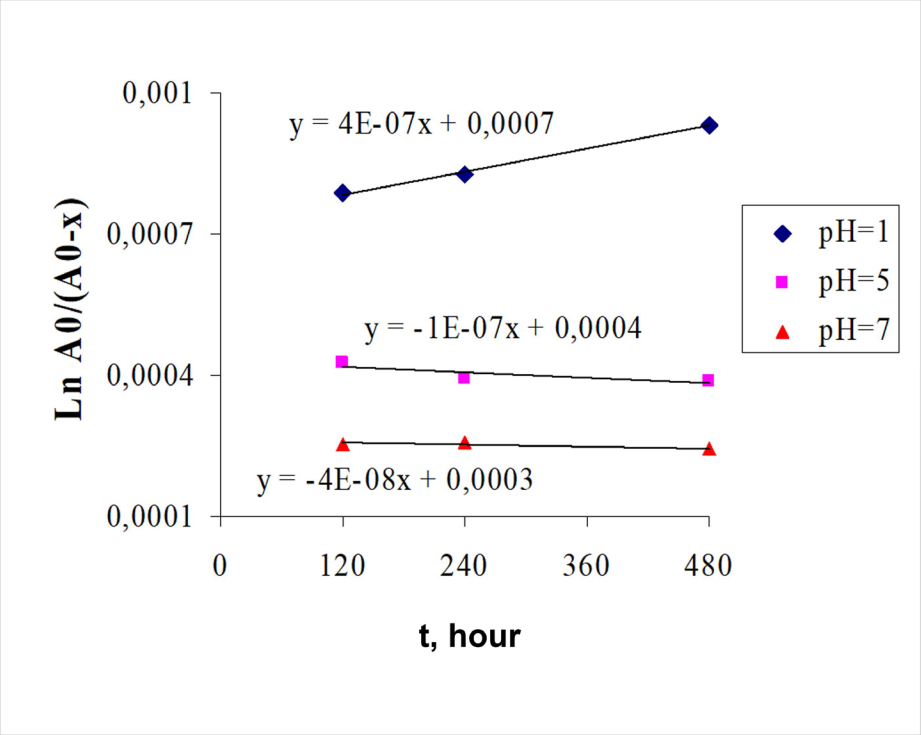

Figure 44. Anamorphosis of the kinetic curve for the oxidation and degradation reaction [160]

An integral method was used to determine the order of the chemical reaction of the oxidation of nanotubes depending on the acidity of the medium. The nature of anamorphoses for various media in coordinates

$$Ln\frac{[A_0]}{[A_0-x]}-t$$

is described by a straight line, which confirms that the process of NT oxidation is a first-order reaction. In this case, for a medium with pH=5 and a neutral medium (pH=7), the rate of oxidation of nanotubes is constant over time, which indicates that nanotubes are slightly susceptible to oxidation processes in non-aggressive environments. SEM images (Figure 45) show the change in the surface degradation of nanotubes under the influence of media with different levels of acidity.

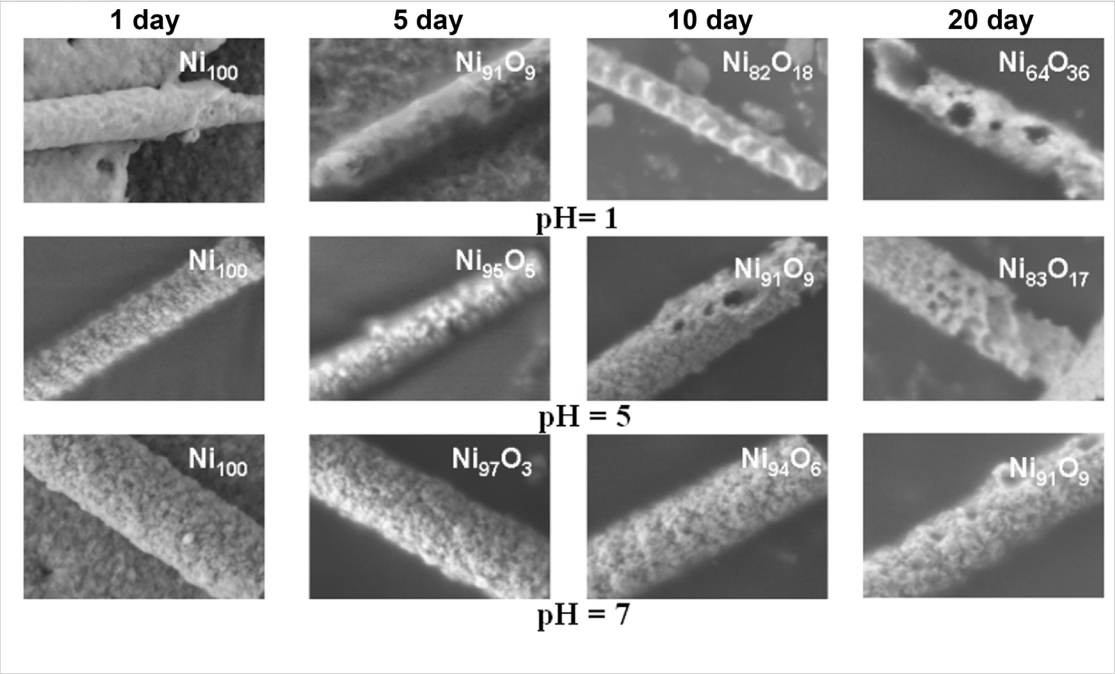

Figure 45. SEM images of changes in the surface morphology of Ni nanotubes depending on the acidity of the medium [160]

Analysis of the obtained images showed that the greatest degradation of the walls of nanotubes is observed for acidic media with pH=1, which confirmed the results of calculations of reactivity, reaction rate constants, and X-ray diffraction analysis. On day 10, for a medium with pH=1, the formation of loose amorphous regions on the outer side of the walls of nanotubes consisting of oxide compounds is observed, according to the energy dispersive analysis. On day 20, there is an increase in the area of amorphous regions and an increase in the atomic oxygen content in the NT structure to 36%, which leads to partial destruction of the walls, while energy dispersive and X-ray phase analyzes showed that the formed amorphous regions are oxide compounds NiO (II) and Ni_2O_3 (III). The scheme of degradation mechanisms depending on the environment is presented in Figure 46, data taken from [161].

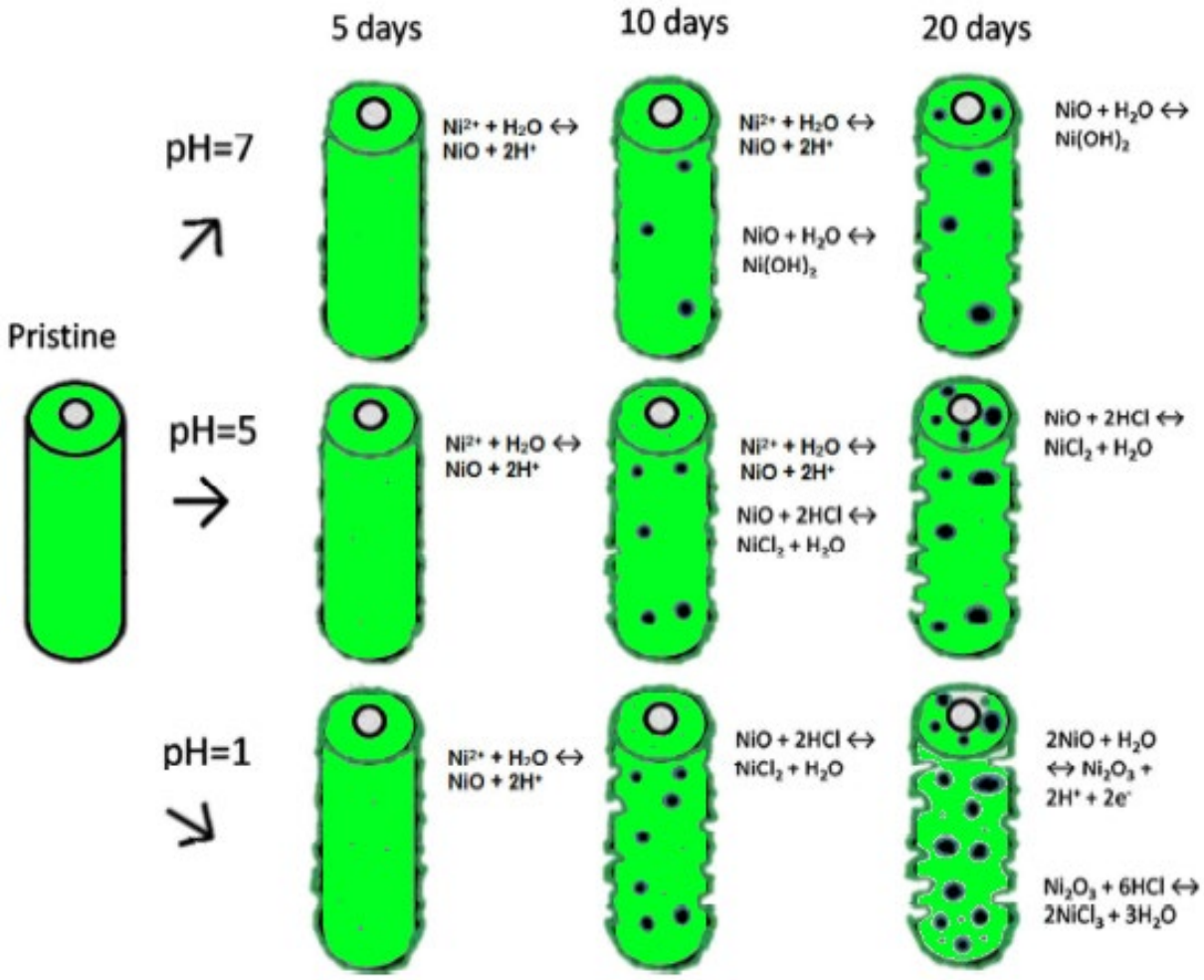

Figure 46. Diagram of the mechanisms of corrosion and degradation of Ni nanotubes [161]

According to the literature [160,161], these compounds are toxic and harmful to organic cells. For media with pH=5 and pH=7, according to the energy dispersive analysis, the appearance of oxygen in the structure is observed on day 5, however, according to x-ray phase analysis, oxide compounds in the crystal structure appear on day 10. The presence of small oxygen impurities on day 5 is due to the oxidation of the surface layer of nanotubes. On day 20, the oxygen content in the structure was 17% and 9% for media with pH=5 and pH=7, respectively. At the same time, for a medium with pH=5, the formation of amorphous regions is observed, causing partial destruction of the NT structure, and for a medium with pH=7, the formation of growths on the surface of the tubes, the average size of which is 30 – 35 nm, consisting of nickel oxide, according to energy dispersive and x-ray phase analysis.

Notes

- The main results of this study were published in [160,161].
- The analysis of structural parameters based on X-ray diffraction patterns and their analysis was carried out jointly with the staff of the Laboratory of Solid State Physics AB of INP.
- Obtaining samples under given synthesis conditions was performed personally by the author at the Laboratory of Solid State Physics AB of INP.
- The determination of the kinetics of degradation was carried out by the author together with the staff of the Laboratory of Solid State Physics AB of INP.

5. Conclusions

This chapter summarizes the obtained results, provides recommendations for future research and possible applications.

The electrochemical synthesis of vertical arrays of nickel nanotubes utilizing nuclear track membranes as templates, as well as the analysis of the geometry, composition, structure, magnetic and corrosion properties of synthesized object were studied. To characterize synthesized Ni NTs we used methods of scanning electron microscopy, transmission electron microscopy, X-ray diffraction analysis, magnetic spectroscopy, and energy dispersive analysis.

The fabricated nickel nanotubes have a number of advantages for bio-application, based on the production method, nanotubes geometry, and the selected material. Usage of PET pore templates allows control on geometric dimensions. Varying parameters of electrochemical deposition allows to vary chemical composition and crystal structure parameters. NTs have uniform magnetic fields, low density compared to NPs, and a large specific surface area. The choice of nickel nanotubes provides a simple possibility of surface functionalization and the potential for detaching the payload by magnetostriction, which is beneficial for targeted delivery of drugs and proteins using a magnetic field.

The scientific novelty of the thesis research is in detailed studies of the fabrication of Ni nanotubes with controlled properties, reactivity and chemical stability, which led to a number of important results:

1. A detailed model of formation of nickel nanotubes in pores of polymer matrices is developed. According to the model, at the initial stage of Ni nanotube formation the transverse component of growth rate prevails, which is responsible for nanotube wall growth in width. At the next stage the equilibrium state sets, characterized by a decrease in current density due to the depletion of the electrolyte solution, the nanotubes grow uniformly in both transverse and longitudinal directions. Next, the concentration of metal ions dominates near the top end of the nanotube, resulting that the longitudinal component of the growth rate of the nanotubes prevails and the tubes grow predominantly along the walls of the pores.

The proposed model of nanotube growth has been successfully applied for electrochemical fabrication of copper, cobalt and zinc nanotubes, as well as two-component nanotubes based on nickel-cobalt, nickel-iron, and copper-nickel compounds [162-166]. These experiments demonstrated good usability of this model of nanotube growth, and were carried out jointly by the research group of Nazarbayev University and the Solid State Physics Laboratory of the Institute of Nuclear Physics.

2. Effect of electrochemical synthesis electrolyte solution temperature and applied potential on Ni nanotubes geometry and crystal structure was established. In particular, it was found that an increase in the applied potentials in the range of 1.5 – 2.0 V and the deposition temperature range 35-50°C leads to the formation of nanotubes with one dominant direction of texture orientation.

3. Possibility of controlled variation of wall thickness of synthesized nanotubes by changing level of electrolyte solution acidity is shown. It was found that lowering the acidity level of the solution leads to a decrease in the wall thickness of nanotubes and the size of crystallites.

Based on the conducted experiments, the most optimal parameters for the synthesis of nanotubes were selected: the difference of the applied potentials is 1.5-1.75 V, pH = 3 and the electrolyte temperature is 25 °C. These parameters were used to fabricate Ni nanotubes for experiments to study the influence of the geometry of the template matrix on the structure of the resulting nanotubes, as well as for corrosion tests experiments.

4. Systematic study of dependence of structural and conducting characteristics of Ni nanotubes from electrolyte composition, temperature and applied voltage was carried out. Electrochemical deposition was carried out in a potentiostatic mode with a potential difference in the range from 1.5B to 2.0B with a pitch of 0.25. Adding ethanol to the electrolyte decreases surface tension of the liquid due to adsorption at the interface, which make possible to more easily distribute and reduce interfacial tension during synthesis. Deposition conditions influence the concentration of micro-stresses and dislocations in crystal structure, as well as parameters characterizing crystal lattice. It has been found that an increase in conductivity for ethanol synthesized samples occurs due to an improvement in the crystal structure and decrease in amorphous inclusions. Amorphous inclusions introduce additional defects in the structure, preventing ballistic electron movement.

5. Arrays of Ni nanotubes with diameters 100-500 nm have been successfully formed by a template synthesis method in pores of PET membranes. Uniform growth of the nanotubes with wall thickness from 25 nm to 140 nm with an outer diameter of 100 nm to 170 nm was demonstrated. Main parameters of Ni nanotubes crystaline structure: lattice parameter, grain sizes, crystallinity and microstrains, as well as texture coefficients were discussed. The main magnetic characteristics of fabricated Ni nanotubes were explored. Ni nanotubes arrays coercivity and squareness ratio exhibit unusual dependence on nanotubes diameter: it rises for samples with nanotubes 100 to 300 nm diameters and fall down for nanotubes 400 and 500 nm diameters. Dependence of nickel nanotubes magnetic characteristics on their morphology and structure was discussed. It is expected that the ability to control the magnetic properties of Ni

nanotubes can open up new opportunities for the design of high-density magnetic memory devices.

6. Kinetic degradation curves of nickel nanotubes in various media were established. Time dependence of deformation of crystallographic parameters on level of medium acidity is obtained. It has been shown that the main mechanism of degradation of nickel nanotubes is the formation of the metastable phase of nickel oxide, which decays due to instability, which leads to partial destruction of the structure. It was found that speed of degradation of nanotubes depends on the degree of crystallinity of the initial nanotubes, as well as the acidity of the solution.

Ni nanotubes can be potentially used in microelectronics, photocatalysis, chemical industry and biomedicine.

The obtained Ni nanotubes have possible useful application as magnetic carriers for targeted drug delivery. For example, in this direction we obtained the first results [27] on the possibility of coating Ni nanotubes with organosilicon compounds to increase the efficiency of corrosion protection of the magnetic core nanotube, as well as to create additional chemical bonds for binding drugs. Further research is planned in this direction.

Another possible development of our research and potential application is to use Ni nanotubes as a base for catalysts for the catalytic reduction of p-nitrophenyl compounds or photocatalysts to enhance the decomposition of organic dyes. The use of Ni nanotubes may significantly increase the rate of photocatalytic reactions, and also allow to remove magnetic nanotubes from aqueous solutions using magnetic separation. During the conducted initial experiments, promising results of the influence of the degree of structural ordering on the catalytic activity of nickel nanostructures were established.

References

1. Fert A., Piraux L. Magnetic nanowires //Journal of Magnetism and Magnetic Materials. – 1999. – Vol. 200. – №. 1-3. – P. 338-358.
2. Quan L. N. et al. Nanowires for photonics //Chemical reviews. – 2019. – Vol. 119. – №. 15. – P. 9153-9169.
3. Vaitiekėnas S. et al. Flux-induced topological superconductivity in full-shell nanowires //Science. – 2020. – Vol. 367. – №. 6485.
4. Wan W. et al. Transition metal electrocatalysts encapsulated into N-doped carbon nanotubes on reduced graphene oxide nanosheets: efficient water splitting through synergistic effects //Journal of Materials Chemistry A. – 2019. – Vol. 7. – №. 25. – P. 15145-15155.
5. Glotov A. et al. Mesoporous metal catalysts templated on clay nanotubes //Bulletin of the Chemical Society of Japan. – 2019. – Vol. 92. – №. 1. – P. 61-69.
6. Chen J. et al. Co-Fe-P nanotubes electrocatalysts derived from metal-organic frameworks for efficient hydrogen evolution reaction under wide pH range //Nano Energy. – 2019. – Vol. 56. – P. 225-233.
7. Sharma V. K. et al. Interactions between silver nanoparticles and other metal nanoparticles under environmentally relevant conditions: A review //Science of The Total Environment. – 2019. – Vol. 653. – P. 1042-1051.
8. Yao K. et al. Plasmonic Metal Nanoparticles with Core–Bishell Structure for High-Performance Organic and Perovskite Solar Cells //ACS nano. – 2019. – Vol. 13. – №. 5. – P. 5397-5409.
9. Scarabelli L. et al. Encapsulation of Noble Metal Nanoparticles through Seeded Emulsion Polymerization as Highly Stable Plasmonic Systems //Advanced Functional Materials. – 2019. – Vol. 29. – №. 14. – P. 1809071.
10. Ahn Y. Y. et al. Surface-loaded metal nanoparticles for peroxymonosulfate activation: Efficiency and mechanism reconnaissance //Applied Catalysis B: Environmental. – 2019. – Vol. 241. – P. 561-569.
11. Han F. et al. High electronic conductivity as the origin of lithium dendrite formation within solid electrolytes //Nature Energy. – 2019. – Vol. 4. – №. 3. – P. 187-196.
12. Ren Y. et al. Direct observation of lithium dendrites inside garnet-type lithium-ion solid electrolyte //Electrochemistry Communications. – 2015. – Vol. 57. – P. 27-30.
13. Zhuo K., Jeong M. G., Chung C. H. Highly porous dendritic Ni–Sn anodes for lithium-ion batteries //Journal of power sources. – 2013. – Vol. 244. – P. 601-605.

14. Wang J. M., Sun X. W., Jiao Z. Application of nanostructures in electrochromic materials and devices: recent progress //Materials. – 2010. – Vol. 3. – №. 12. – P. 5029-5053.
15. Benabbou A. et al. Geometrical modeling of granular structures in two and three dimensions. application to nanostructures //International Journal for Numerical Methods in Engineering. – 2009. – Vol. 80. – №. 4. – P. 425-454.
16. Borisenko V. E. et al. Physics, chemistry and application of nanostructures. – Singapore etc : world Scientific, 1997.
17. Osten H. J. et al. Integration of functional epitaxial oxides into silicon: from high-k application to nanostructures //Journal of Vacuum Science & Technology B: Microelectronics and Nanometer Structures Processing, Measurement, and Phenomena. – 2007. – Vol. 25. – №. 3. – P. 1039-1043.
18. Yan X., Zhu P., Li J. Self-assembly and application of diphenylalanine-based nanostructures //Chemical Society Reviews. – 2010. – Vol. 39. – №. 6. – P. 1877-1890.
19. Zhong L. S. et al. Self Assembled 3D flowerlike iron oxide nanostructures and their application in water treatment //Advanced Materials. – 2006. – Vol. 18. – №. 18. – P. 2426-2431.
20. Xia L., Wei Z., Wan M. Conducting polymer nanostructures and their application in biosensors //Journal of colloid and interface science. – 2010. – Vol. 341. – №. 1. – P. 1-11.
21. Gareth J. Owens, Rajendra K. Singh, Farzad Foroutan , Mustafa Alqaysi, Cheol-Min Han Chinmaya Mahapatra, Hae-Won Kim Jonathan C. Knowles Sol-gel based materials for biomedical applications//Progress in Material Science. – 2016. – P.1-79
22. Hui Pan, Binghai Liu, Jiabao Yi, Cheekok Poh, Sanhua Lim, Jun Ding, Yuanping Feng, C. H. A. Huan, and Jianyi Lin. Growth of Single-Crystalline Ni and Co Nanowires via Electrochemical Deposition and Their Magnetic Properties // J. Phys. Chem. B, 2005, 109 (8), pp 3094–3098
23. Alejandro Pereira, Juan L Palma, Juliano C Denardin and Juan Escrig. Temperature-dependent magnetic properties of Ni nanotubes synthesized by atomic layer deposition // Nanotechnology 27 (2016) 345709 (6pp)
24. K.R.Pirota,D.Navas,M.Hernández-Vélez,K.Nielsch,M.Vázquez. Novel magnetic materials prepared by electrodeposition techniques: arrays of nanowires and multi-layered microwires // Journal of Alloys and Compounds. Volume 369, Issues 1–2, 28 April 2004, Pages 18-26
25. F. Tian, J. Zhu, and D. Wei. Fabrication and Magnetism of Radial-easy-magnetized Ni Nanowire Arrays // J. Phys. Chem. C, 2007, 111 (34), pp 12669–12672

26. Mousa M.A.Imran. Structural and magnetic properties of electrodeposited Ni nanowires // Journal of Alloys and Compounds, volume 455, issues 1-2, May 2008, pages 17-20)
27. Kozlovskiy, Artem L., et al. "Comprehensive study of Ni nanotubes for bioapplications: from synthesis to payloads attaching." Journal of Nanomaterials 2017 (2017).
28. Pereira, Alejandro, et al. "Temperature-dependent magnetic properties of Ni nanotubes synthesized by atomic layer deposition." Nanotechnology 27.34 (2016): 345709.
29. Aziz, Muhammad Ham mad, et al. "Photodynamic effect of Ni nanotubes on an HeLa cell line." PloS one 11.3 (2016).
30. University of California - Santa Barbara. "'Smart' Bio-nanotubes Developed; May Help In Drug Delivery." ScienceDaily. ScienceDaily, 3 August 2005.
31. Qingtao Wang, Guanzhong Wang, Xinhai Han, Xiaoping Wang, and J. G. Hou. Controllable Template Synthesis of Ni/Cu Nanocable and Ni Nanotube Arrays: A One-Step Coelectrodeposition and Electrochemical Etching Method // J. Phys. Chem. B, 2005, 109 (49), pp 23326–23329
32. Sun, Chen, and Valery L. Pokrovsky. "Magnetic properties of a long, thin-walled ferromagnetic nanotube." Journal of magnetism and magnetic materials 355 (2014): 121-130.
33. Leitao, D. C., et al. "Insights into the role of magnetoelastic anisotropy in the magnetization reorientation of magnetic nanowires." Physical Review B 84.1 (2011): 014410.
34. Ahmad, Naeem, et al. "Magnetoelastic anisotropy induced effects on field and temperature dependent magnetization reversal of Ni nanowires and nanotubes." Journal of superconductivity and novel magnetism 24.1-2 (2011): 785-792.
35. Mehmood, Tahir, et al. "Mechanism for formation of fcc-cobalt nanowires in electrodeposition at ambient temperature." Materials Letters 130 (2014): 256-258.
36. Wang, Mingliang, et al. "Growth Orientation Control of Co Nanowires Fabricated by Electrochemical Deposition Using Porous Alumina Templates." Crystal Growth & Design 18.1 (2018): 479-487.
37. Wang, Xue Wei, et al. "Structural control and magnetic properties of electrodeposited Co nanowires." Journal of crystal growth 300.2 (2007): 421-425.
38. Kozlovskiy, A. L., et al. "The influence of thermal annealing on structural properties of Ni nanotubes." Vacuum 153 (2018): 254-261.

39. Sun, Chen, and Valery L. Pokrovsky. "Magnetic properties of a long, thin-walled ferromagnetic nanotube." Journal of magnetism and magnetic materials 355 (2014): 121-130.
40. Leitao, D. C., et al. "Insights into the role of magnetoelastic anisotropy in the magnetization reorientation of magnetic nanowires." Physical Review B 84.1 (2011): 014410.
41. Ahmad, Naeem, et al. "Magnetoelastic anisotropy induced effects on field and temperature dependent magnetization reversal of Ni nanowires and nanotubes." Journal of superconductivity and novel magnetism 24.1-2 (2011): 785-792.
42. Wang, Xue Wei, Zhi Hao Yuan, and Bing Cheng Fang. "Template-based synthesis and magnetic properties of Ni nanotube arrays with different diameters." Materials Chemistry and Physics 125.1-2 (2011): 1-4.
43. Wang, Xue Wei, et al. "Electrochemically synthesis and magnetic properties of Ni nanotube arrays with small diameter." Materials Chemistry and Physics 112.2 (2008): 329-332.
44. Li, Y. L., et al. "Fabrication and magnetic properties of free-standing Ni nanotube arrays with controllable wall thickness."Applied Physics Letters 100.5 (2012): 052402.
45. Chen, P., et al. "Growth of carbon nanotubes by catalytic decomposition of CH4 or CO on a Ni- MgO catalyst." Carbon 35.10-11 (1997): 1495-1501.
46. Choi, G. S., et al. "Carbon nanotubes synthesized by Ni-assisted atmospheric pressure thermal chemical vapor deposition." Journal of applied physics 91.6 (2002): 3847-3854.
47. Yang, Shitong, et al. "Adsorption of Ni (II) on oxidized multi-walled carbon nanotubes: effect of contact time, pH, foreign ions and PAA." Journal of hazardous materials 166.1 (2009): 109-116.
48. Li, Siwen, et al. "Co–Ni Based Nanotubes/Nanosheets as Efficient Water Splitting Electrocatalysts." Advanced Energy Materials 6.3 (2016): 1501661.
49. Qingtao Wang, Guanzhong Wang, Xinhai Han, Xiaoping Wang, and J. G. Hou. Controllable Template Synthesis of Ni/Cu Nanocable and Ni Nanotube Arrays: A One-Step Coelectrodeposition and Electrochemical Etching Method // J. Phys. Chem. B, 2005, 109 (49), pp 23326–23329
50. Yang, Shitong, et al. "Adsorption of Ni (II) on oxidized multi-walled carbon nanotubes: effect of contact time, pH, foreign ions and PAA." Journal of hazardous materials 166.1 (2009): 109-116.

51. Li, Xiangzi, et al. "Boron-doping Ni@ Au nanotubes: Facile synthesis, magnetic property, and in vitro cytotoxicity on Molt-4 cells." Materials Letters 108 (2013): 222-224.
52. Xiaoru Li Synthesis and Growth Mechanism of Ni Nanotubes and Nanowires. // Nanoscale Res Lett. – 2009. – V. 4. – P. 1015–1020.
53. Huaqiang Cao, Liduo Wang, Yong Qiu, Qingzhi Wu, Guozhi Wang, Lei Zhang, Xiangwen Liu. Generation and Growth Mechanism of Metal (Fe, Co, Ni) Nanotube Arrays // ChemPhysChem. 2006. p. 1500
54. Y. Fukunaka, M. Motoyama, Y. Konishi, and R. Ishji. Producing Shape-Controlled Metal Nanowires and Nanotubes by an Electrochemical Method. Electrochemical and Solid-State Letters, 9 (3),C62-C64 (2006).
55. Tao, Feifei, et al. "An Easy Way to Construct an Ordered Array of Nickel Nanotubes: The Triblock-Copolymer-Assisted Hard-Template Method." Advanced Materials 18.16 (2006): 2161-2164.
56. Lin, Shih-Chin, et al. "Synthesis and magnetic properties of highly arrayed nickel-phosphate nanotubes." Solid state sciences 7.7 (2005): 896-900.
57. Yonghui Chen, Chen Xu, Yibo Zhou, Khan Maaz, Huijun Yao, Dan Mo, Shuangbao Lyu, Jinglai Duan and Jie Liu. “Temperature- and Angle-Dependent Magnetic Properties of Ni Nanotube Arrays Fabricated by Electrodeposition in Polycarbonate Templates”. Nanomaterials 2016, 6, 231.
58. Dang, Thanh X., et al. "Helical crystallization on nickel–lipid nanotubes: Perfringolysin O as a model protein." Journal of structural biology 152.2 (2005): 129-139.
59. Proenca, Mariana P., et al. "Distinguishing nanowire and nanotube formation by the deposition current transients." Nanoscale research letters 7.1 (2012): 1-9.
60. Li, Xiaoling, et al. "Nickel/Copper nanoparticles modified TiO2 nanotubes for non-enzymatic glucose biosensors." Sensors and actuators B: Chemical 181 (2013): 501-508.
61. Tao, Feifei, et al. "A facile synthesis method of nickel nanotubes assisted by polyethylene glycol." Polymer Engineering & Science 50.1 (2010): 43-47.
62. Sabzi, Reza Emamali, Krishna Kant, and Dusan Losic. "Electrochemical synthesis of nickel hexacyanoferrate nanoarrays with dots, rods and nanotubes morphology using a porous alumina template." Electrochimica acta 55.5 (2010): 1829-1835.
63. TAO Fei-Fei, XU Zheng. Effective Synthesis of Magnetic Metal Nickel Nanotubes // Acta Phys. Chim. Sin., 2009, 25(5)：977-980

64. Wang, Jianli, et al. "Effect of electrical contact resistance on measurement of thermal conductivity and Wiedemann-Franz law for individual metallic nanowires." Scientific reports 8.1 (2018): 4862.
65. Guo, Chuan Fei, et al. "Metallic nanostructures for light trapping in energy-harvesting devices." Light: Science & Applications 3.4 (2014): e161.
66. Christopher, Phillip, Hongliang Xin, and Suljo Linic. "Visible-light-enhanced catalytic oxidation reactions on plasmonic silver nanostructures." Nature chemistry 3.6 (2011): 467.
67. Jiang, Wen, et al. "Advances and challenges of nanotechnology-based drug delivery systems." Expert opinion on drug delivery 4.6 (2007): 621-633.
68. Wang, Binjun, et al. "Mechanically Assisted Self-Healing of Ultrathin Gold Nanowires." Small 14.20 (2018): 1704085.
69. Serra, Albert, and Elisa Valles. "Advanced electrochemical synthesis of multicomponent metallic nanorods and nanowires: fundamentals and applications." Applied Materials Today 12 (2018): 207-234.
70. Chaure, N. B., et al. "Oriented cobalt nanowires prepared by electrodeposition in a porous membrane." Journal of Magnetism and Magnetic Materials 290 (2005): 1210-1213.
71. Jorritsma, J., and J. A. Mydosh. "Temperature-dependent magnetic anisotropy in Ni nanowires." Journal of applied physics 84.2 (1998): 901-906.
72. Chen, Min, Chia-Ling Chien, and Peter C. Searson. "Potential modulated multilayer deposition of multisegment Cu/Ni nanowires with tunable magnetic properties." Chemistry of materials 18.6 (2006): 1595-1601.
73. Ni, Wei, et al. "Hierarchical foam of exposed ultrathin nickel nanosheets supported on chainlike Ni-nanowires and the derivative chalcogenide for enhanced pseudocapacitance." Nanoscale 6.5 (2014): 2618-2623.
74. Dubois, Sylvain, et al. "Evidence for strong magnetoelastic effects in Ni nanowires embedded in polycarbonate membranes." Physical Review B 61.21 (2000): 14315.
75. Han, Sheng, et al. "Characterization of Ni nanowires after annealing." Materials Letters 61.4-5 (2007): 1105-1108.
76. Yang, Fei, et al. "Ni–Co oxides nanowire arrays grown on ordered TiO 2 nanotubes with high performance in supercapacitors." Journal of Materials Chemistry A 1.3 (2013): 594-601.
77. Zhang, X. Y., et al. "Template synthesis of well-graphitized carbon nanotube arrays." Materials Science and Engineering: A 308.1-2 (2001): 9-12.

78. Zhang, Chunjuan, et al. "Heterogeneous films of ordered CeO 2/Ni concentric nanostructures for fuel cell applications." Physical Chemistry Chemical Physics 12.17 (2010): 4295-4300.
79. Li, Zhe, et al. "Nickel nanotube array via electroplating and dealloying." Thin Solid Films 658 (2018): 1-6.
80. Wegrowe, J. E., et al. "Magnetoresistance of ferromagnetic nanowires." Physical review letters 82.18 (1999): 3681.
81. Kato, S., H. Kitazawa, and G. Kido. "Magnetic properties of Ni nanowires in porous alumina arrays." Journal of magnetism and magnetic materials 272 (2004): 1666-1667.
82. Kamalakar, M. Venkata, and A. K. Raychaudhuri. "Low temperature electrical transport in ferromagnetic Ni nanowires." Physical Review B 79.20 (2009): 205417.
83. Smogunov, Alexander, Andrea Dal Corso, and Erio Tosatti. "Ballistic conductance and magnetism in short tip suspended Ni nanowires." Physical Review B 73.7 (2006): 075418.
84. Lindquist N. C. et al. Engineering metallic nanostructures for plasmonics and nanophotonics //Reports on Progress in Physics. – 2012. – Vol. 75. – №. 3. – P. 036501.
85. Xia Y., Halas N. J. Shape-controlled synthesis and surface plasmonic properties of metallic nanostructures //MRS bulletin. – 2005. – Vol. 30. – №. 5. – P. 338-348.
86. Wu P. et al. Composition-and aspect-ratio-dependent electrocatalytic performances of one-dimensional aligned Pt–Ni nanostructures //The Journal of Physical Chemistry C. – 2013. – Vol. 117. – №. 37. – P. 19091-19100.
87. Velev O. D. et al. A class of porous metallic nanostructures //Nature. – 1999. – Vol. 401. – №. 6753. – P. 548-548.
88. Hecht, David S., Liangbing Hu, and Glen Irvin. "Emerging transparent electrodes based on thin films of carbon nanotubes, graphene, and metallic nanostructures." Advanced materials 23.13 (2011): 1482-1513.
89. Li, Weiyang, et al. "High-performance hollow sulfur nanostructured battery cathode through a scalable, room temperature, one-step, bottom-up approach." Proceedings of the National Academy of Sciences 110.18 (2013): 7148-7153.
90. Chen X.H., Chen C.S., Xiao H.N., Chen F.Q., Zhang G., Yi G.J. Corrosion behaviour of carbon nanotubes – Ni composite coating. Surface & Coatings Technology 191 (2005), 351-356.
91. Koch, C. C. "Top-down synthesis of nanostructured materials: Mechanical and thermal processing methods." Reviews on Advanced Materials Science 5.2 (2003): 91-99.

92. Mercuri, Francesco, Matteo Baldoni, and Antonio Sgamellotti. "Towards nano-organic chemistry: perspectives for a bottom-up approach to the synthesis of low-dimensional carbon nanostructures." Nanoscale 4.2 (2012): 369-379.
93. Patil, U. M., et al. "Photosensitive nanostructured TiO2 grown at room temperature by novel “bottom-up” approached CBD method." Journal of Alloys and Compounds 509.21 (2011): 6196-6199.
94. Ingratta, Mark, Elin Persson Jutemar, and Patric Jannasch. "Synthesis, nanostructures and properties of sulfonated poly (phenylene oxide) bearing polyfluorostyrene side chains as proton conducting membranes." Macromolecules 44.7 (2011): 2074-2083.
95. Liu, Xian-Ming, and Shao-Yun Fu. "High-yield synthesis of dendritic Ni nanostructures by hydrothermal reduction." Journal of crystal growth 306.2 (2007): 428-432.
96. Baffou, Guillaume, and Romain Quidant. "Thermo-plasmonics: using metallic nanostructures as nano-sources of heat." Laser & Photonics Reviews 7.2 (2013): 171-18
97. Yahia, I. S., et al. "Chemically deposited Ni-doped CdS nanostructured thin films: optical analysis and current-voltage characteristics." Journal of Alloys and Compounds 776 (2019): 1056-1062.
98. Shimizu, Toshimi. "Bottom-Up Synthesis and Structural Properties of Self Assembled High Axial Ratio Nanostructures." Macromolecular Rapid Communications 23.5-6 (2002): 311-331.
99. Kai, T. A. O., et al. "Oxidation and hot corrosion behaviors of HVAF-sprayed conventional and nanostructured NiCrC coatings." Transactions of Nonferrous Metals Society of China 19.5 (2009): 1151-1160.
100. He, Dong, et al. "A high-performance supercapacitor electrode based on tremella-like NiC 2 O 4@ NiO core/shell hierarchical nanostructures on nickel foam." Dalton Transactions 46.6 (2017): 1857-1863.
101. Liu, Xian-Ming, Xiao-Gang Zhang, and Shao-Yun Fu. "Preparation of urchinlike NiO nanostructures and their electrochemical capacitive behaviors." Materials Research Bulletin 41.3 (2006): 620-627.
102. Cai, Chao, et al. "The Electrodeposition of Nanostructured Ni-TiN Composite Films." Materials Science Forum. Vol. 620. Trans Tech Publications Ltd, 2009.
103. Feng, Qiu Yuan, et al. "Sediment co-deposition of nanostructured Ni-Al2O3 composite coatings." Key Engineering Materials. Vol. 373. Trans Tech Publications Ltd, 2008.

104. 105 Liu H. et al. Probing ultrathin one-dimensional Pd–Ni nanostructures as oxygen reduction reaction catalysts //Acs Catalysis. – 2014. – Vol. 4. – №. 8. – P. 2544-2555.

105. Zhang X. et al. Controlled synthesis and magnetic properties of Ni nanotubes and nanowires //Materials Research Bulletin. – 2017. – Vol. 95. – P. 248-252.

106. Jung J. S. et al. Fabrication and magnetic properties of Co nanostructures in AAO membranes //Bulletin of the Korean Chemical Society. – 2008. – Vol. 29. – №. 4. – P. 758-760.

107. Qin L. et al. The growth of ordered ZnAl2O4 nanostructures using AAO as a reactive template //Materials Letters. – 2010. – Vol. 64. – №. 24. – P. 2685-2687.

108. Chu S. Z. et al. Fabrication and characteristics of ordered Ni nanostructures on glass by anodization and direct current electrodeposition //Chemistry of materials. – 2002. – Vol. 14. – №. 11. – P. 4595-4602.

109. Козловский А.Л. и др. Электрохимический синтез и кристаллическая структура упорядоченных массивов НТ кобальта. // Вестник КазНУ. Серия химическая. – 2015. – Т.3. – С. 72-80.

110. Shingne N. et al. Formation, morphology and internal structure of one-dimensional nanostructures of the ferroelectric polymer P (VDF-TrFE) //Polymer. – 2013. – Vol. 54. – №. 11. – P. 2737-2744.

111. Wang Z., Brust M. Fabrication of nanostructure via self-assembly of nanowires within the AAO template //Nanoscale research letters. – 2007. – Vol. 2. – №. 1. – P. 34.

112. Shan D. et al. Surface plasmon resonance and interference coenhanced SERS substrate of AAO/Al-based Ag nanostructure arrays //The Journal of Physical Chemistry C. – 2014. – Vol. 118. – №. 41. – P. 23930-23936.

113. Ding J. et al. Morphology and phase controlled construction of Pt–Ni nanostructures for efficient electrocatalysis //Nano letters. – 2016. – Vol. 16. – №. 4. – P. 2762-2767.

114. Tian W. et al. Hexagonal close-packed Ni nanostructures grown on the (001) surface of MgO //Applied Physics Letters. – 2005. – Vol. 86. – №. 13. – P. 131915.

115. Tsuji, Masaharu, et al. "Microwave-assisted synthesis of metallic nanostructures in solution." Chemistry–A European Journal 11.2 (2005): 440-452.

116. Xia, Younan, and Naomi J. Halas. "Shape-controlled synthesis and surface plasmonic properties of metallic nanostructures." MRS bulletin 30.5 (2005): 338-348.

117. Hecht, David S., Liangbing Hu, and Glen Irvin. "Emerging transparent electrodes based on thin films of carbon nanotubes, graphene, and metallic nanostructures." Advanced materials 23.13 (2011): 1482-1513.

118. Hesheng Victor Xu, Xin Ting Zheng, Beverly Yin Leng Mok, Molecular Design of Bioinspired Nanostructures for Biomedical Applications: Synthesis, Self-Assembly and Functional Properties// Journal of Molecular and Engineering Materials. – 2016. – VOL.4(1). – P.33

119. Xiaoqing Yu, Zhenping Wang, Zhiqiang Su and Gang Wei Design, fabrication, and biomedical applications of bioinspired peptide-inorganic nanomaterial hybrids//Journal of Materials Chemistry B. – 2016. – VOL.2 – P.1130-1142

120. Апель, Павел Юрьевич. "Треки ускоренных тяжелых ионов в полимерах/Российская академия наук, институт физической химии." Москва (1998): 5-150.

121. Abu Saleh, Sameer, and Yehuda Eyal. "Porous tracks along wakes of swift uranium ions in polyimide." Applied physics letters 85.13 (2004): 2529-2531.

122. Wang, Pengfei, et al. "Ultrafast ion sieving using nanoporous polymeric membranes." Nature communications 9.1 (2018): 1-9.

123. Kozlovskiy A.L., Shlimas D.I., Shumskaya A.E., Kaniukov E.Yu., Zdorovets M.V., Kadyrzhanov K.K. Influence of Electrodeposition Parameters on Structural and Morphological Features of Ni Nanotubes. Physics of Metals and Metallography, 2017, Vol. 118, No. 2, pp. 164–169.

124. Shlimas D.I., Kozlovskiy A.L., Zdorovets M.V., Kadyrzhanov K.K. Uglov V.V., Kenzhina I.E., Shumskaya A.E., Kaniukov E.Yu. Obtaining of Ni nanotubes with specified properties. Mater. Res. Express 5 (2018) 035024.

125. Guo, Jing, et al. "Microstructures and magnetic properties of Tb-Fe-Co magnetic nanowire arrays prepared by electrochemical deposition." Superlattices and Microstructures 128 (2019): 298-306.

126. Zhang, Guo-Ying, Bing Guo, and Jun Chen. "MCo2O4 (M= Ni, Cu, Zn) nanotubes: template synthesis and application in gas sensors." Sensors and Actuators B: Chemical 114.1 (2006): 402-409.

127. Wang, Xue Wei, Zhi Hao Yuan, and Bing Cheng Fang. "Template-based synthesis and magnetic properties of Ni nanotube arrays with different diameters." Materials Chemistry and Physics 125.1-2 (2011): 1-4.

128. Che, G., et al. "Chemical vapor deposition based synthesis of carbon nanotubes and nanofibers using a template method." Chemistry of Materials 10.1 (1998): 260-267.

129. Cao, Huaqiang, et al. "Generation and growth mechanism of metal (Fe, Co, Ni) nanotube arrays." ChemPhysChem 7.7 (2006): 1500-1504.

130. Xia, Hui, et al. "MnO2 nanotube and nanowire arrays by electrochemical deposition for supercapacitors." Journal of Power Sources 195.13 (2010): 4410-4413.

131. Xu, Qiang, Lu Zhang, and Jing Zhu. "Controlled growth of composite nanowires based on coating Ni on carbon nanotubes by electrochemical deposition method." The Journal of Physical Chemistry B 107.33 (2003): 8294-8296.

132. Tourillon, G., et al. "Electrochemically synthesized Co and Fe nanowires and nanotubes." Electrochemical and solid state Letters 3.1 (1999): 20.

133. Han, Xiu‐Feng, et al. "Structural and magnetic properties of various ferromagnetic nanotubes." Advanced Materials 21.45 (2009): 4619-4624.

134. Shumskaya, Alena, et al. "Evolution of morphology, structure, and magnetic parameters of Ni nanotubes with growth in pores of a PET template." Journal of Magnetism and Magnetic Materials 497 (2020): 165913.

135. Vivas, L. G., et al. "Magnetic anisotropy in ordered textured Co nanowires." Applied Physics Letters 100.25 (2012): 252405.

136. Han, Xianghua, et al. "Influence of crystal orientation on magnetic properties of hcp Co nanowire arrays." Journal of Physics D: Applied Physics 42.9 (2009): 095005.

137. Hu, H. N., et al. "Textured Co nanowire arrays with controlled magnetization direction." Journal of magnetism and magnetic materials 295.3 (2005): 257-262.

138. Kozlovskiy, Artem, et al. "Evolution of Structural and Magnetic Characteristics of Template Synthesized Nickel Nanotubes." Fundamental and Applied Nano-Electromagnetics II. Springer, Dordrecht, 2019. 113-134.

139. Kozlovskiy, A. L., M. V. Zdorovets, and K. K. Kadyrzhanov. "Synthesis and properties of Fe/Ni nanotubes." Crystallography Reports 61.5 (2016): 842-848.

140. Kalkabay, Gulnar, et al. "Influence of temperature and electrodeposition potential on structure and magnetic properties of nickel nanotubes." Journal of Magnetism and Magnetic Materials 489 (2019): 165436.

141. Ferkel, H., B. Müller, and W. Riehemann. "Electrodeposition of particle-strengthened nickel films." Materials Science and Engineering: A 234 (1997): 474-476.

142. Wu, Wangping, Noam Eliaz, and Eliezer Gileadi. "The effects of pH and temperature on electrodeposition of Re-Ir-Ni coatings from aqueous solutions." Journal of The Electrochemical Society 162.1 (2014): D20.

143. Vazquez-Arenas, Jorge, et al. "Co–Ni alloy electrodeposition under different conditions of pH, current and composition." Electrochimica acta 65 (2012): 234-243.

144. Lew, Kyung Seek, et al. "Effect of pH and current density in electrodeposited Co–Ni–P alloy thin films." Materials Chemistry and Physics 112.1 (2008): 249-253.

145. Ji, J., et al. "Surface pH measurements during nickel electrodeposition." Journal of Applied electrochemistry 25.7 (1995): 642-650.

146. Tian, Liangliang, Jincheng Xu, and Songtao Xiao. "The influence of pH and bath composition on the properties of Ni–Co coatings synthesized by electrodeposition." Vacuum 86.1 (2011): 27-33.

147. Su, Xinghua, and Chengwen Qiang. "Influence of pH and bath composition on properties of Ni–Fe alloy films synthesized by electrodeposition." Bulletin of Materials Science 35.2 (2012): 183-189.

148. Haciismailoglu, Murside, and Mürsel Alper. "Effect of electrolyte pH and Cu concentration on microstructure of electrodeposited Ni–Cu alloy films." Surface and Coatings Technology 206.6 (2011): 1430-1438.

149. Motoyama, M., et al. "Effect of surface pH on electrodeposited Ni films." Journal of the Electrochemical Society 153.7 (2006): C502.

150. Kim, Jae-Woo, and Su-Moon Park. "In situ XANES studies of electrodeposited nickel oxide films with metal additives for the electro-oxidation of ethanol." Journal of the Electrochemical Society 150.11 (2003): E560.

151. Hassan, H. B., and Z. Abdel Hamid. "Electrodeposited Ni–Cr2O3 nanocomposite anodes for ethanol electrooxidation." International Journal of Hydrogen Energy 36.8 (2011): 5117-5127.

152. Hassan, H. B., and Z. Abdel Hamid. "Electrodeposited Ni–Cr2O3 nanocomposite anodes for ethanol electrooxidation." International Journal of Hydrogen Energy 36.8 (2011): 5117-5127.

153. Sadler, James E., et al. "Surface functionalization of electro-deposited nickel." Physical Chemistry Chemical Physics 13.40 (2011): 17987-17993.

154. Shibli, S. M. A., K. S. Beenakumari, and N. D. Suma. "Nano nickel oxide/nickel incorporated nickel composite coating for sensing and estimation of acetylcholine." Biosensors and bioelectronics 22.5 (2006): 633-638.

155. Cherigui, El Amine Mernissi, et al. "On the control and effect of water content during the electrodeposition of Ni nanostructures from deep eutectic solvents." The Journal of Physical Chemistry C 122.40 (2018): 23129-23142.

156. Fathi, R., and S. Sanjabi. "Electrodeposition of nanostructured Ni (1− x) Mnx alloys films from chloride bath." Current Applied Physics 12.1 (2012): 89-92.

157. Mernissi Cherigui, El Amine, et al. "Comprehensive study of the electrodeposition of nickel nanostructures from deep eutectic solvents: self-limiting growth by electrolysis of residual water." The Journal of Physical Chemistry C 121.17 (2017): 9337-9347.

158. Stephen, A., et al. "Magnetic properties of electrodeposited nickel–manganese alloys: Effect of Ni/Mn bath ratio." Journal of applied electrochemistry 30.11 (2000): 1313-1316.

159. Kalkabay, G., et al. "Peculiarities of template assisted electrodeposition one dimensional nickel nanostructures from chloride electrolyte." Advanced Physical Research 1 (2019): 5-13.

160. Kalkabay, G., et al. "Study of the reactivity of Ni nanotubes in media with different pH." Crystallography Reports 63.1 (2018): 90-95.

161. Kutuzau, Maksim D., et al. "The behavior of Ni nanotubes under the influence of environments with different acidities." CrystEngComm 20.23 (2018): 3258-3266.

162. Kozlovskiy, A. L., and M. V. Zdorovets. "The study of the structural characteristics and catalytic activity of Co/CoCo2O4 nanowires." *Composites Part B: Engineering* (2020): 107968.

163. Borgekov, Daryn B., et al. "Study of the rate of degradation of permalloy nanowires." Surface and Coatings Technology 389 (2020): 125621.

164. Kaniukov, Egor, et al. "Structural and Magnetic Characteristics of Ferrum Nanotubes Obtained at Different Potentials of Electrodeposition." physica status solidi (b) 257.3 (2020): 1900319.

165. Kadyrzhanov, K. K., et al. "Phase transformations in CoZnO/CoZn nanostructures depending on the difference in applied potentials." Surface and Coatings Technology 386 (2020): 125495.

166. Shumskaya, A. E., et al. "Correlation between structural and magnetic properties of FeNi nanotubes with different lengths." Journal of Alloys and Compounds 810 (2019): 151874.